PREPARATION AND CHARACTERIZATION OF POLYMER COMPOSITES CONTAINING GOLD NANOPARTICLES

A DISSERTATION SUBMITTED TO

THE DEPARTMENT OF CHEMISTRY

AND THE GRADUATE SCHOOL OF ENGINEERING AND SCIENCE

OF BILKENT UNIVERSITY

IN PARTIAL FULFILLMENT OF THE REQUIREMENTS

FOR THE DEGREE OF

DOCTOR OF PHILOSOPHY

By

Eda Yılmaz

September, 2011

I certify that I have read this thesis and that in my opinion it is fully adequate, in scope and in quality, as a dissertation for the degree of doctor of philosophy.

Prof. Dr. Şefik Süzer (Advisor)

I certify that I have read this thesis and that in my opinion it is fully adequate, in scope and in quality, as a dissertation for the degree of doctor of philosophy.

Prof. Dr. Erdal Bayramlı

I certify that I have read this thesis and that in my opinion it is fully adequate, in scope and in quality, as a dissertation for the degree of doctor of philosophy.

Assoc. Prof. Dr. Margarita Kantcheva

I certify that I have read this thesis and that in my opinion it is fully adequate, in scope and in quality, as a dissertation for the degree of doctor of philosophy.

Assist. Prof. Dr. Erman Bengü

I certify that I have read this thesis and that in my opinion it is fully adequate, in scope and in quality, as a dissertation for the degree of doctor of philosophy.

Assist. Prof. Dr. Coşkun Kocabaş

Approved for the Institute of Engineering and Science:

Prof. Dr. Levent Onural
Director of the Institute

ABSTRACT

PREPARATION AND CHARACTERIZATION OF POLYMER COMPOSITES CONTAINING GOLD NANOPARTICLES

EDA YILMAZ

Ph.D. in Chemistry

Supervisor: Prof. Dr. Şefik Süzer

September, 2011

In this study, light-assisted synthesis of gold nanoparticles in polymer films is demonstrated and characterization of gold nanoparticle-polymer composites using various techniques is shown. There are various methods introduced for the synthesis of gold nanoparticles in solution and their integration to the polymer films afterwards. However, synthesizing gold nanoparticles directly inside the polymer matrix is more advantageous for the production of polymer-nanoparticle composites.

An advantage of synthesizing gold nanoparticles within polymer films is the opportunity of photo-patterning. Films having patterns made of regions with and without gold nanoparticles can be produced, using masks designed to cut off the radiation at desired places. Such patterned films were investigated with scanning electron microscope (SEM) and dark regions between irradiated regions and masked regions were observed. These dark regions are shown to be "ion depleted regions", where gold ions diffuse through irradiated regions during the irradiation. These regions of about 10 μm width, suggests a very large distance for gold ions to diffuse through a rigid matrix like Poly(methyl methacrylate)(PMMA), which is very interesting. Supporting evidence for the existence of these regions was obtained from fluorescence studies with Rhodamine 6G molecule and x-ray electron spectroscopy (XPS). The observations made through the formation of ion depleted regions can be used to estimate the diffusion constant of gold ions inside the PMMA matrix. Also the presence of ion depleted regions indicate the stability of photo-patterns created on the polymer film against

smearing during light exposure after the production, by setting an upper limit to the critical feature size.

During the characterization of gold nanoparticle-polymer composites, the electrical properties of PMMA with and without gold nanoparticles were investigated using charge resolved XPS, while applying external bias to the films with and without gold nanoparticles to probe the charging properties of the films. An enhancement of conductivity of PMMA films containing gold nanoparticles was observed using this technique. Additionally charge resolved XPS technique was also used to determine the charge storage characteristics of the polymer surfaces, which is important for the identification of charging mechanisms during contact and other electrification processes. It was shown that the PMMA surface is very susceptible to negative charging and even native negative charges on the PMMA surface can be observed prior to any treatment. Also when the surface is charged carbon and oxygen atoms of the carbonyl and methoxy groups of PMMA were observed to behave differently from the backbone of the polymer, which shows the chemical specificity of the charge accumulating spots on the surface.

Keywords: Gold nanoparticle, PMMA, XPS, Charge resolved XPS, Photo-patterning, Ion depleted region, Contact electrification

ÖZET

ALTIN NANOPARÇACIKLARI İÇEREN POLİMER KOMPOSİTLERİNİN HAZIRLANMASI VE KARAKTERİZASYONU

EDA YILMAZ

Danışman: Prof. Dr. Şefik Süzer

Eylül, 2011

Bu çalışmada altın nanoparçacıklarının polimer filmleri içerisinde ışık yardımıyla sentezlenmesi ve çeşitli teknikler kullanılarak altın nanoparçacığı-polimer kompositlerinin karakterizasyonu gösterilmektedir. Altın nanoparçacıklarının çözelti fazında sentezini ve sonradan polimer filmlerine bütünleştirilmesini gösteren başka çalışmalarda mevcuttur. Fakat bu uygulamalara nazaran altın nanoparçacıklarının polimer filmleri içerisinde sentezlenmesi, polimer-nanoparçacık kompositlerinin üretimi açısından daha basit ve avantajlıdır.

Altın nanoparçacıklarının polimer filmleri içinde sentezlenmesinin bir avantajı, bu tekniğin ışıkla desenleme uygulamalarına imkan sağlamasıdır. Bu yöntemle UV ışığını istenen bölgelerde kesen maskeler kullanılarak, polimer içinde altın nanoparçacığı içeren ve içermeyen bölgelerden oluşan desenler oluşturulabilir. Bu şekilde oluşturulan desenli filmlerin taramalı elektron mikroskobu ile incelenmesi sırasında, maskelenmiş ve radyasyona maruz bırakılmış bölgeler arasında mikroskopta koyu gözüken bölgeler tespit edilmiştir. Bu koyu bölgeler "İyondan arındırılmış bölgeler" olarak adlandırılmış olup oluşumları sırasında altın iyonlarının radyasyona maruz bırakılmış bölgelere doğru hareket ettiği düşünülmektedir. İyonların bu bölgeleri oluştururken katı bir polimer filmi içerisinde 10 μm gibi uzun bir mesafe kat etmesi ilgi çekicidir. Bu bölgelerin varlığı ile alakalı destekleyici kanıtlar Rhodamine 6G molekülünü kullanan floresans çalışmalarından ve x-ışını fotoelektron spektroskopisinden (XPS) elde edilmiştir. İyondan arındırılmış bölgelerde yapılan incelemelerden yola çıkılarak, altın iyonlarının poli(metil metakrilat) (PMMA) filmleri

içerisindeki hareket kabiliyetlerine ait difüzyon katsayısı hesaplanabilir. Bunun yanı sıra iyondan arındırılmış bölgelerin varlığı, daha dayanıklı, ışıkla temas sonucu kusma yapmayan desen oluşumunda çok önemlidir.

Altın nanoparçacığı-polimer kompositlerinin karakterizasyonu bağlamında, yük çözümlemeli XPS tekniği ile altın nanoparçacığı içeren ve içermeyen PMMA filmleri, dışarıdan voltaj uygulanarak incelenmiştir. Bu çalışmalar sonucunda altın nanoparçacığı içeren PMMA filmlerinin iletkenliklerinin arttığı gözlemlenmiştir. Buna ek olarak, yük çözümlemeli XPS tekniği ayrıca polimer yüzeylerinin yük toplama özelliğinin incelenmesi için kullanılmıştır. Bu özellik yalıtkan malzemelerin temasla elektriklenmesi olayının aydınlatılması için büyük önem taşımaktadır. Bu çalışmalarda PMMA yüzeyinin eksi yükleri toplamaya çok yatkın olduğu gösterilmiş ayrıca yüzeyde hiçbir etki olmaksızın yerel eksi yüklerinde bulunduğu gözlemlenmiştir. Ayrıca yüzey yüklü olduğu durumlarda PMMA'nın karbonil ve metoksi gruplarının polimerin iskeletinden daha farklı davrandığı görülmüştür. Bu durum özellikle yük toplama noktalarının kimyasal özelliklerinin tayini için önem arz etmektedir.

Anahtar kelimeler: Altın nanoparçacığı, PMMA, XPS, Yük çözümlemeli XPS, Işıkla desenleme, İyondan arındırılmış bölge, Temasla elektriklenme.

ACKNOWLEDGEMENTS

I would like to express my deepest gratitude to Prof. Dr. Şefik Süzer for his excellent supervision and his support during 7 years starting from my undergraduate to my Ph.D. graduation. I would like to thank Dr. Gülay Ertaş for always answering my questions and helping me in every possible way. I'm also grateful to my committee members for their valuable contributions during the preparation on this thesis.

I'm indebted to my husband and my family for all their support and self-sacrifice on my behalf.

I also would like to thank my present and past groups members, Hikmet Sezen, İlknur Tunç, Ivalina Avromova, C. Pinar Cönger, Hacı Osman Güvenç and Merve Taner, for their support.

Finally, I would like express my gratitude to TÜBİTAK for the financial support during my studies.

Table of Contents

List of Figures

List of Tables

1 Introduction

Nanotechnology has been one of the most popular fields of science for the last 20 years and the attention towards this area continues to increase. Nanotechnology includes a wide range of applications in the interest of many different fields. For that reason, interdisciplinary approaches are generally essential for the creation of novel methods or materials within the scope of nanotechnology. “Nano” term in nanotechnology, in general, refers to materials with features in the 1 nm - 100 nm size range. In this size range materials behave differently from their bulk and atomic forms, hence materials which were previously unknown to us have been synthesized utilizing these properties. In addition to producing new materials, nanotechnology is also important to build smaller components for many applications like new generation electronics, computers etc.. In this respect, there is an ever-increasing demand for smaller components for technology with increased capacity to create more compact devices than before. Especially for the computers, the transistor technology we have now is not sufficient to build machines with higher capacity. New ways to fit more transistors or other circuit elements to smaller chips are required. To achieve this mission, scientists now use nanotechnology to create smaller and more powerful transistors, capacitors and other circuit components for such systems. Of course this example is only a very small fraction of the studies conducted in the field of nanotechnology. Such approaches to build smaller and more efficient materials are employed in many different fields like biotechnology, catalysis chemistry, environmental chemistry, sensor design, energy related research etc.

One of the most studied materials in nanotechnology is probably metal nanoparticles, sometimes referred as Quantum Dots (QD) as well. Nanoparticles are basically particles made of any material that are again within the size range of 1-100 nm. The reason of the demand for nanoparticles in various applications is their fascinating size-related properties. [1-3] Each metal nanoparticle behaves different and has specific properties depending on its size, shape and composition. The electronic properties of metals differ drastically, as one compares bulk metal to metal nanoparticles and molecular forms of the metals, due to change in density of electronic states as shown in Figure 1.1.[4, 5]. Nanoparticles neither have bandgaps as wide as molecules nor as small as bulk metals. The bandgap structure of most nanoparticles can be described as discrete energy levels with a small energy gap. This change in the bandgap structure grants many different properties to the nanoparticles. In addition, the increased

surface/volume ratio imparts some nanoparticles more reactivity than their bulk counterparts and enables them to catalyze reactions more efficiently and/or some nanoparticles gain superior electrical properties making them excellent candidates for the next generation electronic devices. Of course how their properties change is strongly related to the material they are made of. Nanoparticles can be synthesized from noble metals atoms like gold, platinum or silver or transition metals like manganese, iron etc. or even the oxides of the transition metals. In addition to that, nanoparticles consisting of two or more different metals can also be synthesized. Core-shell nanoparticles and alloy nanoparticles are examples for this kind of nanoparticles. Creating such bimetallic (or multimetallic) nanoparticles enables us to achieve properties that cannot be achieved with monometallic nanoparticles. Whatever they are made of, the band structure imparted in nanoparticles is particularly important and enables many applications in electronics[3, 6], optics[7, 8], catalysis[9, 10] and biotechnology[11, 12].

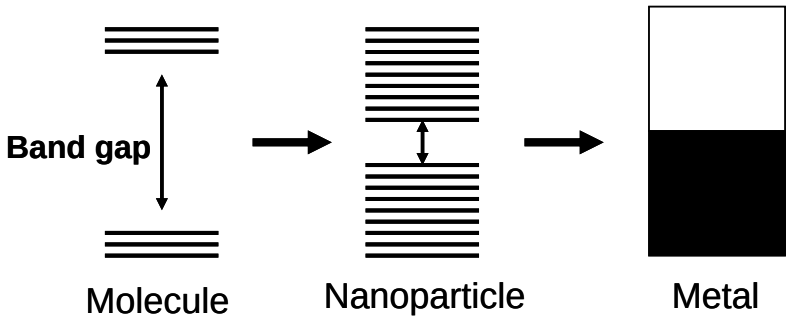

Figure 1.1 Evolution of electronic states of a metal from molecule to bulk

As mentioned, nanoparticles of noble metals like gold or silver can be synthesized and they have exciting chemical, optical and physical properties unlike their bulk metals. For example, although the bulk form of gold is an inert material, the nanoparticle form of gold is highly reactive and can catalyze many different reactions. [13-16] Also they have interesting optical properties. A strong absorption band in visible range is observed for most of these noble metals, which is called Surface Plasmon Resonance (SPR) band. SPR band is usually a very strong absorption band which makes the nanoparticles having this band, especially in the visible range, very valuable for optical applications. In the upcoming chapters, the extraordinary properties of gold nanoparticles and the applications related to these properties will be discussed in more detail for a better understanding of the motivation for this work.

.

1.1 Applications of Gold Nanoparticles

Although gold nanoparticles have become popular for the last decade but they are not newly discovered. They have been used by many cultures from Egypt to China as a colorant for glass or ceramics throughout the history. We can still admire stained glass windows in churches colored with colloidal gold from centuries ago. Considering the elapsed time we've been using gold nanoparticles, the detailed characterization to classify them as nanoparticles is very recent. After realization of the special electronic structure of gold nanoparticles and introduction of synthesis methods with excellent control on the particle size and shape, the research considering the possible applications of gold nanoparticles has increased tremendously for the last 50 years. Nowadays gold nanoparticles are even being used in some commercial applications created with certain nanotechnology approaches. There are also numerous applications of gold nanoparticles in different fields. Brief insights to some of these fields will be mentioned in the following sections to demonstrate the importance of gold nanoparticles in science and technology.

1.1.1 Gold Nanoparticles in Electronics

In the electronics, the most demanding objective is to build smaller devices with higher performance and with less energy consumption. The current semiconductor technology cannot fulfill these requirements any further since it has reached its physical limit. In place of the current systems, more capable new materials should be developed. An important candidate for such technologies is single electron device concept, which uses quantum dots as its components. The single-electron devices are expected to employ "switchable" quantum dots and quantum channels with correlated electrons that can offer order of magnitude smaller components for the new generation electronics. This can result in new generation of computers, supersensitive electrometers, near infrared receivers and very simple miniature lasers. Gold nanoparticles can be employed to produce such devices as shown in a study by Sato et al. in which a single-electron transistor has been constructed using alkanedithiol-stabilized gold nanoparticles as tunnel junctions.[17]

When metallic nanoparticles with a diameter in the range of a few nanometers are arranged with an interparticle distance of about 1nm, they build tunnel junctions with low electrical capacitances. [18] With this process controlled charge transport between the particles can be achieved by single-electron tunneling (SET) events at room temperature. SET devices can range from a single conductive nanoparticle between two microelectrodes to 2D-3D

arrays of nanoparticles with SET property in contact with a STM tip. For example, scanning tunneling spectroscopy has been used to observe SET effects on nanoparticle monolayers of Au_{55} nanoparticles in contact with a tip and "Coulomb staircase" behavior (single electron transfer steps in current-potential curve) was observed even at room temperature and the capacitance of the nanoparticles was calculated as 3.9×10^{-19} F. [19] Combining many SET elements to develop computing devices is still challenging. Although construction of single nanotransistors is not a hard task, combining 10^{12} transistors to form a transistor network is yet a dream. But judging from the current studies, gold nanoparticles are excellent candidates for the components of such devices.

1.1.2 Gold Nanoparticles in Catalysis

Normally gold is known as a chemically inert element and indeed it is one of the most stable elements. But gold nanoparticles are surprisingly very active catalysts for many different reactions. For example, Haruta et al. reported that gold nanoparticles dispersed on Co_3O_4, Fe_2O_3 or TiO_2 substrates are highly active catalysts for CO and H_2 oxidation, NO reduction, water-gas shift reaction, CO_2 hydrogenation and catalytic combustion of methanol. [13-16] This surprising catalytic activity again is a result of the intermediate electronic structure of gold nanoparticles between bulk metal and atomic state. Catalytic performance can be sensitive to particle size since the surface structure and electronic properties can change greatly with the size of the nanoparticles. One of the most important studies about gold nanoparticle catalysts was by Valden et al. [20]. They produced a highly active model gold catalyst where gold nanoparticles are spread uniformly on a Ti_2O_3 surface that showed ~50 fold improvement in the performance of realistic, high surface area catalysts.

Besides improved electronic structure suitable for catalysis, gold nanoparticles are also preferred as catalysts for their large surface/volume ratio. For catalysis the area of the catalyst interacting with the substrate is of great importance. For the same amount of catalysts the ones with larger surface/volume ratio have greater activity than the others if all other conditions are equal. For this reason generally catalyst species are attached to mesoporous or microporous structures for heterogeneous catalysis to achieve the largest possible area for interactions with the substrate. In this aspect, gold nanoparticles serve as a practical solution for this problem with their easy synthesis and naturally large surface/volume ratio. [1]

For instance a final note on catalysis with gold nanoparticles is, as can be realized from the list of the important reactions that are catalyzed by gold nanoparticles, most of the

reactions are related to degradation of harmful gases that cause air pollution and global warming. For this reason gold nanoparticle based catalyst research is a very hot topic and better catalysts for the exhaust of the cars or other pollution sources are anticipated in the near future.

1.1.3 Gold Nanoparticles in Biotechnology

Gold nanoparticles are also widely used in biology and biotechnology for various applications, mostly on the basis of attaching different groups on nanoparticles and functionalizing them as sensors or for targeted drug delivery. Currently, DNA-gold nanoparticle assemblies for biological sensors, gold nanoparticle enhanced immuno-sensing, gold nanoparticle sugar sensors and other gold nanoparticle bioconjugates like peptides, lipids, enzymes, drugs and viruses are some of the areas of interests. Conjugates of gold nanoparticles with oligonucleotides are of great interest because of the potential use of the programmability of DNA base pairing to organize nanoparticles in space and the multiple ways of providing a signature for the detection of precise DNA sequences. With these properties such conjugate systems have many applications in the fields of biosensors, disease diagnosis and gene expression. [21] [22] [23] For example, in a study of Mirkin's group DNA and RNA oligonucleotides attached to gold nanoparticles was monitored using surface-enhanced Raman spectroscopy (SERS) and with the shifts of the corresponding Raman signals matching with the target oligonucleotides was detected. [24] Like this example, by changing the attached groups on gold nanoparticles many of the biological molecules could be detected since biological systems are generally based on pair matching mechanisms. Using this basis, it is possible to design biosensor chips, consisting of gold nanoparticles with different recognition groups as an array on the chip and a single drop of specimen can be detected for many different threads at the same time.

1.1.4 Gold Nanoparticles in Characterization

Gold nanoparticles are also used for the improvement of instrumentation techniques and detection methods. The mostly known example in this area is SERS effect of gold nanoparticles. [25] Generally Raman signals of most molecules are hard to detect since the signals are very weak and the concentration must be very high to conduct a reliable measurement. But for cases like molecular biology generally the amount of the molecule to be detected may be very small and some kind of signal enhancement is needed at such cases.

Surface plasmon resonance of gold nanoparticles enhances Raman signals and enables non-detectable amounts of materials to be detected.

Besides, gold nanoparticles can also be used for analytical detection of desired elements or molecules, changing the attached groups. An example of such studies is given by Kim et al. for detection of small concentrations ("spectroscopically silent") of aqueous heavy metal ions, including toxic metals like lead, cadmium, mercury, was accomplished using simple calorimetry. [26] In this study, functionalized gold nanoparticles were aggregated in solution in the presence of divalent metal ions by an ion-templated chelation process and this caused an easily measurable change in the absorption spectrum of the particles.

1.2 Applications of Nanoparticle-Polymer Composites

Polymer composites have been produced and used for decades for various applications. Probably the most famous and widely used polymer composite is Bakelite, which is a clay reinforced resin that was developed in the early 20th century. Nevertheless the true importance of polymer composites was not fully realized until the end of 20th century. With the growing attention towards nanomaterials such as nanoparticles, carbon nanotubes and nanowires, the investigations towards possible applications of these materials in polymer composites has also became popular. Addition of nanoparticles or other nanomaterials to the polymer matrix enables the modification of polymer properties or sometimes implies addition of new properties to the polymers. These new materials with superior properties have many applications in different areas like optics, microelectronics, piezoelectrics, batteries, organic solar cells and biomedical sciences etc. and the application areas still continue to increase. Some of the most popular applications will be reviewed briefly in this section.

There are several ways to produce polymer-nanoparticle composites depending on the desired properties and the area of use. Nanoparticles can either be integrated to the polymer matrix to produce homogeneous composite films or can be capped with polymers to produce nanoparticle-core/polymer-shell composite nanoparticles. To produce homogeneous composite films of polymer-nanoparticle composites nanoparticles can either be synthesized beforehand and integrated to the polymer or can be synthesized within the polymer. For both cases homogeneous distribution of the pre-synthesized nanoparticles is important. In the former synthesis method, ligands that are used to stabilize nanoparticles against agglomeration, can be immiscible with polymer and prevent homogeneous distribution in some cases. The ligand choice should be carefully made for the synthesis of nanoparticles for that reason. However in the latter case, which is the synthesis of the nanoparticles directly within the polymers, the homogeneous distribution of nanoparticles in polymer is granted for most cases. Comparing the distribution of metal pre-cursors to nanoparticles, the distribution of metal pre-cursors can be more easily achieved because of their small size and high miscibility with the polymer.

Another important criterion to be watched for the nanoparticle-polymer composites is maintaining the interaction and full integration of nanoparticles in the polymer matrix. In this case ligands around the nanoparticles can again be a problem since even if the ligand is

miscible with polymer and enables homogeneous distribution, it still forms a barrier between nanoparticle and polymer. Especially in applications for electronics, full integration of nanoparticles with the polymer is needed for improved electron transfer between nanoparticles and polymer. For this reason ligand hinderance should be kept at a minimum. The synthesis of nanoparticles inside polymer matrices is again advantageous for such cases since the nanoparticles synthesized with this method in the polymer don't need ligands for the stabilization. Polymer maintains the particle size of nanoparticles and prevents them against agglomeration by its limited pore size and low diffusion rate within. For that reason better interaction of polymer with nanoparticle can be maintained using this synthesis technique.

One of the most important effects of nanoparticles on polymer materials is changing their optical properties. For example, the addition of nanoparticles can change the refractive index of the polymers, as shown by many different studies[27-32]. TiO_2 is one of the most widely used materials to modify the refractive index of the polymers, but there are also studies employing ZrO_2, Al_2O_2, ZnO and PbS for this purpose. The modification of refractive index of polymers is especially important for applications like microoptics and optical data transmission. Photoluminescence of nanocomposites is another interesting property of nanoparticle-polymer composites and it has a high potential for applications. For example epoxy nanocomposites containing ZnO nanoparticles can be used as solid state lightning[33] and ZnO-polymer core-shell nanoparticles can be used for in vitro cell imaging[34].

Combination of Fe_2O_3, Fe_3O_4 or ferrite nanoparticles with polymers creates the opportunity to produce polymeric materials with magnetic properties. Polymer nanocomposites with desired magnetic properties free of hysteresis at room temperature and in some cases transparent can be produced this way.[35, 36] For polymers with magnetic properties there are many potential applications in different fields such as in industry; as microwave absorbing material[37], as contrast agent for magnetic resonance imaging[38, 39], in cancer treatment by local hyperthermia[40, 41], as drug carriers[42, 43] or as biocompatible ferromagnetic fluid[44, 45].

Polymer composites with interesting dielectric properties can be synthesized with the addition of conductive metal nanoparticles to polymers. The most aspiring advantage of using polymer composites as parts of integrated circuits is the opportunity of "printing" the polymers on the boards to create these circuits. Such an opportunity would bring down the production costs tremendously compared to the current technology. Also polymers can be synthesized with low cost methods and there is practically unlimited amount of resources

compared to the limited resources of silicon, which is used as the base material of the current electronic devices. Additionally light and flexible devices can be produced using polymer composites as the main material which is an advantage regarding the preferences of the consumers towards such products. Studies continue to grow aiming to produce suitable nanocomposites as components for electronic applications. [3, 46] For example there are many attempts to design materials with high permittivity to be used as capacitors. $BaTiO_3$ composites with polymers are promising candidates for such applications because of the high permittivity of $BaTiO_3$. [47, 48] In another study the capacitive and resistive characteristics of ionic polymer metal composites are discussed in length. [49] Although there are encouraging examples of polymer composites demonstrating excellent capacitance or conductance abilities for the design of circuit components, the integration of those into circuits and devices still has a long way to go and studies will continue to overcome many hardships in this way.

Another important potential application field for the polymer-nanoparticle composites is employing them as electrodes in lithium-ion batteries. Nanocomposites based on inorganic nanoparticles and carbon are very advantageous as anode materials in lithium-ion-batteries and are expected to increase the performance of the batteries significantly since reducing dimensions using nanomaterials increases the diffusion rate of lithium insertion and removal due to short diffusion lengths. [50] Also the electron transfer between nanoparticles is enhanced and the high surface/volume ratio enables high contact area with the electrolytes. Nanocomposites containing SnO_2 seems very promising as anode materials since they have higher specific capacities than the standard carbon anodes. The most important point to improve about nanocomposite anodes is the cyclability of the anode. The current cyclability of the nanocomposites are quite low comparing to the current systems and studies to improve this problem continue. Combining nanoparticles with carbon based materials gives promising results for increasing the number of cycles the anode can go through. Zhang et al. demonstrated a high number of cycles (100 cycles with 34% decay) for metallic Sn nanoparticles encapsulated in an elastic carbon sphere. [51]Carbon encapsulation of SnO_2 also results in high reversible specific capacity according to a study by Park et al. [52]

1.3 Synthesis of Nanoparticles

Synthesis methods for nanoparticles are typically grouped into two categories: (i) top-down and (ii) bottom-up approaches. The top-down approach involves division of a bulky solid into smaller portions, using milling, chemical methods and volatilization of a solid followed by condensation of the volatilized components. The bottom-up approach uses condensation of atoms or molecular species from the gas phase or the solution. Both methods have advantages and disadvantages in different aspects. The top-down approach employing lithography and etching techniques can advantageously be used to generate required nanostructures in a spatially controlled manner. This property is important for integration and interconnection of nanoparticles into circuit elements and/or to design other specific applications. On the other hand, the bottom-up approach is very powerful in creating monodisperse nanoparticles with atomic precision and this precise synthesis is important for applications in need of well-defined nanoparticles. Also the machinery and the costs of both approaches differ considerably. For the top-down techniques generally expensive machinery and careful maintenance are needed. While for the bottom-up techniques, reactions generally take place in a test tube and the cost of reagents are a lot cheaper compared to the costs of machinery used in the top-down approach. There are strong and weak sides of both approaches and one would select the most suitable method for their own application.

1.3.1 Synthesis of Gold Nanoparticles in the Solution Phase

As mentioned before, nanoparticles can be produced with many different techniques, gold nanoparticles are no exception to that. Nevertheless solution phase synthesis is the most commonly used synthesis approach for gold nanoparticles, because of its well defined nature and the accuracy of the synthesized nanoparticles.[1, 53] The solution phase synthesis generally consists of two steps; reduction of gold salt ions in the solution with a mild reducing agent and capping the nanoparticles with an organic molecule to prevent the further agglomeration of the particles. The reducing agent reduces Au^{3+} ions to Au^{0} atoms and Au^{0} atoms coalesce to form nanoparticles since they are thermodynamically more stable. To prevent further aggregation of the formed nanoparticles, organic capping agents are used to result in stable and dispersed nanoparticles.

Among the commonly used synthesis methods of gold nanoparticles the most popular one is Turkevitch method, introduced by Turkevitch in 1951.[54] The Turkevitch method

employs citrate reduction of $HAuCl_4$ in water. Gold nanoparticles of about 10-30 nm can be synthesized with this method. Also a method for the synthesis of nanoparticles with pre-chosen size was introduced by Frens in 1973. [55] It was shown that the derivation of the ratio between the reducing/stabilizing agents can lead to nanoparticles size between 16 nm – 147 nm size range. Turkevitch synthesis is generally used to produce nanoparticles with a loose shell of ligands (citrate ions) around the gold nanoparticle core.

Another method used widely for gold nanoparticle synthesis is the Brust-Schiffrin method. [56, 57] This method was proposed in 1994 and had quite an impact on the field since it enabled the facile synthesis of thermally stable and air-stable gold nanoparticles with reduced dispersity and controlled size for the first time. Nanoparticles synthesized by this method can be repeatedly isolated and redissolved in common organic solvents without aggregation and decomposition so they can be easily handled like stable organic molecules. This synthesis method uses thiol ligands that strongly bind gold, because of the soft character of both gold and sulfur. $AuCl_4^-$ is transferred to toluene using tetraoctylammonium bromide as the phase transfer agent and reduced by $NaBH_4$ in the presence of dodecanethiol. The color of organic phase changes from orange to deep brown within a few seconds upon the addition of $NaBH_4$. Gold nanoparticles synthesized with this method are in the size range of 1 nm – 3 nm, the size of the nanoparticles can be controlled adjusting the gold/thiol ratio and also the temperature of the reaction medium. Fast reductant addition and cooled solutions produce smaller and more monodispersed nanoparticles with this method.

Other than the synthesis methods mentioned above there are many other methods to produce gold nanoparticles with pre-chosen size and morphology. In these methods the size and shape of the nanoparticles are generally controlled by changing the medium temperature, the concentration of gold salt, the concentration of the reducing agent, adding reactants slower or faster or by variation of stirring conditions.

Thus, using solution phase synthesis methods, particle size, composition and life-time of nanoparticles may be controlled very accurately. However integration of the synthesized nanoparticles into solid materials like polymers or films is a big problem for this synthesis method if one wants to produce nanoparticle-polymer composites. Especially the spatial control on the distribution of nanoparticles throughout the polymer matrix is very hard using this synthesis method.

1.3.2 Synthesis of Nanoparticles in Polymer Matrix

Polymer-nanoparticle composites are important candidates for new age technological devices as mentioned in the previous sections and ongoing research by many different groups is performed for production and characterization of these systems. Polymers can be used as platforms to support gold nanoparticles as substrates. For example, in many biological applications polymers are used as carrying media for nanoparticles to their targets, or in catalysis polymers can be used as supports for nanoparticle catalysts. As much as polymers are good candidates for supporting nanoparticles, nanoparticle-polymer composites can also be functionalized to produce new materials using both properties of gold nanoparticles and polymers. Flexible, low weight, advanced electronic devices can be designed using such materials in the production. But as mentioned before the primary problem that we must overcome to produce such systems is the integration of nanoparticles in to the polymers homogeneously and for some applications with a spatially controlled manner.

Nanoparticles may be synthesized before the integration to polymer or within the polymer to produce composite systems. For example, Vitale et al.[58] synthesized Au nanoparticles and dispersed these dodecanethiol functionalized Au nanoparticles, in poly[platinum-bis(tributhylphosphine) diethynylbiphenyl] afterwards, whereas Horiuchi et al. demonstrated that Pd nanoparticles may be produced in polymethylmethacrylate films, through adsorption of $Pd(acac)_2$ vapor to irradiated polymer films.[59] With the method proposed by Horiuchi et al. patterned polymer films of diblock-co-polymers or polymer blends can be produced using the varying adsorption tendencies of $Pd(acac)_2$ vapor to different polymers. However, this process needs high temperature conditions (180^oC) for the evaporation of Pd metal into the polymer matrix thus is not appropriate for systems working at room temperature.

At room temperature, an efficient approach, used for the production of nanoparticles within the polymer matrix is employment of irradiation. Energetic light is a widely used element to produce electrons within in the synthesis medium for reduction of metal salts and it is both used in the solution phase synthesis as well as, in the solid state synthesis. Gachard et al. has reported a synthesis method, which employs γ-rays to induce reduction in an aqueous solution of 2-propanol and polyvinyl alcohol with gold salt.[60] In another study, we reported that x-rays can also be used to reduce gold ions into gold atoms followed by formation of gold nanoparticles[61]. Not only highly energetic light like γ-rays and x-rays are employed for reduction, but also less energetic UV irradiation can also be used for this

purpose. Korchev et al. proposed that silver nanoparticles can be produced in sulfonated poly(ether−ether)ketone−poly(vinyl alcohol) films by direct irradiation with 350 nm UV light[62]. Alexandrov et al. used UV light to initiate the gold nanoparticle growth in PMMA films and finalized the synthesis by annealing the samples at different temperatures from 20°C up to 80°C[63].

In our work, we used light of various wavelengths to produce electrons within the polymer matrix to reduce gold ions into gold atoms. The produced gold atoms then, nucleate and grow into gold nanoparticles inside the polymer matrix(Figure 1.2). During the irradiation of the polymer, cross-linking of the polymer also takes place and this process may limit the growth of the nanoparticles after a critical particle size. This *in-situ* reduction method

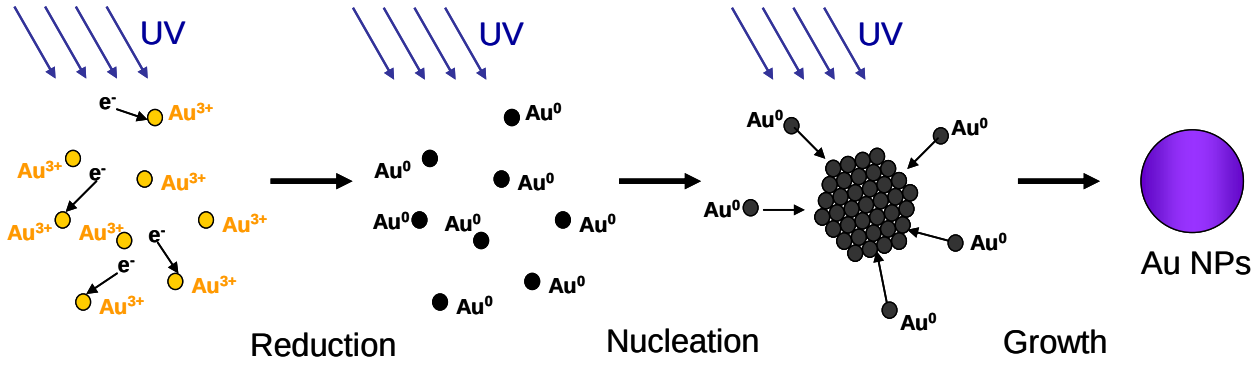

Figure 1.2 Schematic representation UV radiation induced, reduction of Au^{3+} ions to Au^{0} atoms and nucleation and growth of Au nanoparticles in polymer matrix

has many advantages and enables different applications. With this method we can overcome a very important obstacle in the nanoparticles/polymer composite studies, which is the integration of nanoparticles to the polymer films after their synthesis. As much as it benefits from the degradation of the polymer, this method doesn't destroy the polymer completely, and only a very small percentage of the polymer is degraded. Also with this method reduction process and nucleation and growth processes of gold can be entangled and followed step by step with UV-Vis spectrometer since the rates of these processes in polymer are much slower than in solution, in which gold ions are reduced instantly and nanoparticle formation is completed in the following minutes. Photo-patterning and direct writing are possible applications and another advantage of this production method. Using a light impermeable mask, patterns of all sorts and of a large range of sizes can be imprinted on the polymer.

1.4 Advantages of Poly(methyl methacrylate) as a Synthesis Medium

PMMA is a well known, utilized and extensively studied polymer, which is an important dielectric element in electronics. One of the advantages of using PMMA as a substrate is the ease of processibility and preparation of PMMA films. PMMA can be dissolved in acetone relatively easier compared to the dissolution of other polymers in their particular solvents. Acetone was selected as the solvent since it can both dissolve PMMA and $HAuCl_4$ and is not as hazardous as other organic solvents. Film preparation with acetone is also fast and easy since acetone can evaporate at room temperature very quickly compared to many other solvents.

Besides the ease of preparation, PMMA is also appropriate for its stability. PMMA matrix is more rigid compared to many other polymers, hence nanoparticles can be confined to specific sites after their preparation within the matrix. For example, PVA was also used in our studies in earlier stages and for specific purposes and gold nanoparticles can also be prepared in PVA matrices, but our experiences showed us that PVA films containing gold nanoparticles were not as stable as PMMA films. There were also reports concerning this fact in the literature. [64] After their preparation PMMA films conserve their spectroscopic properties for a long time (3 years of stability was observed until now). For PVA films change in the absorption of surface plasmon resonance band was observed after 1 year and distortion on the photo-patterns printed on PVA was also observed. On the other hand, photo-patterns printed at PMMA films were stable.

1.5 Photo-Patterning of Polymer Composites

Patterning of polymer composites is a technologically important process for many different applications. In polymer-nanoparticle composite preparation, besides being able to achieve homogeneous distribution of nanoparticles inside polymer films for successful composites, pattern creation on or in polymer films using nanoparticles is another important issue, especially for optical and electronic applications. There are many different techniques employed to create patterned polymer films. One of the most used techniques for achieving patterns, consisting of regions with and without nanoparticles, is to use the immiscibility of various polymer blends to selectively adsorb nanoparticles in one of the immiscible polymers. In such a study Horiuchi et al. demonstrated the selective reduction $Pd(acac)_2$ vapors by poly(styrene)(PS) matrix in PMMA-PS blends. [59] They subjected PS-PMMA blends to $Pd(acac)_2$ vapor in N_2 atmosphere, the blend adsorbed Pd vapor and only PS matrix selectively reduced Pd ions to Pd nanoparticles because of the PS's high reduction power towards Pd ion. PMMA matrix on the other hand didn't produce any Pd nanoparticles since the reduction power of PMMA is rather low. This study showed with selective production of Pd nanoparticles by different polymers in a blend, one can produce patterned films according to the blend's structure. Nevertheless the control on the pattern morphology is very hard to achieve with such a technique. In another study, Horiuchi et al. found a way to increase PMMA reducing power externally to modify the printed patterns. [65] In which they subjected PMMA films to UV irradiation for an increased reduction power of PMMA towards adsorbed Pd ions and with this method they produced patterns consisting of UV irradiated Pd nanoparticles containing regions and non-irradiated Pd ion containing regions.

Another technique that can be used to achieve such patterns on polymer films is to start with a dispersed metal precursor and selectively reducing required regions for the pattern to produce nanoparticles within. [66] This technique is the one we used to produce patterns consisting of regions with and without gold nanoparticles within the PMMA matrix. With this technique using a photomask impermeable to light, any pattern can be printed on the polymer films consisting of regions with and without nanoparticles. The stability of the printed patterns is an important issue in this technique and the production of stable patterned films was achieved and this issue will be discussed in the upcoming chapters.

1.6 Ultraviolet-Visible Spectroscopy

Ultraviolet-Visible (UV-Vis) spectroscopic technique measures the absorption spectra of samples in the ultraviolet and visible range of the electromagnetic spectrum by recording the amount of light adsorbed by the sample in different wavelengths. The absorption spectra in this range include electronic transitions which are generally the transition of an electron from a ground state to an excited state in the molecular orbitals. In addition, some vibrational transitions may also be observed when the spectrum is of a gas phase molecule. The electronic transitions observed in the UV-Vis spectroscopy generally appear as broad peaks because of the interactions of molecules with each other and the solvent molecules. For example the UV-Vis spectrum of a molecule dissolved in water, generally includes the effects of hydrogen bonding and molecular interactions in addition to its own electronic transitions. To get rid of this broadening is only possible if the spectrum is recorded in gas phase and/or in inert matrices, but this may not be possible for many samples.

UV-Vis spectroscopy is a widely used technique since it's very easy to use and relatively cheap compared to many other techniques and can give valuable information for different types of samples. The most fundamental formulation used in UV-Vis spectroscopy for the quantification of measured absorption values is the Beer-Lambert law:

$$A = \epsilon \cdot b \cdot C$$

In this formulation, A is the measured absorbance at a specific wavelength, ϵ is the molar absorptivity or extinction coefficient at a specific wavelength, b is the path-length through the sample and C is the concentration of the absorbing species. Thus, one can calculate the concentration of the absorbing species in a sample by simply measuring the absorption of the sample and using the molar absorptivity at a specific wavelength. Of course the only information UV-Vis provides about the sample is not its concentration. At least, the applications of UV-Vis spectroscopy in nanotechnology are more. Especially, in the nanoparticle characterization UV-Vis spectroscopy is widely used for the determination of many different properties. For example, for quantum dots, the UV-Vis spectroscopy can be used to calculate the average particle size and more importantly the band-gap of the nanoparticles. The particle size has an important role in the determination of the absorption spectrum in UV-Vis range, since, even though the material which makes up a nanoparticle, defines its intrinsic energy signature, the effect of nanoparticle's size significant at energies near the bandgap. The noble metal nanoparticles like gold or silver are also no exceptions.

They have distinct surface plasmon resonance bands in the visible region, which gives them their characteristic color. Surface plasmon resonance band will be discussed in length in the following section.

1.6.1 Surface Plasmon Resonance Band of Gold Nanoparticles

As mentioned above, nanoparticles of noble metals like silver and gold have very specific absorption peaks in the visible region called surface plasmon resonance (SPR) band, which make those nanoparticles important in optical applications. SPR band originates from the quantum size effect of the nanoparticles, since nanoparticles have neither atomic nor metallic electronic properties, because of their confined energy levels. Their electronic properties strongly depend on the particle size, interparticle distance, nature of the protecting shell and the shape of the nanoparticles. The quantum size effect is seen when the de Broglie wavelength of the valance electrons is of the same order as the size of the particle itself. When this happens, particles behave electronically as zero-dimensional quantum dots. Freely mobile electrons get trapped in such metal boxes and show a characteristic collective oscillation frequency of the plasma resonance, which is called surface plasmon resonance band.

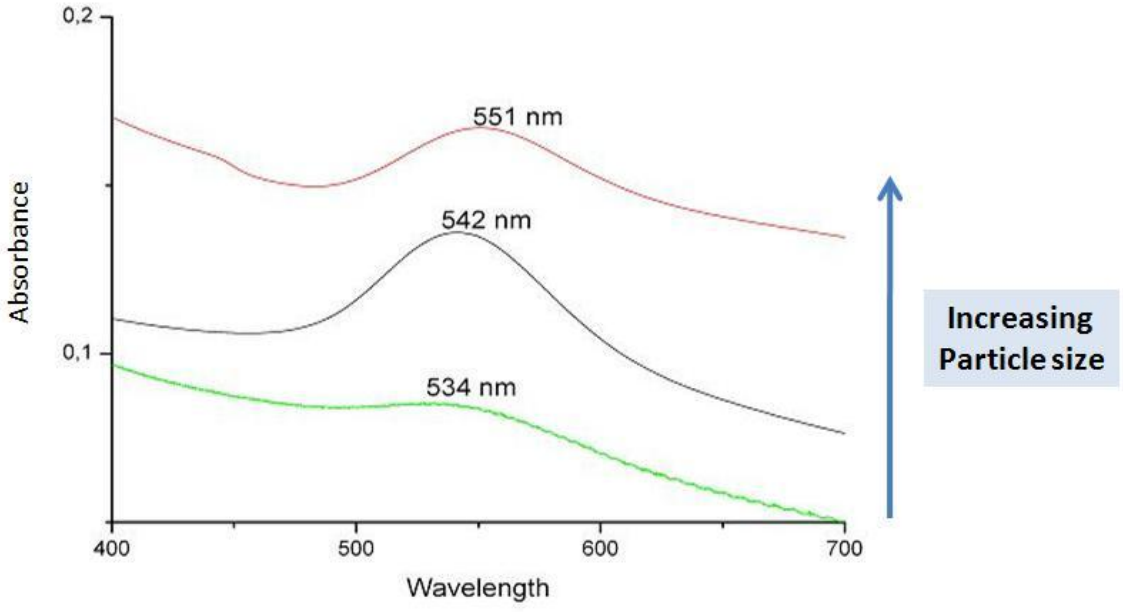

Figure 1.3 A UV-Vis spectrum showing the dependency of SPR band to the particle size.

For gold nanoparticles, the SPR band appears in between 500 nm – 600 nm depending on the particles size, and its position is strongly related to particle size as shown in Figure 1.3. Gold nanoparticles, smaller than 5 nm, are hard to distinguish and yield broad peaks as their SPR bands. But after 5 nm of particle size, SPR band becomes more easily noticeable. For smaller nanoparticles, the SPR band shifts to smaller wavelengths which is called blue shift, and for larger nanoparticles SPR band shifts to higher wavelengths which is called the red shift.

The UV-Vis spectroscopy of gold-nanoparticles and gold ions will be frequently used for characterization purposes throughout the rest of the thesis.

1.7 X-Ray Photoelectron Spectroscopy

X-ray Photoelectron Spectroscopy (XPS) is a non-destructive technique that gives both quantitative and qualitative information about surfaces. In XPS, x-rays of known energy are directed to the sample and photoelectrons are ejected from the sample as a result. Those photoelectrons are collected by a detector and their energies are measured. This process is expressed with the following Einstein's relation;

$$E_B = h\nu - E_K - \Phi$$

E_B is binding energy of the ejected electron, $h\nu$ is the energy of the incident photon, E_K is the measured kinetic energy of the ejected electron and Φ is the work function which relates to the minimum energy required to eject an electron from the solid matrix to the vacuum level. A schematic representation of a XPS measurement is shown in Figure 1.4. Subtracting the measured kinetic energies of the photoelectrons from the energy of x-rays gives us the binding energies of the electrons. Since binding energies are specific to each atom for its specific energy level, and elements besides hydrogen can be detected and their relative amounts can be easily determined with this technique. Chemical specificity is a big advantage of XPS. Besides determination of the types of atoms on the surface, XPS can even give information about the oxidation states of those atoms. The chemical state of the atoms strongly influences the binding energy of the ejected electrons. The binding energy would be large for tightly bound electrons, hence for positively charged species a larger binding energy than the neutral state is measured.

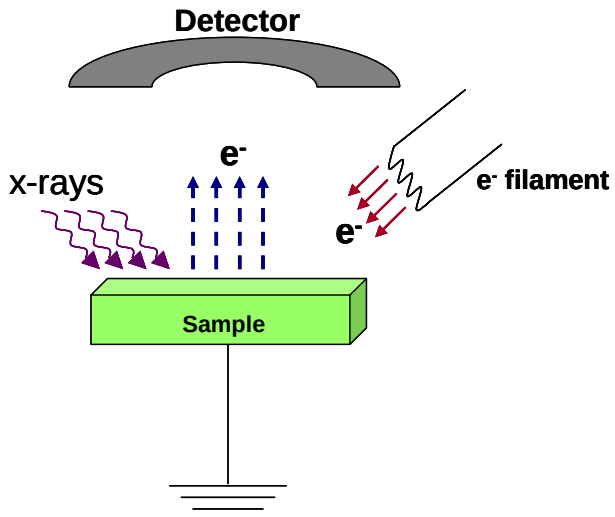

Figure 1.4 Schematic representation of XPS measurement

XPS is also a very surface sensitive technique. X-rays can penetrate through microns of depth into the sample, but ejected electrons without energy lost can only come from the top 10 nm or less (depending on the type of material the sample is made of) of the sample because the photoelectrons cannot travel through larger distances without loss of energy. To have information from depths deeper than 10 nm x-rays with high energies should be used and such measurements can be performed only at synchrotron facilities. Conventional XPS instruments usually work with x-rays at two different energies, Al Kα has 1486.6 eV and Mg Kα has 1253.6 eV x-ray energies.

Using the small mean free path of the electrons, some additional information may be extracted using angle resolved XPS. Angle resolved XPS measurements are made at different take-off angles of electrons and at different angles the electron yield coming from a certain depth changes according to the angle. Figure 1.5 shows an angle resolved XPS measurement schematically. For instance, if we make the measurement at 90^o (Figure 1.5(a)), this corresponds to the normal XPS measurement and a mean free path of **d** can be achieved. But if we decrease the angle to θ, we start to collect more electrons from the surface and the sampling depth equals to **d.sinθ**. As the mean free path decreases, our surface sensitivity increases and we can distinguish topmost layers on our sample.

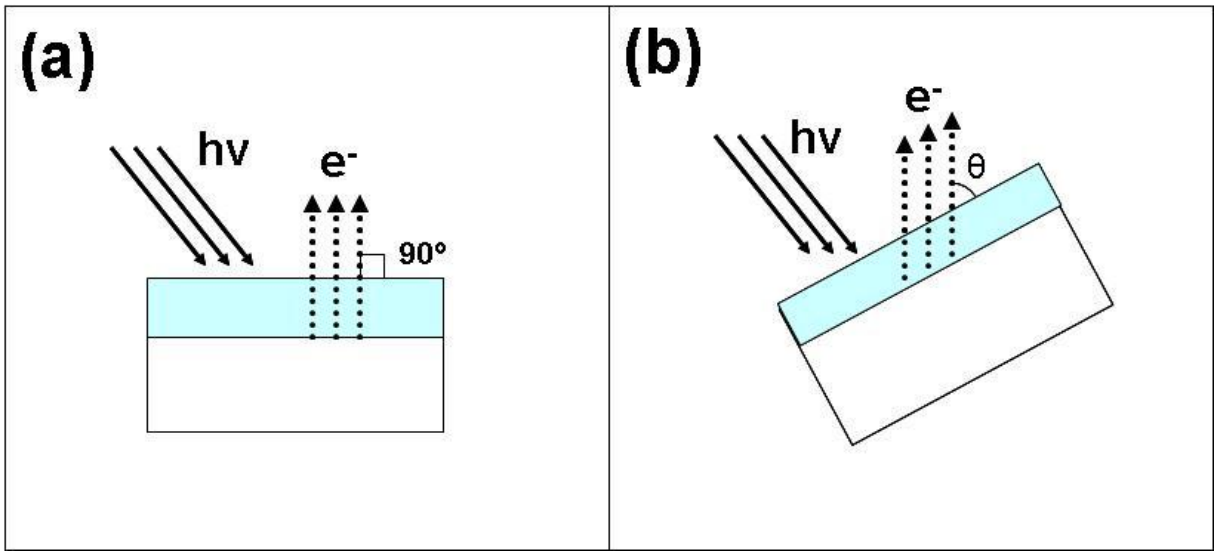

Figure 1.5 Schematic representation of angle resolved XPS measurement.

1.7.1 Using Charging as a tool in XPS

In XPS measurements, a current is generated by the flow of photoelectrons and secondary electrons from the sample to the vacuum. Normally, the generated charge on the surface of the sample is neutralized by the electrons coming from the ground and no effect of this charging is seen through the measurements. But if the sample is non-conducting, the neutralization of the surface charging cannot be achieved and shifts at line positions are observed during the measurements, because of the charging. In the early years of XPS experiments, the charging of non-conducting samples had been considered as a nuisance and many successful techniques were developed to overcome this problem. For example, an electron filament can be added to the system to generate extra low energy electrons for the sample to ease the neutralization as shown in Figure 1.4.

Indeed charging phenomena causes shifts in the binding energies and inconsistent results can be produced. But it is also proved to be true that when used correctly, additional information about the samples can be harvested using charging as a tool. Applying external voltage bias to the sample during a XPS measurement causes shifts in the positions depending to the nature of the sample. For conducting samples positions shift as much as the applied bias, but for non-conducting samples the shift is observed to be nonlinear due to charging. This nonlinear behavior contains additional molecular and structural information. For example, it was shown by Ulgut et al.,[67] that the thickness of SiO_2 films on Si substrates can be measured, with the application of positive and negative biases to the sample. Also in another paper the structure of a composite film was extracted again using charging as a tool for extracting additional information.[68]

One way to use charging in XPS is applying a DC bias to sample at various voltages. For conducting samples if +10 V is applied to the sample an exact 10 eV shift towards higher binding energy is observed for its corresponding lines, this process is shown in Figure 1.6. If we have a non-conducting sample, according to its charging properties a smaller shift is observed in its line positions. This result points out the accumulated negative charge on the surface. When positive 10 V is applied to the non-conducting sample, the line position shifts +10 eV, but the positive potential on the surface attracts more low energy electrons from its surroundings than normal, thus the line positions start to shift to lower binding energies depending on the resistance of the sample. Overall, line shifts are smaller than the applied

voltage. For negative potentials an opposite situation takes place. During measurement electrons are repelled from the surface by the negative potential, thus the already shifted line positions start to shift to even larger apparent binding energies because of the positive charging generated at the surface. Again the overall observation is the shifting of the lines to lower binding energies less than a -10 eV difference in the case of applied -10 V. Such measurements give us information about the resistance of the sample since in this case the resistance of the sample prevents electrons to neutralize the charges created on the surface.

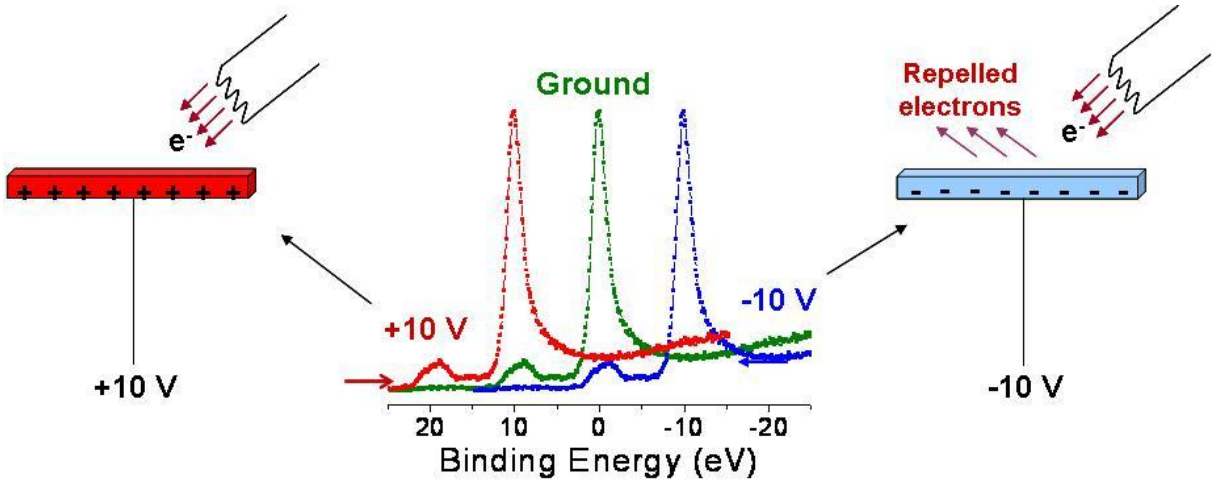

Figure 1.6 Shifting of the XPS peaks due to +/- 10 V DC bias in a conducting sample.

Another method to generate charging on the sample surface and using it as an additional information source is applying square wave pulses to the sample. During DC potential measurements, we can get information about to what extent the sample can charge in the given potential interval but we can't predict how fast the sample responses to the potential changes. Knowing the response time gives us useful information about another electrical property of the sample which is the capacitance. Response times can be observed using potentials altering with different time intervals, and this can be easily achieved using square wave (SQW) pulses. SQW pulses are alternating potentials at a given frequency and with a given potential value. Generally +/- 10 V pulse is applied to the sample with different frequencies and in between 100 Hz to 10^{-3} Hz and data is collected. Since we apply two different potentials during data acquisition, we observe two peaks of a given line one for -10 V and one for +10 V. If the sample is not charging the binding energy difference between

these two peaks can be observed as 20 eV. But in the case of charging the binding energy difference between these two peaks starts to decrease with the increase in charging.

Basically the working principle behind the SQW potential and the DC potential measurements is the same. But for SQW potential measurements, additionally we can have information about capacitance property of the sample as mentioned before. The reason for that is in the case of SQW we can switch between negative and positive potential with a given frequency, thus we can see how quick the sample responses to the change of the potential in the frequency range we apply. For example, at high frequencies like 100 Hz, the potential switches from -10 V to +10 V so quickly that our polymeric samples cannot follow them , as a result we see no charging changes and observe an exact 20 eV binding energy difference, even though the sample itself maybe is in a charged state. Samples cannot find enough time to build up charge on them at frequencies so high. But for example, at frequencies like 10^{-2} Hz the potential switches from negative to positive at every 100 seconds, so the sample has enough time to build up charge and we can see binding energy differences smaller than 20 eV at such frequencies for non-conducting polymeric samples. The charge build up is of course different for every sample since this property depends on the dielectric properties of the sample, for example using this difference we can obtain capacitance for these samples by taking measurements at different frequencies and following the trend of each sample. At very low frequencies like 10^{-4} or 10^{-5} Hz the binding energy difference reaches to a point where it doesn't decay anymore and this point gives us the same binding energy difference as the DC potential measurements give. So SQW measurements give us information both on resistance and on capacitance of the sample.

1.8 Contact Electrification of Insulating Materials

The XPS charge resolved experiments performed on insulating materials like polymers, provides us a chance to investigate the response of insulating materials to charge accumulation on the surface. Finding out how the materials behave when surface is charged and how and where the charges are stored on the surface may give us important clues about the mechanism of electrification of insulating materials. Contact electrification of insulator materials is well known to men for a very long time, and is successfully used in many industrial applications. However, the detailed molecular nature of this phenomenon is still unknown to us. There are several studies proposing different mechanisms for the causes of electrification. [69-73] Among those, two major ideas emerges as the source of electrification. Some claim that electron transfer is the reason for the electrification, while the others think ion transfer takes place during rubbing or contact of two insulators and this is the source of electrification. There are convincing evidences for both sides and the case is still controversial.

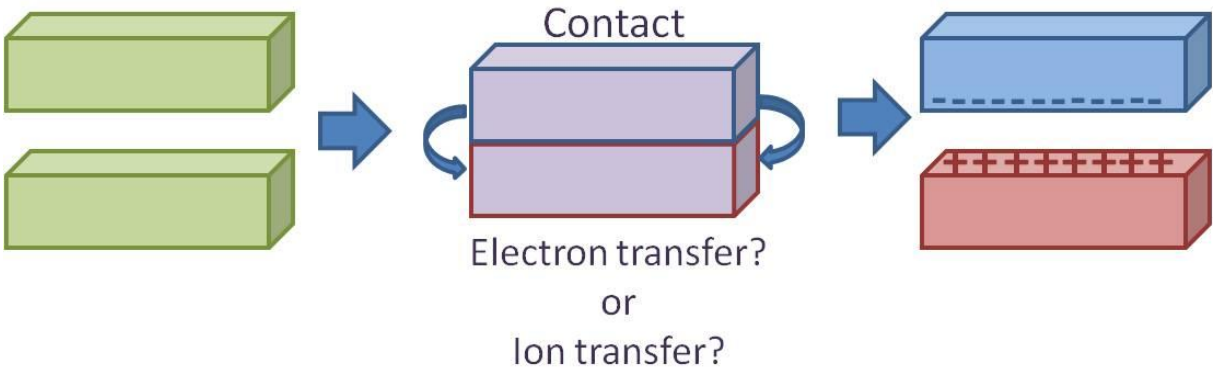

Figure 1.7 Schematic representation of contact electrification.

The main reason for this continuing debate is the difficulty of characterizing the nature of the charge on an insulating material. The present methods generally give an idea if there is any net charge on the surface but they cannot tell whether this charge originates from accumulation of electrons or ions. To overcome this problem Liu et al. proposed chemical characterization of the charge by subjecting it to redox reactions. [74, 75] They showed that the charge on a PTFE surface can reduce ions like Ag^{+}, Cu^{2+}, Pd^{2+} after contacting with PMMA, offering a solid evidence for the presence of electrons. Likewise the rubbed PMMA can change the pH of a solution by proton transfer, showing the presence of exchanged protons on

the surface. Supporting Liu et al. suggestion, Jacobs et al. show that there is no detectable material transfer during contact electrification, regardless of the ion transfer claims, and they propose, proton transfer occurs between carboxylic acid groups of PDMS and carbonyl groups of PMMA during contact. [69, 76] On the other hand, McCarthy et al. claim that electron transfer is not energetically plausible, since it involves many demanding processes like removing an electron from a material, transferring it through separation of charge across an interface and adding an electron to another material and these processes can occur at room temperature for only materials with zero bandgap. [73, 77] They proposed that ion transfer is the source of contact electrification for insulating electrets. Likewise Diaz et al. nominated ions as the source of charge during contact electrification and constructed a model explaining the role of ions during charging process on polymers. [70, 78, 79]

Understanding the reason of contact electrification process is important for the advancement of many applications and preventing problems arising from the contact electrification. Understanding of electrification process is also important for the development of electroactive polymers and elastomers. In a recent article by Carpi et al. the importance of dielectric elastomer actuators for applications like touch screens for consumer electronics and artificial muscles. [80] As shown by Brochu et al. artificial muscles can exceed the performance of natural muscles using dielectric elastomers. [81] One other application possibility, mentioned by Carpi et al. is using dielectric elastomer transduction in reverse way and producing electrical energy from the mechanical energy, which would be groundbreaking if applicable. A better understanding of the electrification process will definitely help realization of such applications and should be pursued. Therefore, within the scope of this thesis, XPS is used for the purpose, hoping that with its chemical specificity, and at the same time being sensitive to charge accumulation/dissipation may offer new insight(s) at the molecular level.

1.9 Objective of the Study

The scope of this study can be summarized under two main objectives; (i) synthesis of gold nanoparticles within polymer matrices, (ii) characterization of polymer-gold nanoparticle composites.

Photo-irradiation assisted synthesis of gold nanoparticles within polymer films was conducted for the first part of this study. Prominent synthesis methods of gold nanoparticles were discussed in length in the previous sections while addressing the advantages and disadvantages of various synthesis methods. As mentioned, synthesis of gold nanoparticles within polymer matrices is especially advantageous to produce polymer-gold nanoparticle composites. Also the slower, detectable rate of the reaction within the polymer matrices and the opportunity to conduct photo-patterning applications are also additional advantages of this synthesis method. Photo-patterning of PMMA films with gold nanoparticles was successfully achieved and the presence of ion depleted regions was observed during these processes. Ion depleted regions are formed by the diffusion of gold ions from and near the borders of the masked regions to the irradiated regions. Observation of the ion depleted regions enabled us to calculate a rough diffusion constant for the diffusion of gold ions inside these polymer matrices, which was not elaborated in the literature. Additionally, the presence of these ion depleted regions has important implications on the stability of the photo-patterns. It was shown that ion depleted regions can be as wide as 10 μm at the border regions, providing an upper limit to the dimensions of stable photo-patterned features.

Characterization of gold nanoparticle-polymer composites was performed using various different characterization techniques, but the most important part of this study consists of charge resolved XPS measurements performed on these composites. As explained in the charge resolved XPS part of the introduction, this technique uses the surface charging on insulating materials, which was considered as a nuisance before, for obtaining more information about the electrical characteristics of the samples. Resistance and capacitance values of PMMA films with and without gold nanoparticles were measured using this technique. The effects of gold nanoparticle on the dielectric properties of PMMA films were evaluated.

As well as observing the cumulative effect of charging on the surfaces of polymeric films, detailed studies, regarding the effects of the accumulated charges at the molecular level,

were also performed, using this novel charge resolved XPS technique. Determining the nature of charge accumulation on the surface is especially important for understanding the mechanism of electrification process at the molecular level on electret materials, which has been in the center of a recent debate. Detailed examination of these processes is very important for both industrial applications and development of new materials. Experiments with PMMA films were conducted using the charge resolved XPS technique, to understand the storage of negative and positive charges on the surface and the effects of these stored charges to the backbone carbons, carbonyl and methoxy groups of the polymer. It was shown that carbon and oxygen atoms of carbonyl and methoxy groups behave differently with charge accumulation. The studies showed that the polymer surface is very susceptible for accumulation of negative charges during XPS measurements. It was also observed that some native negative charges existed even at the onset of our measurements on the surface prior to any induced charges. These studies give clues that electrons play important roles as charge carriers in certain electrification processes on the polymer surfaces. The effect of gold nanoparticles within the polymer films on the surface charge accumulation was also demonstrated during these studies.

2 Experimental

2.1 Materials

Poly(methyl methacrylate) (PMMA), poly(vinyl alcohol) (PVA), Hydrogen tetrachloroaurate ($HAuCl_4$), Silver nitrate ($AgNO_3$), benzophenone and rhodamine 6G were purchased from Aldrich and used without further purification. Absolute acetone with a purity >99.5% was used for the preparation of all samples. Deionized water was used for the cleaning and sample preparation purposes.

2.2 Preparation of Samples

PMMA films containing gold ions were prepared by firstly dissolving both $HAuCl_4$ and PMMA in an appropriate common solvent, which was acetone for most of the experiments. Then the solutions of both reagents were mixed in various ratios to prepare the mixture to cast the films. $HAuCl_4$ solution concentration can vary from 10^{-2} M to 10^{-4} M depending on the experiment type and PMMA solution concentration can vary in between 0.5% and 10% (w/w) depending on the required film thickness.

Thickness of the prepared films depends on a couple of factors. Firstly, the concentration of the polymer solution is important. Thick films can be produced using higher concentrations of PMMA solution. The second factor affecting the film thickness is the preparation method. Uniform films of PMMA can be prepared either with spin-coating, or room temperature casting in which the polymer solution is casted on a flat surface and the solvent is evaporated at room temperature slowly. In our studies thick films were produced from ~5-10% (w/w) solutions by room temperature casting on flat surfaces (glass or polypropylene substrates), the fully dried films then can be extracted as free standing polymer films. During evaporation process an acetone rich atmosphere around the sample may be necessary for obtaining clear films. On the other hand, thin films was prepared in the range of tens to hundreds of nanometers thicknesses by the spin coating technique, which is schematically described in Figure 2.1. During spin coating process, excess amount of the solution for the targeted film is dropped on the substrate surface while the substrate spins at full speed and homogeneous films can be produced with the aid of centrifugal force. For spin coated PMMA films, ~0.5-2% (w/w, depending on the desired thickness) PMMA solution is

dropped on the Si substrates during spinning and homogeneous films are obtained. Spin velocities between 1000 rpm to 3500 rpm can be used depending on the desired film thickness and presented solution concentration.

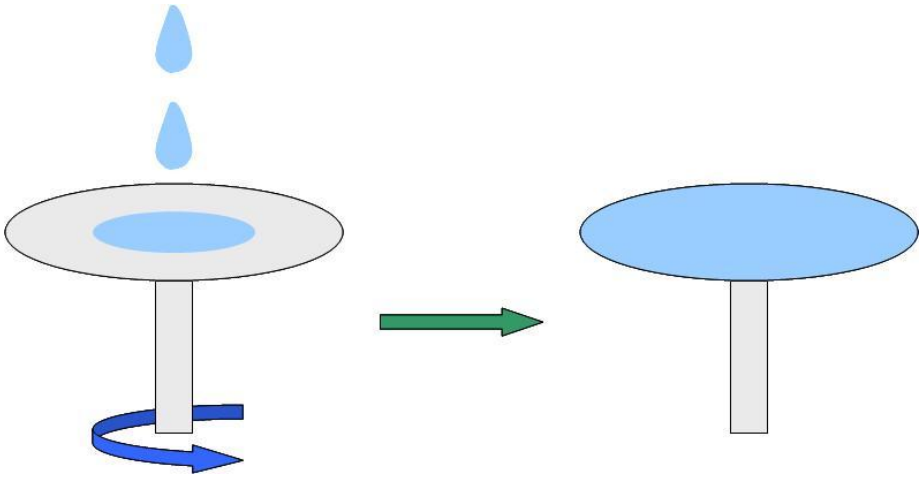

Figure 2.1 Schematic representation of spin coating procedure.

The polymer films were prepared on Si substrates for XPS and SEM measurements to have thinner samples to avoid excess charging. Si substrates cleaned with hydrofluoric acid (HF) prior to film casting. HF is used to etch the native SiO_2 layers on Si substrates, which may act as a non-conductive barrier between Si substrate and the polymer film. Good contact to the Si substrate is especially important for XPS and SEM measurements for again avoiding the excess charging of the sample.

Irradiation of films was done using different light sources depending on different experiments. The light source used in most cases was a low pressure 10 W Hg lamp of 254 nm wavelength. This wavelength can supply enough energy for the degradation of PMMA matrix and preparation of gold nanoparticles. For experiments performed with different irradiation wavelengths a brighter light source, 500 W mercury lamp with Oriel Cornerstone 130 1/8m monochromator was used. Irradiation times can vary depending on the brightness of the light source and the gold concentration of the film. For low pressure Hg lamp samples were irradiated for 24 hours to ensure not to leave any unreduced species, while we later observed that sufficient reduction can also be achieved in about 6 hours for most samples.

Photo-patterning studies were performed using a quartz photomask with masking features made of deposited metal regions. The films were pressed to the mask firmly to avoid

any loose contact or shadowing from the mask. Glass slides were used to clamp the films to the mask surface from behind. During irradiation of the photo-patterns, a low pressure 10 W Hg lamp of 254 nm wavelength was used and generally films were irradiated for 24 hours for the complete annihilation of gold ions at the irradiated regions. For the second irradiation of the films, if necessary, the mask was removed and the film was irradiated for a second time without the mask on. For photo-patterning applications thick and thin films were prepared depending on the application. Thick films were necessary for optical microscope, fluorescence microscope and Raman spectroscopy characterizations, while thin films on Si substrates were used for SEM and XPS characterizations.

2.3 Instrumentation

The UV-Visible spectra were recorded using two different spectrometers; a Varian Cary 5 and an Oceans Optics HR4000 spectrometer. Varian Cary 5 is a double beam-in-time instrument with superior optical properties. The measurements with this instrument were performed against a reference sample. During measurements solid sample holders were used for the polymer films. For PMMA films on polypropylene, a sample holder of the same size as the sample holder of the sample was used as reference, since polypropylene does not have any peaks at the probed region. However, for samples on glass, clean glass substrates about the same thickness were used as reference. The measurements were performed between 200 nm-800 nm with a scanning rate of 200 nm/min. The Ocean Optics HR4000 spectrometer was used for experiments performed with Oriel Cornerstone light source for swift measurements. Ocean Optics HR4000 spectrometer is a compact size spectrometer, designed for fast measurements and this spectrometer can be coupled with fiber optic cables for the measurement. This property enabled a lot of versatility during the fast measurements of polymer spectra. With both spectrometers, UV-Vis spectra of polymer films were recorded, so sample holders for solid films were used.

A Bruker Tensor 27 FT-IR spectrometer was used for infrared measurements. Samples were free standing polymer films without any supporting substrate like polypropylene or glass. Only peaks coming from the polymer films were observed in the measured spectra. Thick films were prepared to have good signal strength from the samples.

XPS measurements were performed with two different XPS instruments. The first one was a Kratos ES300 spectrometer with a Mg Kα (not monochromatized) source at 1253.6 eV.

This instrument analyzes the signal coming from nearly all the sample surface instead of focusing to one spot, so the spectra taken with this instrument are always an average of the signal from the sample. Charging experiments on PMMA films with and without gold nanoparticles were performed using this instrument while applying DC bias or square wave pulses of +/-10 V to the sample holder. An electron filament was used in some measurements for the neutralization of the sample surface against excess charging.

The second instrument used for the XPS measurements was a Thermo Sceintific K-Alpha XPS spectrometer with a monochromatized source with 1486.68 eV photon energy. This spectrometer can probe the sample with a small x-ray spot size between 30 μm-400 μm. And it's equipped with a flood gun as an external electron and ion source for the neutralization of the sample surface when necessary. Using this instrument charge resolved XPS measurements can be performed with DC bias or SQW pulses and as well as other measurements like line scan or area scan on the sample. One advantage of this instrument was collecting snapshot spectra of the sample very fast and being able to monitor the movement in peak positions in very small time intervals. Snapshot spectra mode was used especially with charge resolved XPS technique using SQW pulses to monitor the changes in the sample during the charging events. A schematic representation of charge resolved XPS measurements with SQW pulses monitored with snapshot mode and its interpretation is given in Figure 2.2. As can be seen in the figure, the spectra of the relevant lines were collected step by step with this technique very swiftly (0.01 – 1.0 sec for each spectrum depending on the experiment conditions) and as a result the collection of these spectra clearly shows the movement of the line during biasing. Then those spectra can be fitted and the line positions can be calculated and plotted for the quantification of the charging event.

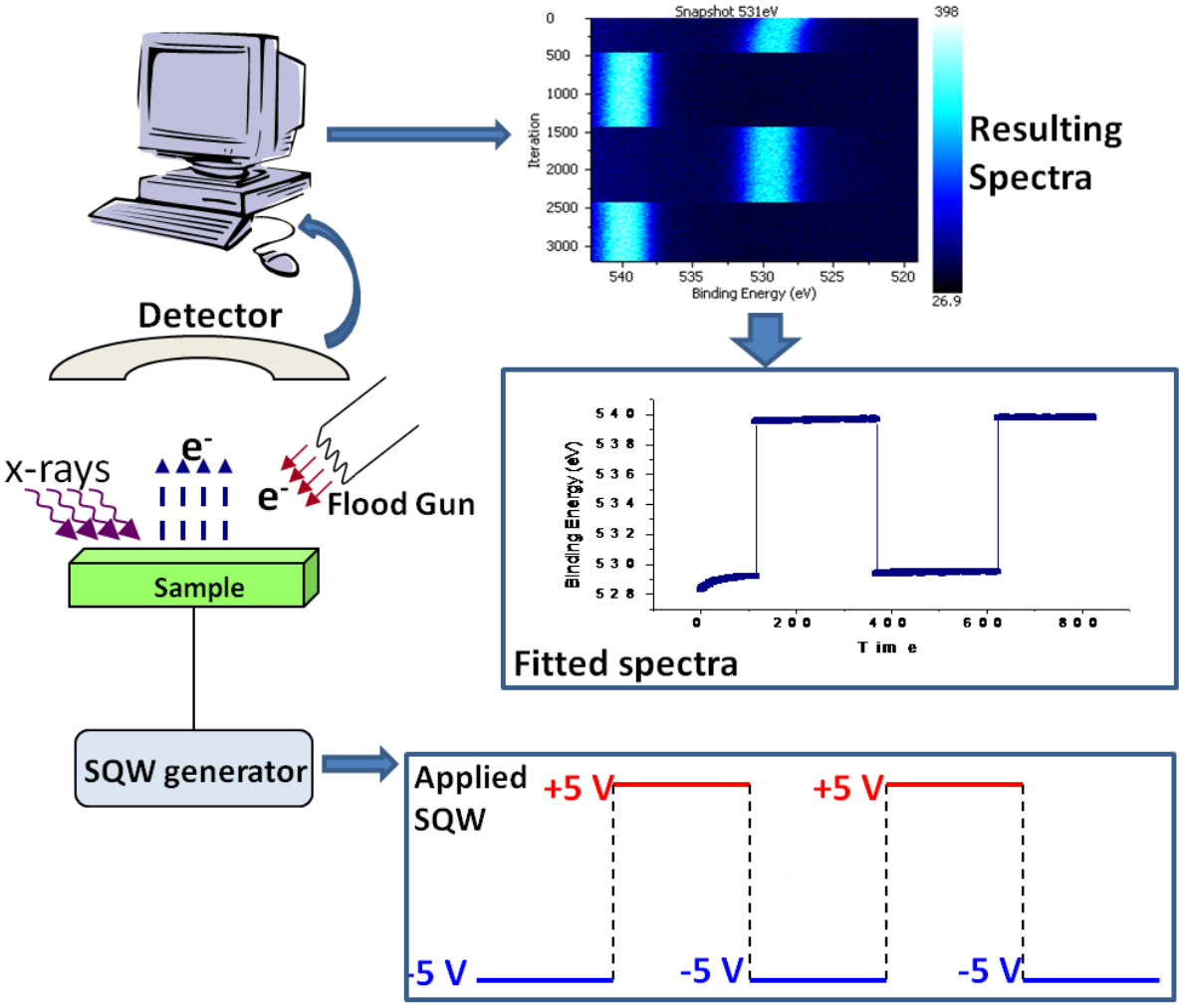

Figure 2.2 Illustration of experimental setup for the SQW voltage applied measurement on PMMA films.

The XPS spectra data obtained were fitted using the XPSPEAK 4.0 fitting program for individual spectra and automatically fitted by Avantage program for the snapshot experiments. Then those data were plotted using Origin 7.5. The data were normally recorded at a 90° electron takeoff angle.

Scanning electron microscope images were taken by a Zeiss EVO 40 electron microscope. This instrument can provide electron beam brightness up to 30 kV, but our measurements were generally performed at beam energies between 5 kV to 10 kV since polymer films can easily burn at high energy electron beams. Both secondary electron detector and backscattered electron detector were available and measurements with both of them were performed. SEM was especially used for the imaging of photo-patterns in this study. Regions containing gold nanoparticles of the photo-patterns appeared brighter than the other regions because of the high secondary electron yield of gold nanoparticles. This instrument was also equipped with an energy dispersive x-ray detector, which can analyze the

x-rays emitted from the sample along with the secondary electrons for chemical characterization of the sample. We also tried to use this technique for the characterization of our patterned films, but we couldn't obtain consistent results because of the low energy of the beam. For good results in energy dispersive x-ray technique high beam voltages should be employed, which in our case results the burning of the polymer films.

Zeiss Axio Imager A1 was used for our fluorescence microscope imaging. Our samples contained Rhodamine 6G dye molecules, which emits fluorescence strongly between 500 nm and 700 nm when excited with 480 nm light. This microscope is a polarized light microscope which was originally designed for the fluorescence studies in biological systems. By our trials we also found out that FITC filter, which excites at around 490 nm and collects around 520 nm, was the most efficient filter for our samples.

3 Results and Discussion

3.1 Light Induced Production of Gold Nanoparticles

As mentioned in Section 1.3.2, our route to produce gold nanoparticles is light directed synthesis within the polymer matrix. We employ UV radiation for the reduction of gold ions into gold atoms (reduction) in polymer matrix, and the reduced gold atoms form gold nanoparticles (nucleation and growth) by further irradiation (Figure 1.2). The reduction and nucleation and growth processes may be followed separately by UV-Vis spectrometer as shown in Figure 3.1. In the UV-Vis spectrum, the peak at 315 nm belongs to Au^{3+} and results from ligand to metal charge transfer, and the peak between 500-600 nm is surface plasmon resonance band of Au nanoparticles and its peak position depends on the size of the nanoparticles. In Figure 3.1, the arrow pointing down at 315 nm represents the decrease in the Au^{3+} peak during the reduction of gold ions and the arrow pointing up at 530 nm represents the development of the surface plasmon resonance band during the nucleation and growth of gold nanoparticles.

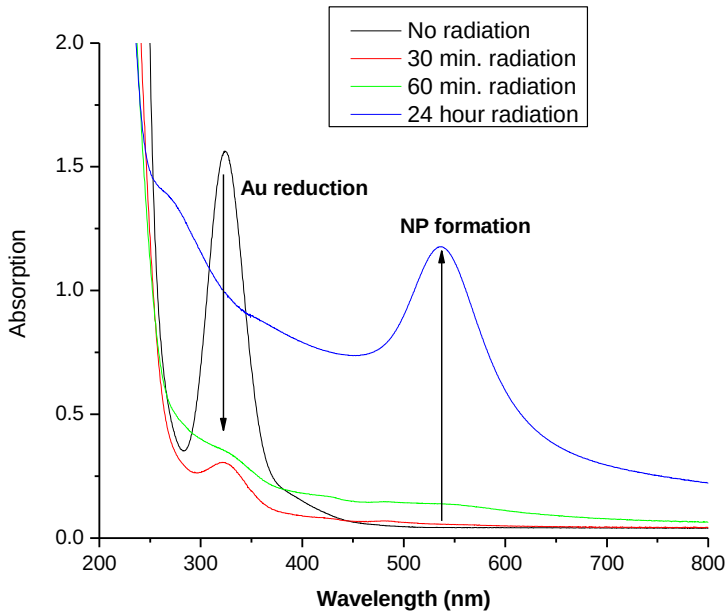

Figure 3.1 UV-Vis Spectrum of PMMA/Au film; reduction of Au3+ and nucleation and growth of Au NPs

An advantage of synthesizing gold nanoparticles in polymer matrices is the slowed, detectable reaction rates as mentioned earlier. In the solution synthesis methods the reduction of gold takes place in seconds or less and the nucleation and growth of gold nanoparticles is completed in minutes. Such a fast reaction is impossible to control and detect. On the other hand, synthesis of gold nanoparticles is several orders of magnitude slower in polymer matrix since the degradation of polymer and the diffusion of gold atoms are slow processes and can be easily monitored. We can follow the reduction and nucleation and growth processes step by step with spectrum acquisition in appropriate time intervals, and we can deduce the effects of different factors on these processes, comparing their relative rates for each case. In experiments concerning the effects of temperature during irradiation and Pt ions addition, we observed that, these factors increase the growth/nucleation of gold nanoparticles, whereas they do not have any significant effect on reduction rate of gold ions. As seen in Figure 3.2[*,†] the nucleation and growth (N/G) rate was smallest for non-heated sample with only gold and the addition of Pt ions increases the N/G rate, but without a doubt the most effective way of increasing the N/G rate is heating according to these results, heating causes a 6-fold increase in N/G rate and the largest N/G rate is observed for the heated case with Pt ions present in the film. Nevertheless these factors can increase N/G rate while they don't have any effect on the reduction rate of gold ions.

The reduction rate of gold ions in polymer matrix is mainly limited to the degradation rate of the polymer in light assisted synthesis. A slowly degrading polymer means less electron source for gold ions to be reduced. Thus finding a way to increase the degradation of polymer can also increase the reduction rate of gold ions. One perfect candidate for such a purpose can be photosensitizer molecules. Photosensitizer molecules generally sensitize photoreactions by an energy transfer mechanism, which consists of the one-step transfer of electronic excitation from an excited donor molecule to an acceptor molecule.

---

[*] The first experiments regarding this subject was performed during my senior year in undergraduate and the results will be only referenced here briefly in Figure 3.2 to explain the second part of this work better, which is related to my Ph.D. studies.

[†] The values in the y-axis of this graph are calculated by dividing the area of surface plasmon resonance band to the area of gold ion peak at 330 nm. This formulation enables us to eliminate the effect of concentration variation of gold in each PMMA film and gives the surface plasmon band peak growth regardless of the gold concentration in the beginning.

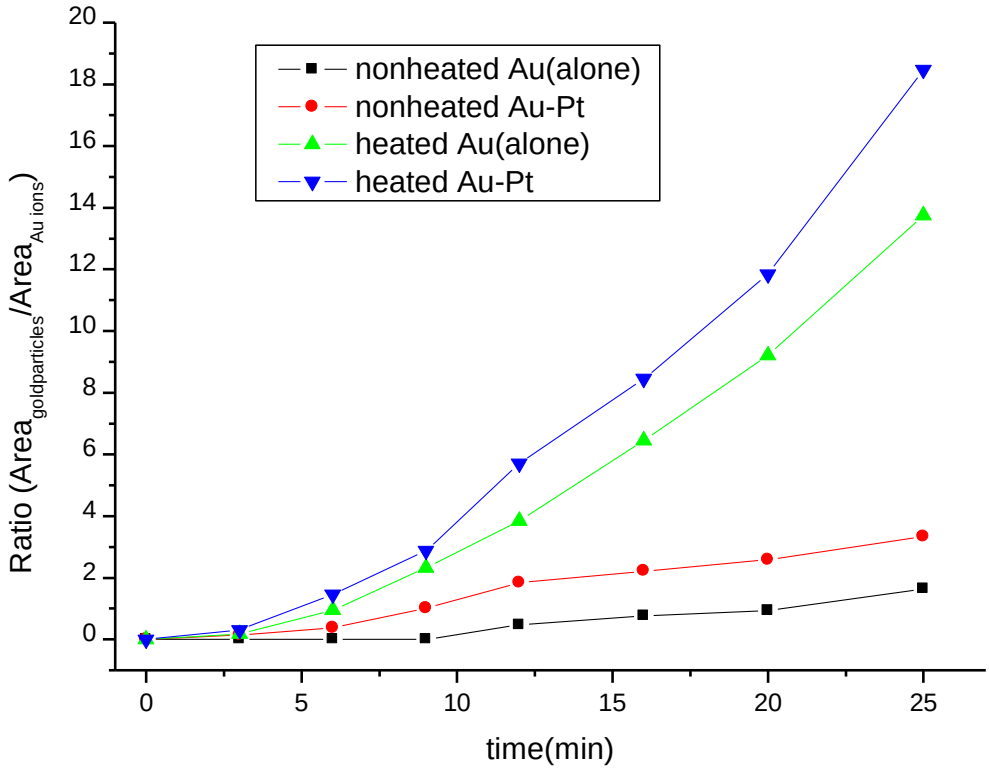

Figure 3.2 Effect of heating and addition of Pt ions on NP formation vs. Au3+ reduction. It 's seen that both heating and Pt ions addition increases NP formation without affecting reduction rate.

Thus reduction of gold ions could be accelerated with increased rate of degradation of polymer with the energy transfer from the photosensitizer molecule to the polymer. For such an energy transfer to take place the photosensitizer molecule should adsorb the light in the irradiation wavelength and use its energy to transfer an electron or accept a proton. Benzophenone is a good candidate for such an application, since it absorbs radiation at 260 nm and it was already demonstrated that benzophenone could be used to increase UV assisted polymer degradation [82]. The structure of benzophenone is given at Figure 3.3. With absorption of a photon, a $n \rightarrow \pi^*$ transition is promoted and benzophenone translates from singlet state to triplet state. Then the excited benzophenone molecule abstracts a proton from the polymer to relax back to its ground state. The produced polymer radical is then expected to reduce Au ions to Au atoms.

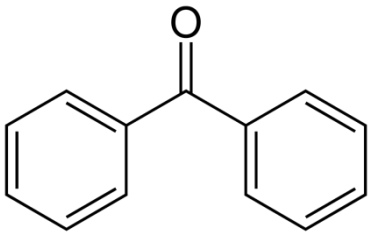

Figure 3.3 Structure of benzophenone

To test this hypothesis, PMMA films containing gold salt with and without benzophenone, were prepared and the UV-Vis spectra of these films were recorded for appropriate irradiation time intervals as shown in Figure 3.4. Contrary to expectations, these results show that benzophenone doesn't increase the rate of reduction of gold but decreases it. Although the amount of gold nanoparticles produced is close for both cases, the gold ions are completely reduced in 45 minutes for gold only case, while it takes about 2 hours for film containing the benzophenone.

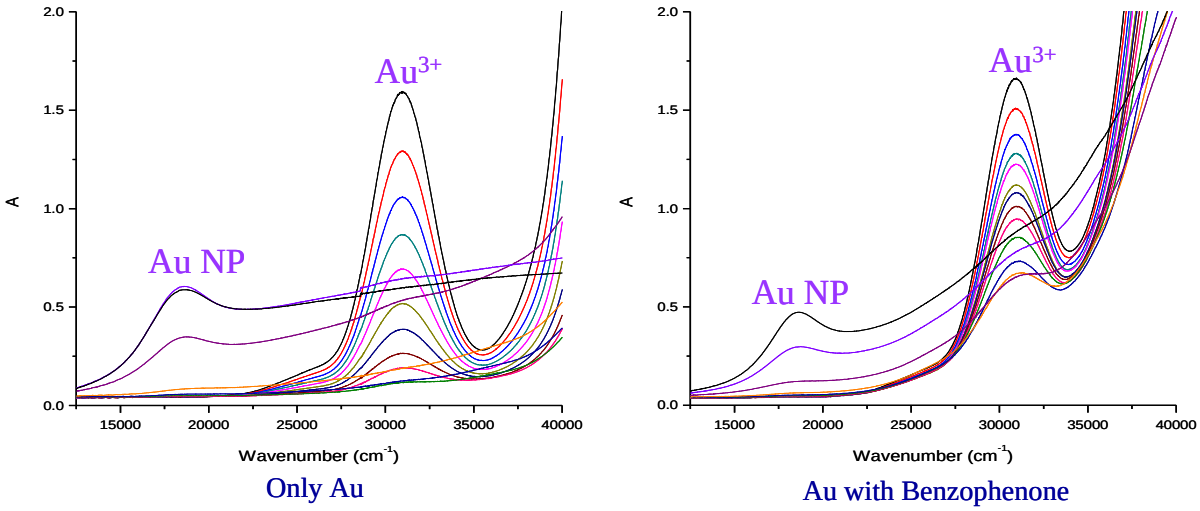

Figure 3.4 UV-Vis spectra of PMMA/Au films with and without benzophenone taken in appropriate time intervals

On the other hand, benzophenone increases the reduction rate of silver ions in PVA matrix as shown in Figure 3.5. For this experiment $AgNO_3$ was used instead of $HAuCl_4$ since there was no common solvent for PVA, benzophenone and $HAuCl_4$ but the principle is

basically the same for both metal salts. Silver ions can also be reduced by the radicals produced by the degradation of the polymer and they form silver nanoparticles within the polymer matrix. Silver nanoparticles have their plasmon resonance band between 300-400 nm and this distinct absorbance band can both be used to determine the silver nanoparticle presence and to calculate the particle size of the nanoparticles. As can be seen in Figure 3.5, with benzophenone presence in the film production of silver nanoparticles is increased around 4-fold, this increase can be related to the increased rate of reduction of silver ions since benzophenone shouldn't have any effect on nucleation and growth processes. This result shows the difference between the degradation of PMMA and PVA and its effects on reduction and nucleation and growth processes.

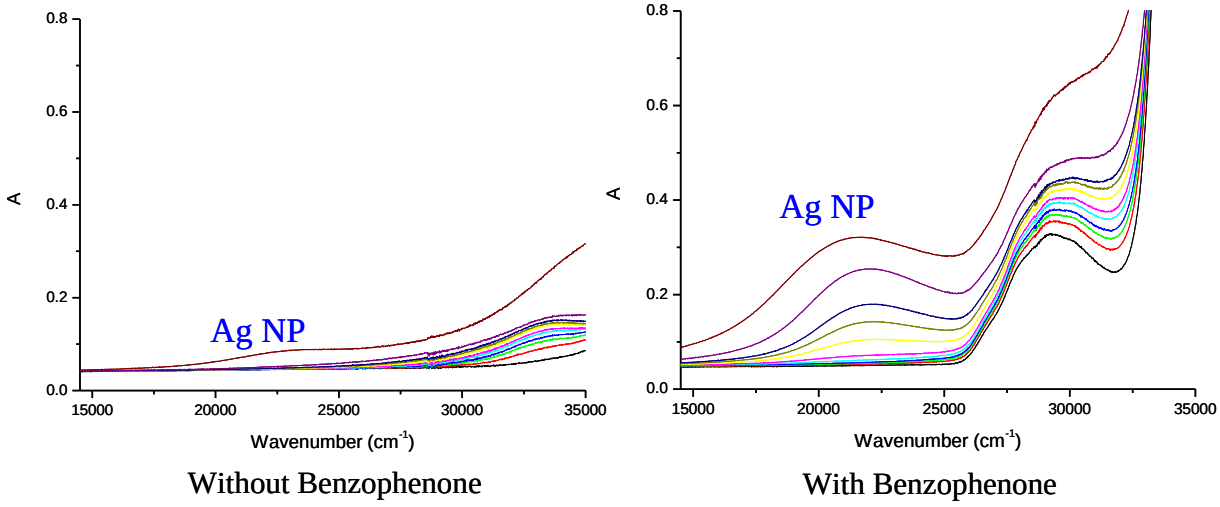

Figure 3.5 UV-Vis spectra of PVA/Ag films with and without benzophenone taken in appropriate time intervals

The proposed mechanism of reduction of gold ions in PVA matrix by Korchev et al. via degradation of polymer is as follows; [62, 83]

$$[R'RCOH]_n \rightarrow [R'RC^*OH]_n \quad \text{(by UV)}$$

$$[R'RC^*OH]_n + Au^{3+} \rightarrow [R'RC{=}O]_n + Au^0 + 3\,H^+$$

While the mechanism suggested for degradation of PMMA is as follows [65];

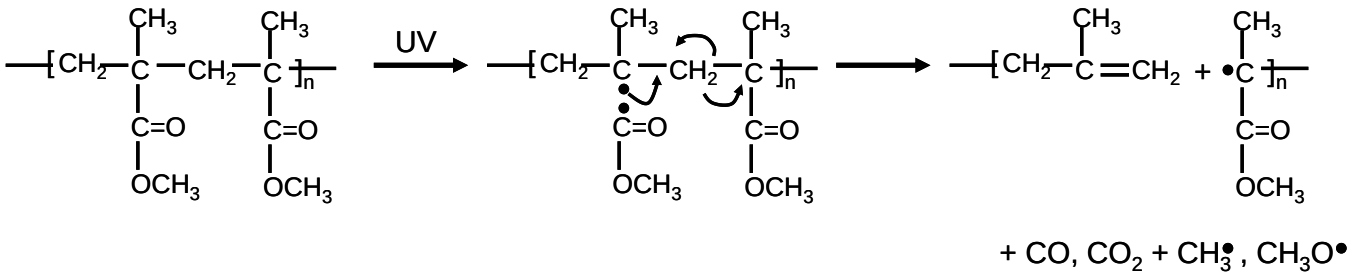

The changes in the chemical structure of the polymer during irradiation process can be monitored using FT-IR spectroscopy. In the degradation of PVA, a carbonyl group is produced from the alcohol group, and the detection of carbonyl group is easy in IR, because of its high cross-section. To see the effect of irradiation on PVA in the presence of gold ions, pure PVA films and PVA films containing Au^{3+} ions were prepared and subjected to 254 nm UV radiation. IR spectra were taken in appropriate time intervals during irradiation and the formation of carbonyl peak at about 1710 cm^{-1} wavenumber was followed.

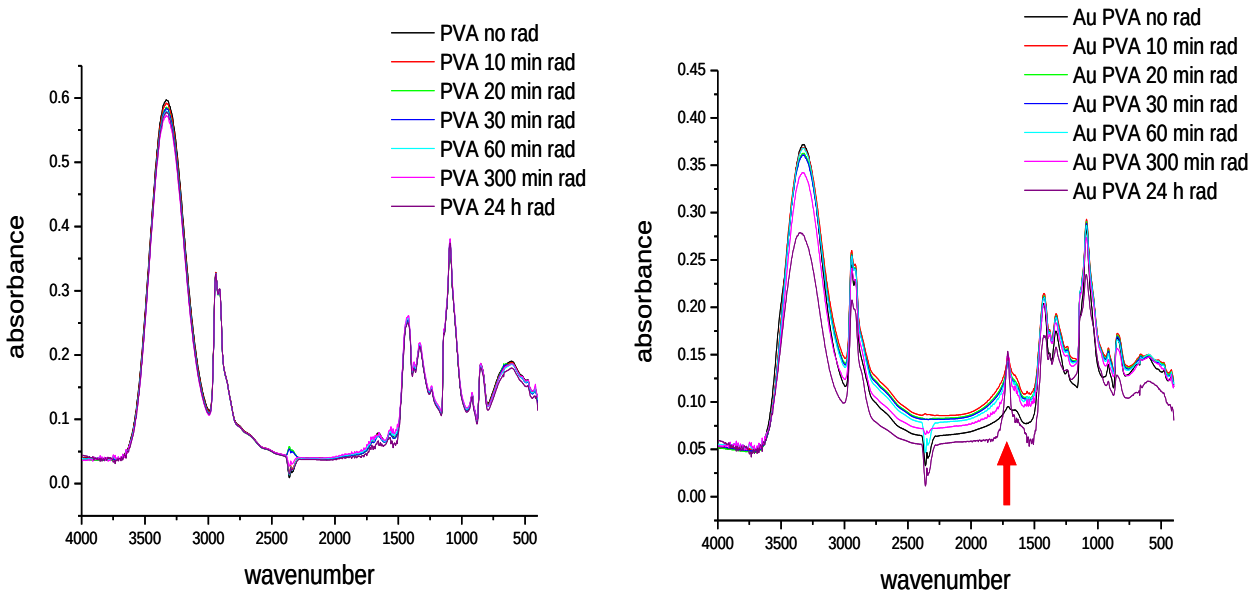

Figure 3.6 IR spectra of Au-PVA and PVA films taken after appropriate irradiation times

As Figure 3.6 shows, while no change was observed at pure PVA film during irradiation, formation of a carbonyl peak at 1708 cm^{-1} and decrease in the area of OH peak at 3340 cm^{-1} was observed for PVA film containing Au^{3+} ions. This result clearly shows that carbonyl groups are produced only in the presence of gold ions and this is due to the reduction of gold ions by the polymer during irradiation. On the other hand, FT-IR studies cannot show the

degradation of PMMA films clearly, since PMMA already has a carbonyl group and the changes induced by the degradation are too small to detect.

The difference between the degradation mechanisms of PMMA and PVA, can be observed more clearly observing their susceptibility towards degradation as a function of irradiation energy. For this purpose, PVA and PMMA films containing gold ions were prepared and subjected to light having wavelength starting from 600 nm low energy region to 300 nm high energy region and the reduction of the gold was monitored for light at different wavelengths. The spectra of PMMA and PVA films containing Au^{3+} ions, irradiated for 30 minutes at each wavelength are given in Figure 3.7 and Figure 3.8. Black lines show the spectra of films before irradiation and red lines show spectra after irradiation. It was observed that PVA is more susceptible to degradation than PMMA since most of the Au^{3+} ions were reduced at 400 nm irradiation whereas the same extend of reduction of Au^{3+} ions was observed at 300 nm for PMMA.

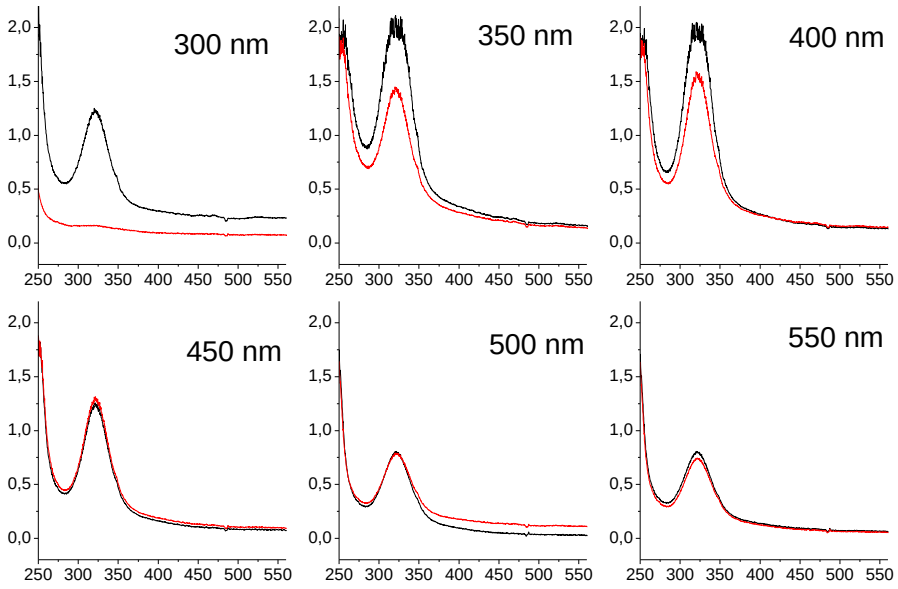

Figure 3.7 Reduction of Au^{3+} in PMMA by different wavelengths of UV-Vis radiation

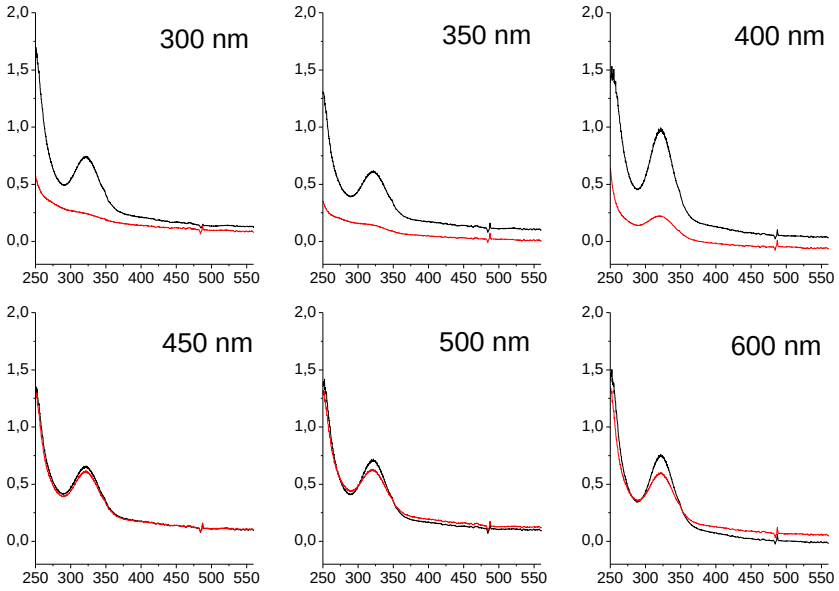

Figure 3.8 Reduction of Au^{3+} in PVA by different wavelengths of UV-Vis radiation

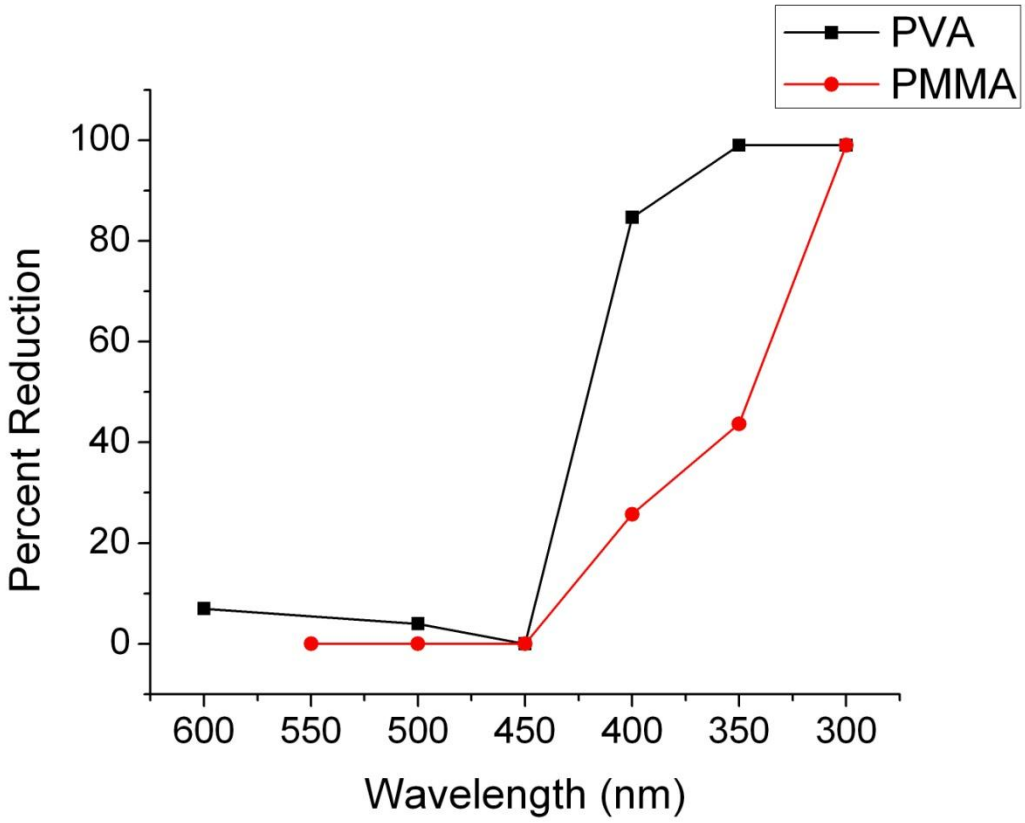

Figure 3.9 Graph summarizing the reducing effects of different wavelengths of light on PVA and PMMA.

The results of Figure 3.7 and Figure 3.8 are summarized in Figure 3.9. In this graph the percent reduction of gold ions is plotted as a function of the wavelength of the light used for the reduction process. It is clearly seen that the reduction process begins in PVA at a much larger wavelength than PMMA, although their curves meet at the end.

Hence, our studies on the reduction and nucleation and growth rates of gold ions/nanoparticles have revealed us that, nucleation and growth rates can be increased mechanically via heating, by increasing the rate of diffusion or via addition of another metal, while the reduction rate can only be modified chemically and have strong dependence on the polymer used for the application. Benzophenone was used as a photosensitizer molecule to increase the reduction rate of metal ions within the polymer matrices, and it was seen that benzophenone increases the reduction rate in PVA while it decreases the reduction rate in PMMA. Such a difference between two polymers, can be the result of different degradation mechanisms of both polymers with the UV irradiation. As shown by the experiments with IR spectroscopy the degradation mechanisms offered for PVA is in agreement with our results. Furthermore, irradiation experiments with PMMA and PVA containing gold ions using light at different wavelengths showed that, PVA and PMMA differ in their degradation mechanisms and the effect of benzophenone may be different due to these differences. Nevertheless, these studies reveal that the reduction rate of metal ions within polymer matrices can be increased using suitable photosensitizer molecules for different polymer matrices, as in the PVA-benzophenone case.

3.2 Photo-patterning and Investigation of Ion Depleted Regions

As mentioned before, one of the advantages of using polymer matrices is the ability to use a photomask impermeable to light for photo-patterning of any shape in different sizes on the polymer films containing dispersed gold ions. These patterns consist of two regions, the region containing gold nanoparticles within, which is the region exposed to radiation and the virgin region, which is not exposed to the radiation. Photo-patterns of micron range can be produced with this method as well as larger ones. Light microscope images can show the contrast between regions containing nanoparticles and virgin regions for films with thickness of tens of micrometers with large mask features as shown in Figure 3.10. In this picture, purple strips are the regions containing gold nanoparticles and the surface plasmon resonance of gold nanoparticles gives the purple color to these regions. The colorless strips are virgin regions that are masked during irradiation. The scale bar in this picture represents 10 μm.

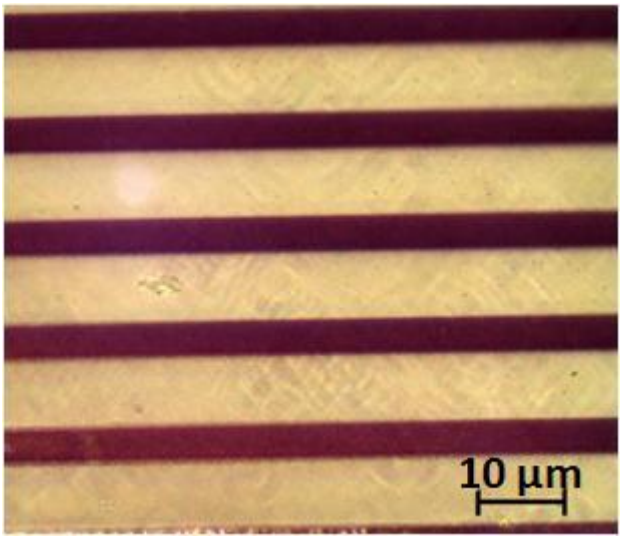

Figure 3.10 Light microscope image of the photo-pattern produced on Au-PMMA film[‡]

In addition to optical characterization of photo-patterns using microscopy, Raman spectroscopy can also be used to identify the regions forming these photo-patterns. Using the pronounced SERS effect of gold nanoparticles, the Raman signal coming from regions

[‡] Reprinted with permission from { E. Yilmaz, G. Ertas, E. Bengu and S. Suzer, Journal of Physical Chemistry C **114** (43), 18401-18406 }. Copyright {2010} American Chemical Society.

containing gold nanoparticles and from regions without gold nanoparticles can be distinguished easily. Figure 3.11 shows the Raman spectra taken from different regions of the photo-patterned film. Spectrum of the film before light exposure doesn't yield a significant Raman signal (a), but after exposure, the irradiated regions give large SERS signals corresponding to the well-known D and G bands of an organic matrix surrounding the gold nanoparticles (d). [84] The masked regions don't yield any Raman signal like the virgin film (b-c). This result, in agreement with the optical microscope images, clearly shows the presence of nanoparticles in irradiated regions and the absence of nanoparticles in virgin regions.

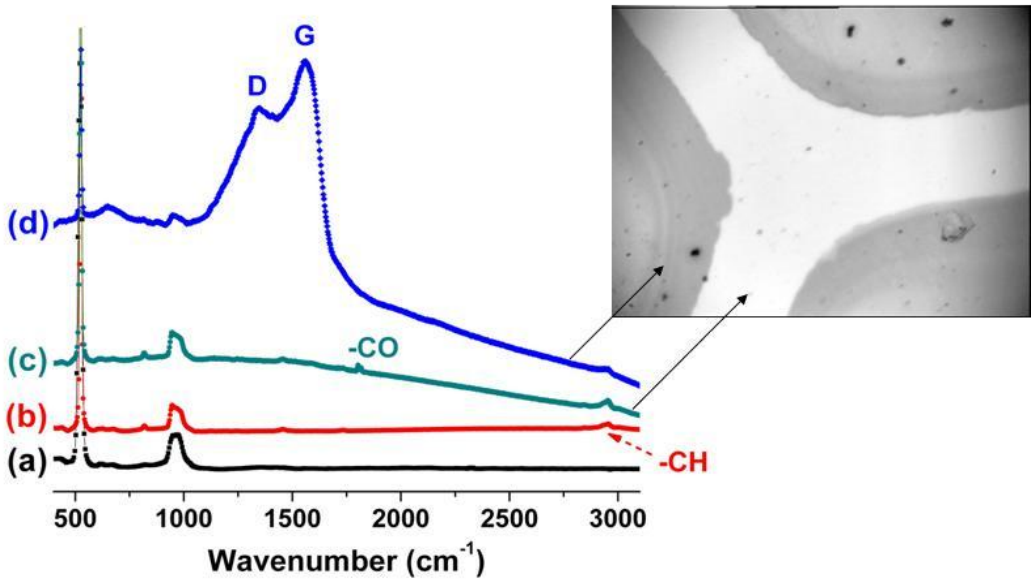

Figure 3.11 Raman spectra recorded from different regions of the photo-patterned film on a silicon wafer substrate[§]

For thick films we can get good images of photo-patterns with optical microscope but for thin films on Si substrates with a thickness in the range of tens of nanometers, it's impossible to use optical microscope. For this kind of samples with small sized features, scanning electron microscope (SEM) can be used. SEM can provide the contrast difference between regions with and without gold nanoparticles because of the high secondary electron

[§] Reprinted with permission from { E. Yilmaz, G. Ertas, E. Bengu and S. Suzer, Journal of Physical Chemistry C **114** (43), 18401-18406 }. Copyright {2010} American Chemical Society.

yield of gold atoms or ions. Also with the use of backscattered electron detector in SEM, the regions containing high Z elements and nanoparticles can be distinguished by the high backscattering properties of these systems. Figure 3.12 shows a SEM image of a photo-patterned PMMA film, prepared by spin coating on Si wafer substrate. The image on the left is the secondary electron detector image, while the image on the right is the backscattered electron image, and in both images, regions containing gold nanoparticles appear brighter than the other regions because of the aforementioned reasons.

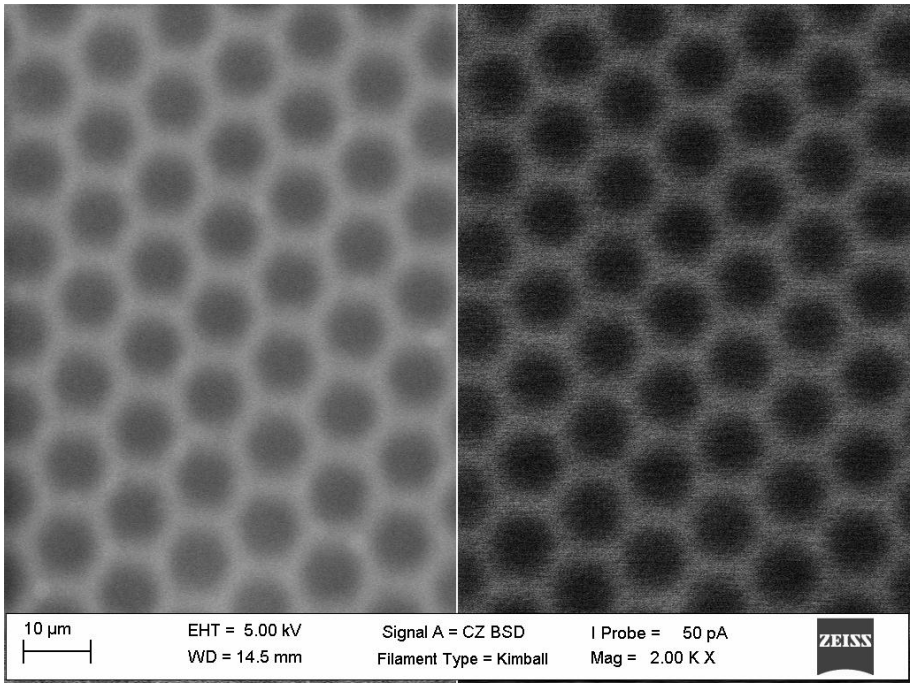

Figure 3.12 Secondary electron (left) and backscattered electron (right) images of a photopatterned Au-PMMA film

One interesting thing about the produced photo-patterns was, even after the mask is removed and the films were irradiated for an additional 24 hours without the mask, photo-patterned features were still intact after the 2nd UV treatment. In addition, to our big surprise, there was no significant change in the unexposed regions as well. Normally the virgin regions would be containing the unreacted gold ions after the first UV treatment, and it was expected that they would undergo further photoreaction during the second UV treatment and reduce gold ions to gold nanoparticles like the original irradiated regions. This should have resulted in the disappearance or blurring of the photo-patterns. In contrary as seen in Figure 3.13, such a photo-patterned film irradiated for the second time after the mask was removed, didn't show any decay in its photo-pattern (image on the right). The film does not lose its photo-patterned features after the second 24 hours irradiation without the mask. This result is rather interesting

and suggests an accompanying diffusion mechanism of gold ions or atoms during the original photo-production of gold nanoparticles.

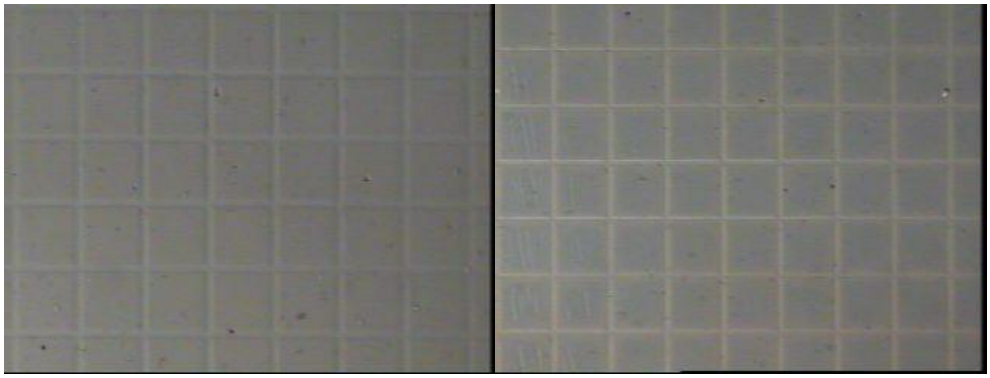

Figure 3.13 Light microscope image of photopattern produced on Au-PMMA film by 200 µm x 200 µm mesh, the film was irradiated for another 24 hours after the mask was removed.

Detailed analysis of these doubly irradiated films showed, similar features during SEM analysis. Completely dark regions between the first irradiated and the second irradiated regions were observed in these films as shown in Figure 3.14.

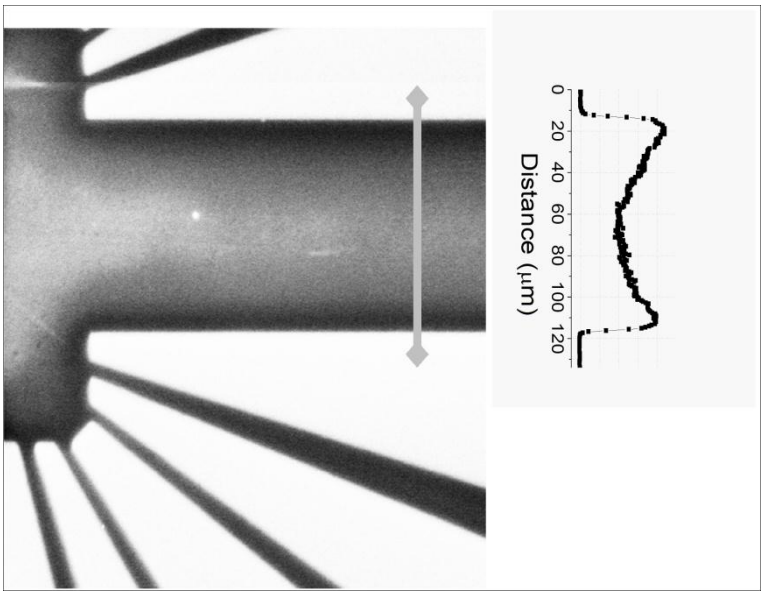

Figure 3.14 SEM image of the photopatterned Au-PMMA film after second UV treatment[**]

[**] Reprinted with permission from { E. Yilmaz, G. Ertas, E. Bengu and S. Suzer, Journal of Physical Chemistry C **114** (43), 18401-18406 }. Copyright {2010} American Chemical Society.

The composition of these regions is a mystery, and the most probable reason for these regions appearing darker in SEM image was the metal concentration in these regions being much smaller than other regions. The most convincing explanation for the decreased metal concentration in these regions is the possibility of migration of gold ions from these regions to others, so these dark regions are called "ion depleted regions". Ion depleted regions are observed in the border between the irradiated regions and virgin regions. Our hypothesis about the identity of these regions is that, they contain very little or no gold, compared to the virgin region and irradiated region.

Since both of the regions, under and outside the mask, are irradiated, there are gold nanoparticles everywhere except in the ion depleted regions. A profile through these regions as in Figure 3.14, shows the contrast difference more clearly and it reveals that the ion depletion has a width of about 10 microns. A detailed figure, illustrating our hypothesis

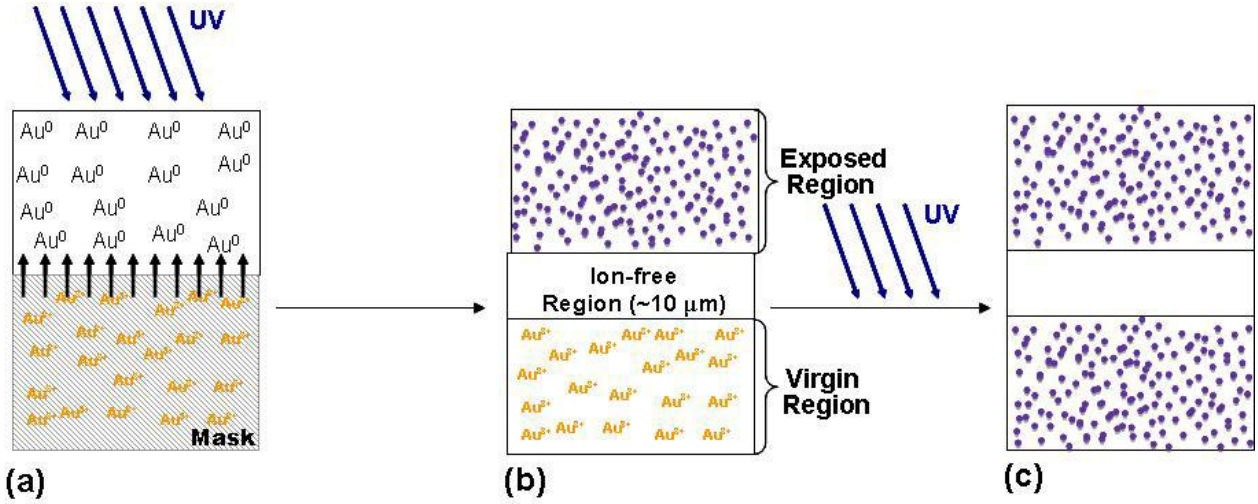

Figure 3.15 Illustration of ion migration during irradiation and the ion depleted region at the border, after mask is removed and after second UV treatment.[††]

explaining the action of ions during the irradiation and the picture after mask is removed is given in Figure 3.15. As shown in the figure when the mask is on for the first irradiation, the gold ions at the border between masked region and irradiated region diffuse towards the irradiated regions (Figure 3.15 (a)) and this process leaves behind a ion depleted region (Figure 3.15 (b))Afterwards when the film is irradiated for the second time, the masked

[††] Reprinted with permission from { E. Yilmaz, G. Ertas, E. Bengu and S. Suzer, Journal of Physical Chemistry C **114** (43), 18401-18406 }. Copyright {2010} American Chemical Society.

regions in the first irradiation also produces gold nanoparticles while the ion depleted region stays free of gold nanoparticles (Figure 3.15 (c)).

For more evidence supporting the proposed mechanism and the presence of ion depleted regions, fluorescence studies were conducted on photo-patterned films. Using fluorescent dyes as contrast agents in the presence of metal ions or nanoparticles is not a new concept. It was shown in many studies that Au ions or Au nanoparticles quench or enhance fluorescence of various fluorescent molecules, respectively. Using this property as a tool, presence of ions, atoms or nanoparticles can be differentiated with the aid of fluorescence studies in composite systems. The fluorescence quenching/enhancing of gold nanoparticles was demonstrated by many groups. It was shown by Xu et al.[85] that Au^{3+} ions quench fluorescence of Rhodamine B, whereas Au nanoparticles do not have a significant effect on its fluorescence. Later, this property was used to design a three-dimensional multi-layered optical memory by Tanaka et al.[86]. On the other hand, Sen et al.[87] claimed that resonance energy transfer from Rhodamine 6G (R6G) to gold nanoparticles takes place, thus quenching of fluorescence of R6G is observed when it is within the vicinity of gold nanoparticles. These studies indicate that the response of the fluorophore to Au ions and Au nanoparticle may be different depending on its type, but still as long as it can be used as a contrast marker it is useful for our purpose. In experiments performed to find the effect of gold species on R6G fluorescence were performed separately and the fluorescence quenching of R6G by gold ions was observed. R6G was then chosen for our experiments.

PMMA films containing Au salt and R6G (PMMA/Au/R6G) and PMMA films containing only R6G (PMMA/R6G) were prepared and subjected to 254 nm UV for 24 hours with the photo-patterning mask on. The fluorescence images of the resulting films were taken by a fluorescence microscope. As can be seen from the Figure 3.17 regions with more fluorescence at the border of irradiated and virgin regions can be observed in Au/PMMA/R6G films. These bright regions are similar in size to the ion depleted regions we observed in SEM images and they seem to prove our hypothesis about movement of ions during irradiation.

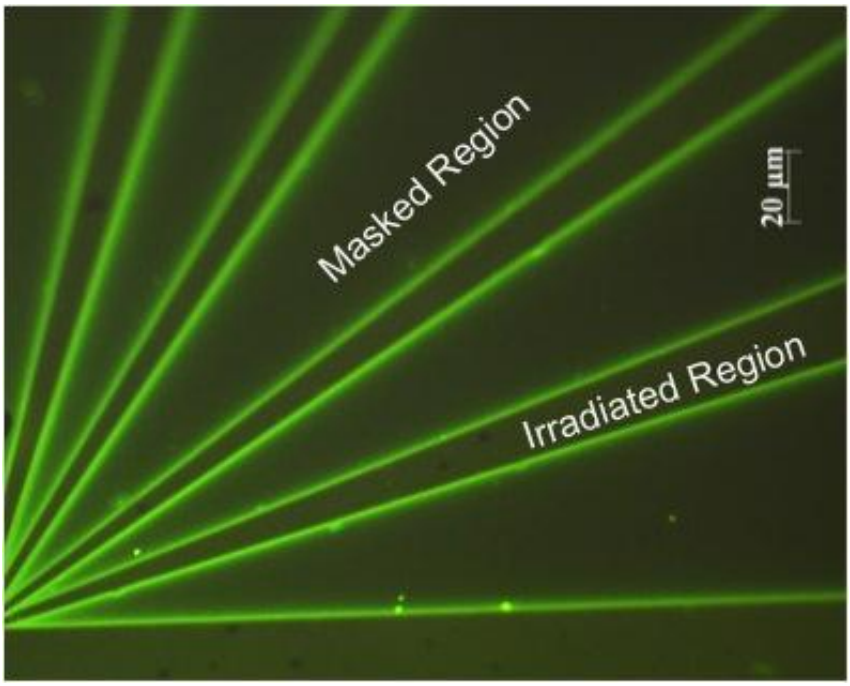

Figure 3.16 Fluorescence microscope image of a photo-patterned Au/R6G/PMMA film.

In order to ensure that these bright border regions are due to the gold content of the film and not some defect created by the photomask, films consisting of only PMMA and R6G without any gold were also prepared. Figure 3.17 shows the fluorescence image of two films, PMMA/Au/R6G and PMMA/R6G, clearly showing that the bright border regions are only observed for when gold is present in the film (Figure 3.17(a)). In the PMMA/R6G film (Figure 3.17.(b)) the dark areas are irradiated areas. In these regions R6G molecules are degraded during UV irradiation and lose their fluorescence, so after the mask is removed these areas appear dark in the fluorescence microscope. The bright areas in Figure 3.17(b) on the other hand, stay under the mask during irradiation and are not affected during irradiation. Additionally the fluorescence is also not quenched by anything since there is no gold in this film.

Figure 3.17.(a) and Figure 3.16, shows three different types of regions; dark areas, quenched areas and bright areas. Dark areas contain UV degraded R6G as in the PMMA case and appear dark in fluorescence images because of this degradation. The areas under the mask however aren't contacted to UV light the difference, between the border and the middle regions under the mask, is solely due to the gold content. The middle regions, less fluorescent than the borders, contain Au^{3+} ions which quench the R6G fluorescence, while the border regions aren't affected by this quenching since the gold ions in these regions migrated through

the irradiated region during the irradiation, thus they appear brighter in the fluorescence microscope. These results support our hypothesis about the migration of gold ions in the border regions between irradiated regions and masked regions and shows the results obtained from SEM really represent the gold content in the photo-patterned films.

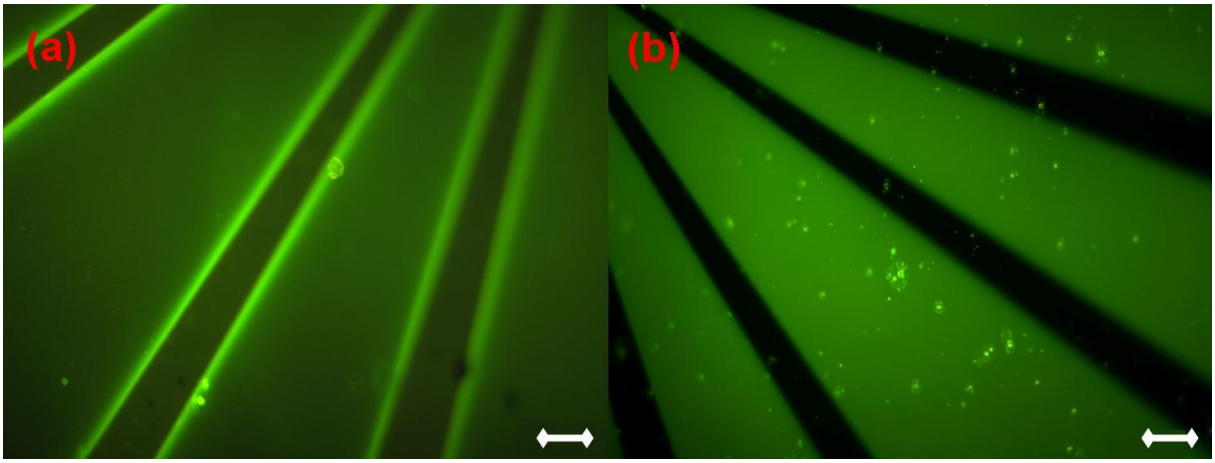

Figure 3.17 Fluorescence images of photo-patterned (a) Au-PMMA and (b) PMMA films with R6G taken by fluorescence microscope.[‡‡]

Although, Figure 3.17 shows clearly that the bright regions at the border observed in fluorescence microscope aren't a result of any defect of the photomask, suspicion may arise if the border regions are a part of the masked regions or the irradiated regions. To determine the origin of the borders, images taken from photo-patterned PMMA/Au/R6G and PMMA/R6G films using the same photomask were superimposed as shown in Figure 3.18. As can be seen from the figure, the bright border regions on PMMA/Au/R6G films overlap with the borders of the masked regions in the PMMA/R6G film. This interception provides solid proof that these bright regions in PMMA/Au/R6G film are the borders of the masked regions.

[‡‡] Reprinted with permission from { E. Yilmaz, G. Ertas, E. Bengu and S. Suzer, Journal of Physical Chemistry C **114** (43), 18401-18406 }. Copyright {2010} American Chemical Society.

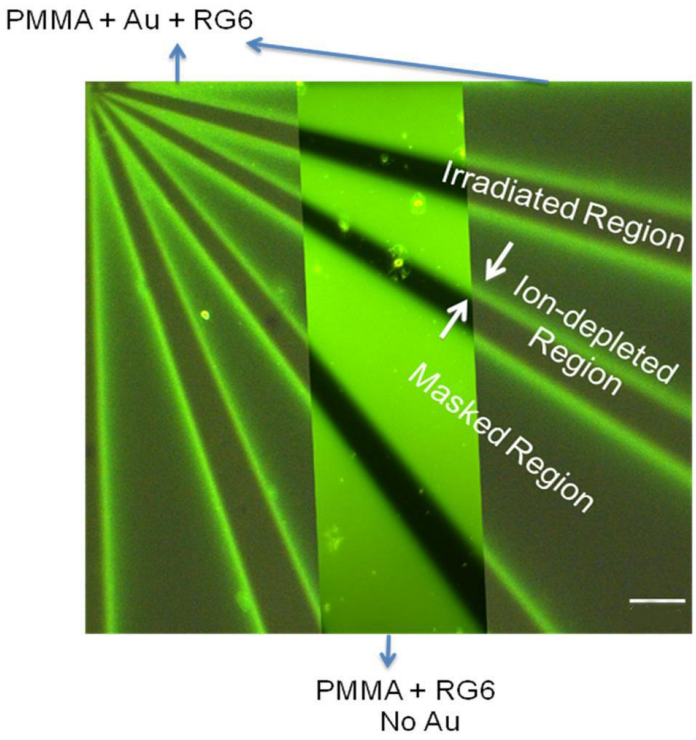

Figure 3.18 Fluorescence microscope images of PMMA with gold and R6G, the middle of which contains that of only R6G film overlapped.[§§]

Ensuring the dark borders observed in SEM images and bright borders observed in fluorescence microscope belong to the same region for both images is another important issue. To determine the observed regions are the same for both techniques, the images of the same film were taken using SEM and fluorescence microscope and overlapped on each other. The difficulty to perform this experiment was normally SEM samples should be as thin as possible to avoid charging of the sample while the fluorescence studies samples should be fairly thick to collect the maximum fluorescence from the sample. Thus the sample used for both measurements couldn't ensure the best image quality with both techniques. Nevertheless optimization of the film was done to get meaningful results from both techniques. For this experiment a spin-coated thin film of PMMA/Au/R6G mixture was cast on glass substrate and fluorescence image and SEM image of this film was recorded. Figure 3.19 shows the overlapped images of SEM and fluorescence microscope at the same sample. It can be easily seen that the regions appearing dark on SEM image appear brighter at the fluorescence

[§§] Reprinted with permission from { E. Yilmaz, G. Ertas, E. Bengu and S. Suzer, Journal of Physical Chemistry C **114** (43), 18401-18406 }. Copyright {2010} American Chemical Society.

microscope image. This image clearly shows that the dark regions observed during SEM measurements are the same as the bright regions observed during fluorescence studies.

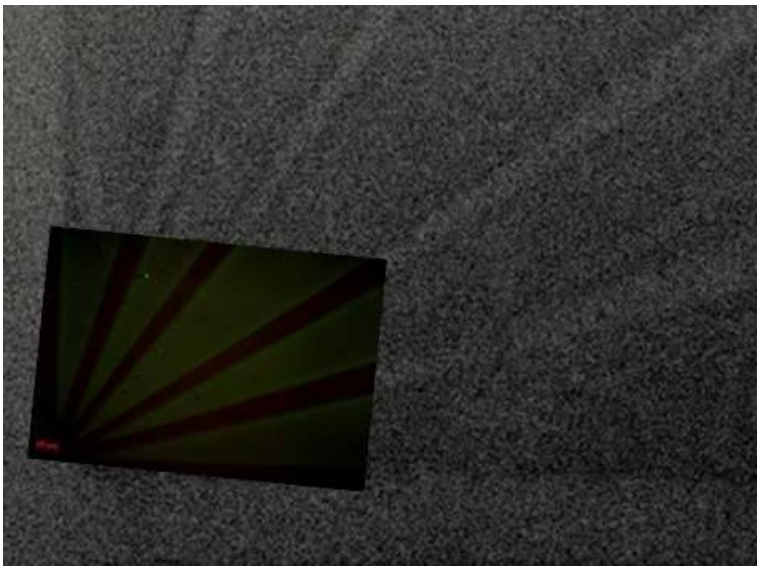

Figure 3.19 Overlapped images of SEM and fluorescence microscope of the same sample

The formation of ion depleted regions is very interesting and can be observed clearly with fluorescence studies conducted with R6G molecule. Another interesting property of these regions is that their formation is dependent on time. Figure 3.20 shows the formation of ion depleted regions as a function of time, with fluorescence images taken within different irradiation time intervals. As can be seen from the figure these regions are formed slowly with time. Bright border regions are not observed after 30 minutes of irradiation (Figure 3.20.(a)), after 1 hour of irradiation (Figure 3.20.(b)) they start to become noticeable and image taken after 24 hours of irradiation (Figure 3.20.(c)) shows the final state of these regions. This slow time dependent formation of ion depleted regions requests a diffusion controlled mechanism for these regions. The proposed mechanism explaining the formation of ion depleted regions already suggests the diffusion of gold ions from the border of masked regions through the irradiated regions. The results demonstrated in Figure 3.20 supports the proposed mechanism in that respect.

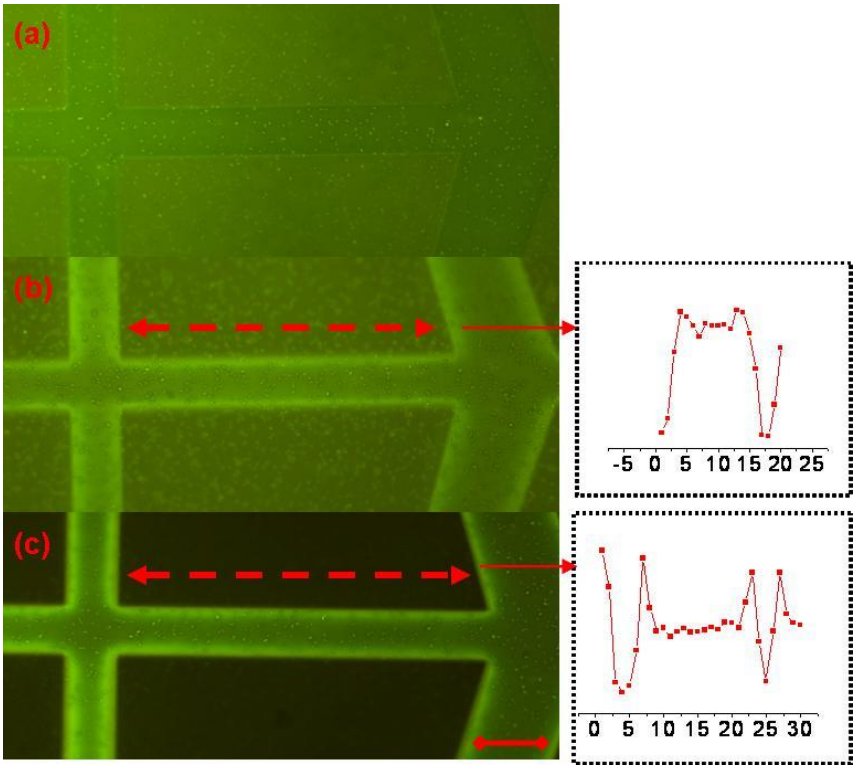

Figure 3.20 Fluorescence images of PMMA film with Au and R6G irradiated for 30 minutes, 1 hour and 24 hours. Inlet: XPS line scans of the Au4f peak intensity[***]

Besides fluorescence images demonstrated, XPS profiles obtained from line scans on the sample are also given in the inlets in Figure 3.20. Line scan in XPS is another technique that can provide information on the distribution of gold ions, atoms and nanoparticles in a patterned film. Although imaging techniques with XPS are newly emerging, they are very powerful. One can do very detailed XPS analysis combined with imaging using specialized XPS equipments. Thermo Fisher K-alpha provides spatial resolution of about 10-20 μm in that respect, it may not be a very fine resolution, but still meaningful data for our purpose can be harvested on the gold content. For such measurements, a roundabout way for the analysis of gold distribution should be used. The irradiated regions of Au/PMMA films tend to yield a lot more gold signal than the masked regions, so for better signal strength during line scans instead of taking a line scan from the masked region and observe low gold signal coming from the ion depleted region at the border, a line scan was performed on the irradiated region and increased gold content was observed at the borders, due to the migrated ions from the ion

[***] Reprinted with permission from { E. Yilmaz, G. Ertas, E. Bengu and S. Suzer, Journal of Physical Chemistry C **114** (43), 18401-18406 }. Copyright {2010} American Chemical Society.

depleted region to the irradiated region, was observed. XPS line scan measurements performed on irradiated regions of photo-patterned PMMA/Au/R6G films are given in Figure 3.20.Inlet. After 1 hour of irradiation we can see some small increase of gold signal at the borders of the irradiated region compared to the middle region. And after 24 hours of irradiation the Au concentration at the border is about two folds higher than of the middle region This is a clear evidence that gold diffuses from masked region to the irradiated region during irradiation and this diffusion results in a highly concentrated region at the border of the irradiated region and most probably a poorly concentrated border region at the border of the masked region which we call ion depleted region.

The measurements performed on photo-patterned Au/PMMA films clearly show the presence of ion depleted regions as we suggested. The presence of ion depleted regions is important for the production of stable photo-patterned films, since knowing the ions at the border between irradiated regions and masked regions will be cleared for 10 μm distance, films consisting of regions containing only gold nanoparticles and no other ion can be produced with features smaller than 10 μm. Without ion depletion process in photo-patterned films, the films can produce nanoparticles in the masked regions after the mask is removed with sun light exposure and patterns would be lost.

Another important implication of the presence of ion depleted regions is the insight they provide for the diffusion of gold ions in PMMA films. Diffusion of metal ions and atoms in polymer films have been studied by many groups before, but the diffusion mechanisms and diffusion constants provided are not very consistent. Although somewhat scattered, there are several reports regarding the diffusion of gold atoms inside polymer matrices. Alexandrov et al. [63] reported the diffusion coefficient (D) of gold atoms in PMMA matrix at 348 K as 2×10^{-7} cm^2 s^{-1}, which is quite large compared to other reports about diffusion of metal atoms in polymers. For example, in a detailed paper about diffusion of metal atoms in polymers by Faupel et al. [88], the corresponding diffusion coefficients are given for gold atoms in different polymer matrices (like BPA-PC and TMC-PC) at temperatures about 500 K. These reported values are in the range of 10^{-13}-10^{-16} cm^2 s^{-1}, smaller by about 7 orders of magnitude. In contrast to several studies on metal atoms, no corresponding reports are available dealing with diffusion of metal ions (i.e., $AuCl^{4-}$) in polymer matrices. An approximate value can now be obtained by using our experimental results and the Fick's First Law of diffusion;

$$s=-D/c(\partial c/\partial x)$$

where s denotes the terminal speed of the ions, D is the diffusion coefficient, c is the concentration, and $\partial c/\partial x$ is the concentration gradient. For a movement of 10 μm = 0.001 cm within 24 h, we can get an estimate of 1.2×10^{-8} cm/s for s, and an upper limiting value for the concentration gradient can be estimated as c /10 μm, by assuming total consumption of the ions within the irradiated regions.

$$D = 1.2 \times 10^{-8} \text{ cm} / \text{s} * 0.001 \text{ cm}$$

This rough procedure yields an unreasonably large diffusion constant of 10^{-11} cm^2/s for ions to move in polymer matrices at RT. The reason behind this large estimation may be a driving force for the gold ions to move from masked regions to irradiated regions. Such a force would definitely accelerate the motion of gold ions and may result in diffusion constants much larger at room temperature.

It is well-known that gold atoms tend to come together, following their photoreduction step, which results in formation of gold nanoparticles, because of their large cohesive energy (366 kJ/mol), but we are yet to know of a factor to force the gold ions to diffuse at a 10 μm distance from the masked regions toward the irradiated ones at RT, and in the absence of external electrical potentials. Development of an electrochemical potential due to depletion of ions as result of photoreduction in the irradiated regions can be thought of as the thermodynamic driving force, but its magnitude can be estimated as ca. 120 mV (11 kJ/mol) for an extreme concentration difference of a factor of 100 between the two regions. Even this value is about 30 times smaller than the driving force for the gold atoms. Thus the nature of the driving force behind this unusual movement of gold nanoparticles is yet to known but we can observe its effects in our photo-patterned films with the formation of ion depleted regions.

In addition to the preparation of gold nanoparticles in PMMA films, we can also produce gold nanoparticles in PVA films as mentioned beforehand. Such films can also be photo-patterned using masking method. In order to see if there were similar ion depletion processes in PVA/Au films, PVA/Au/R6G films were prepared and photo-patterned by UV irradiation. SEM images and fluorescence images of PVA/Au/R6G film can be seen in Figure 3.21. As can be seen from the figure, both SEM image shows dark regions at the borders and fluorescence image shows the bright regions at the borders like those observed in the PMMA films. This result ensures us that similar ion depletion process also takes place in PVA matrix. This result shows that the ion depletion process is not specific to the polymer, but it is probably a process depending only on the gold ions and their reduction processes.

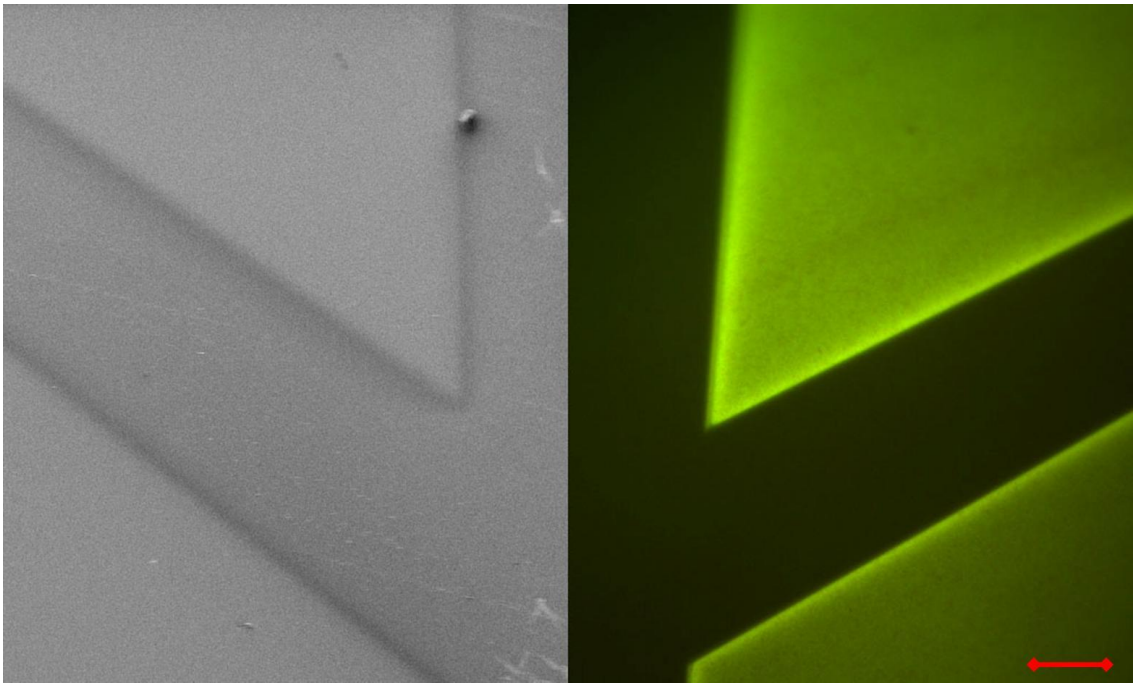

Figure 3.21 Photo-patterned PVA film containing Au nanoparticles and R6G, left hand-side shows SEM image right hand-side shows fluorescence image.[†††]

As a conclusion, in this section photo-patterning of PMMA films with gold nanoparticles was demonstrated. Photo-patterned thick Au/PMMA films were imaged in optical microscope while for thin photo-patterned films SEM imaging was employed. During SEM studies dark regions, between masked regions and irradiated regions of the photo-patterned films, were observed. Close investigation of these dark regions with fluorescence studies, hinting the gold content of the patterned films, concluded the formation of ion depleted region between masked regions and irradiated regions, due to the migration of gold ions from the masked regions through the irradiated regions. Ion depleted region are as wide as 10 μm, which is surprisingly large for an ion to diffuse through a polymeric substance. The presence of ion depleted regions is especially important for the production of durable photo-patterned films with feature size less than 10 μm and using the data we obtain during the formation of ion depleted regions, diffusion constant of the gold ions in PMMA matrix can be calculated.

[†††] Reprinted with permission from { E. Yilmaz, G. Ertas, E. Bengu and S. Suzer, Journal of Physical Chemistry C **114** (43), 18401-18406 }. Copyright {2010} American Chemical Society.

3.3 Effect of Gold Nanoparticles on the Dielectric Properties of PMMA

Normally PMMA is used as a dielectric component in electronic applications due to its high resistivity. [89] On the other hand, the change in resistivity of PMMA by the addition of conducting species to the matrix is also point of concern. [90, 91]Also, the effect of gold NPs on PMMA conductivity is a well-discussed issue in previous studies of different groups. Abyaneh et al. [92] showed the decreased resistivity of PMMA films with increasing gold NP content. In their experiments oleylamine capped gold NPs were mixed with PMMA by different weight percentage ratios and I-V measurements were performed with a Keithley 238 current/voltage sourcemeter unit. In another recent study, the increased conductivity of PMMA by gold ions was studied by Salvadori et al. [93] with a buried conducting layer of metal/polymer nanocomposite which was formed by very low energy gold ion implementation. The measurement was made through electrical contacts attached to the film with silver glue and covered by a thin Pt film for better contact. The gold ions penetrated through 2.7 nm depth of the 50 nm PMMA film and it was shown that the conductivity of PMMA increased drastically with the increasing amount of gold ions within the polymer. In our study, we focus mainly on the charging properties of PMMA and Au NPs/PMMA films to understand the effect of Au NPs on the electrical properties of PMMA films and we present a new method to investigate the conductivity of gold nanoparticle-PMMA composites using XPS.

Using charging as a tool to investigate the resistivity of PMMA films in XPS has many advantages. The currents measured from polymer films are usually very low in the range of nanoamperes due to high resistivity. The common method of measuring resistivity of a film, the I-V measurement, needs very good electrical contacts to the sample film and sensitive equipment to perform a meaningful measurement. Additionally the measurement must be insulated from the surroundings so that the measurement is not altered by the environmental factors. At the other hand, XPS measurements don’t need taxing contacts, since the information comes directly from the surface of the film. Also needless to say that, the sample is already isolated from the surrounding factors. Hence, more reliable results can be obtained using XPS as a tool for resistivity and capacitance measurements of insulating samples.

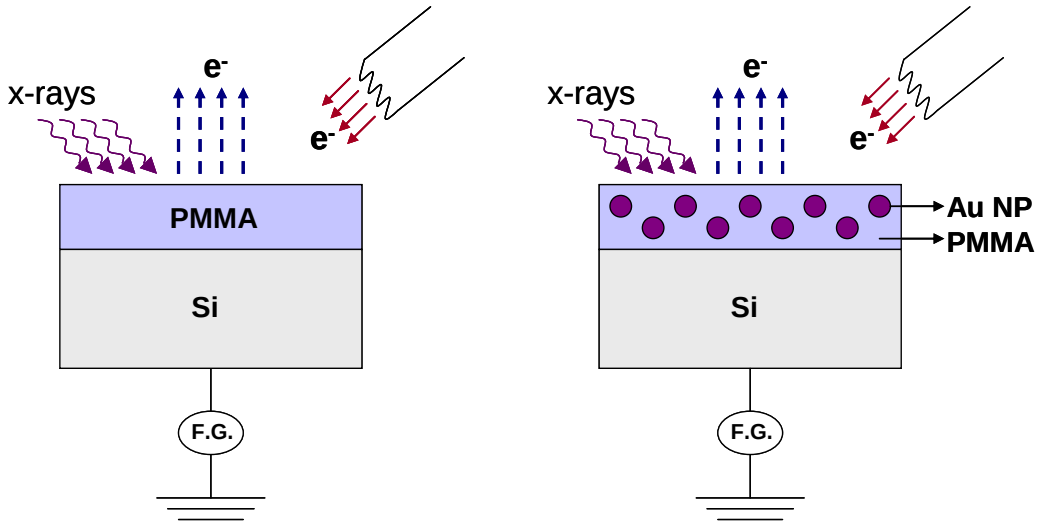

Figure 3.22 The scheme of samples used for XPS measurement

Our experimental setup for our XPS measurements is given in Figure 3.22. The C1s spectra of the PMMA and Au NP/PMMA films, subjected to -/+ 10 V voltages and grounded, are given in Figure 3.23 (a) and (b). Both films were irradiated for 12 hours to have the same conditions except for the presence of gold NPs. For PMMA film without gold nanoparticles the total binding energy difference between the -10 V and +10 V measurements is 11.3 eV, whereas the binding energy difference for PMMA film containing gold nanoparticles is 16.0 eV. The bigger difference in binding energy for Au NP/PMMA film indicates us less charging on film as explained before, thus we can claim that gold nanoparticles decrease the resistivity of PMMA films. Additionally as shown in the spectra at Figure 3.23(c), with increasing concentration of gold nanoparticles in PMMA film we can reach to a point where no charging on the surface is observed. This concentration, which PMMA almost acts like a conductive material was also shown by other studies. [93] But using XPS, this concentration can be observed at lower quantities than the other techniques since it is a non-contact technique, which also shows the power of this technique.

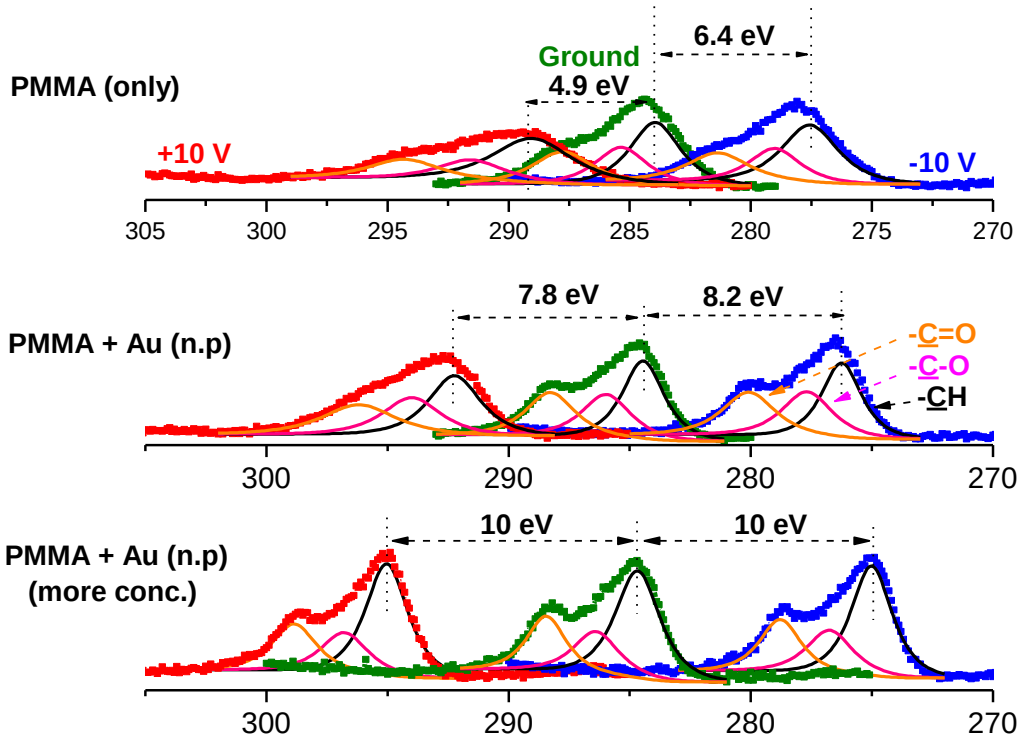

Figure 3.23 Charging behaviour of C lines of PMMA films a) without gold nanoparticles, b) with gold nanoparticles and c) with a large amount of gold nanoparticles[‡‡‡]

Besides applying -/+ 10 V to the films, measurements with square wave (SQW) potentials at different frequencies can be performed as mentioned before. With such measurements, not only information about resistivity of the sample but also information about capacitance of the sample can be obtained. When the XPS spectra of O1s and C1s lines of PMMA films are measured by applying 10 V square wave voltage with different frequencies the following are observed: In the high frequencies, since the applied voltage changes in between -10 V and +10 V rapidly the film doesn't charge and the binding energy difference observed between the separated peaks is nearly 20 eV. But in the low frequencies, the time interval of the applied voltage is longer and this causes more charging on the surfaces of the films and for charging samples binding energy differences less than 20 eV is observed. So any

[‡‡‡] Reprinted from Applied Surface Science, Vol. 256, Yilmaz E., Suzer S., "Au nanoparticles in PMMA matrix: In situ synthesis and the effect of Au nanoparticles on PMMA conductivity", 6630-6633, Copyright (2010), with permission from Elsevier.

charging difference made by the addition of gold NPs can be observed by comparing binding energy differences at high and low frequencies.

Binding energy difference vs. Frequency plot is given in Figure 3.24 for graphite, PMMA and Au NP/PMMA films. At high frequencies 20 eV binding energy difference is observed for all samples which is natural since at high frequencies samples can't charge due to rapidly changing potentials (from -10 V to +10 V). But at low frequencies the time intervals between potential changes become larger and non-conducting samples start to charge whereas conducting samples remain unaffected. As can be seen at Figure 3.24 graphite shows 20 eV binding energy difference between the two C 1s lines at every frequency. But PMMA and Au NP/PMMA films shows charging gradually with decreasing frequencies. At the very low frequencies, the binding energy difference converges to the values observed at the DC potentials measurements. In these particular samples, we see for PMMA it is about 12.8 eV and for Au NP/PMMA it is about 16 eV, and is in agreement with the binding difference energies observed at DC potential measurements. Information about capacitance properties of the sample on the other hand, is deduced from the frequency dependence of the decrease of the binding energy difference. From decay constant we have by fitting curves to the binding energy difference vs. frequency plot, we can calculate the capacitance values for the sample alongside to the resistance. (Table 3.1) Of course it should be noted that the values in this table, are not related with the bulk properties of the samples directly. The resistance and capacitance values demonstrated here are related to the conductivity and the dielectric properties of the samples, respectively.

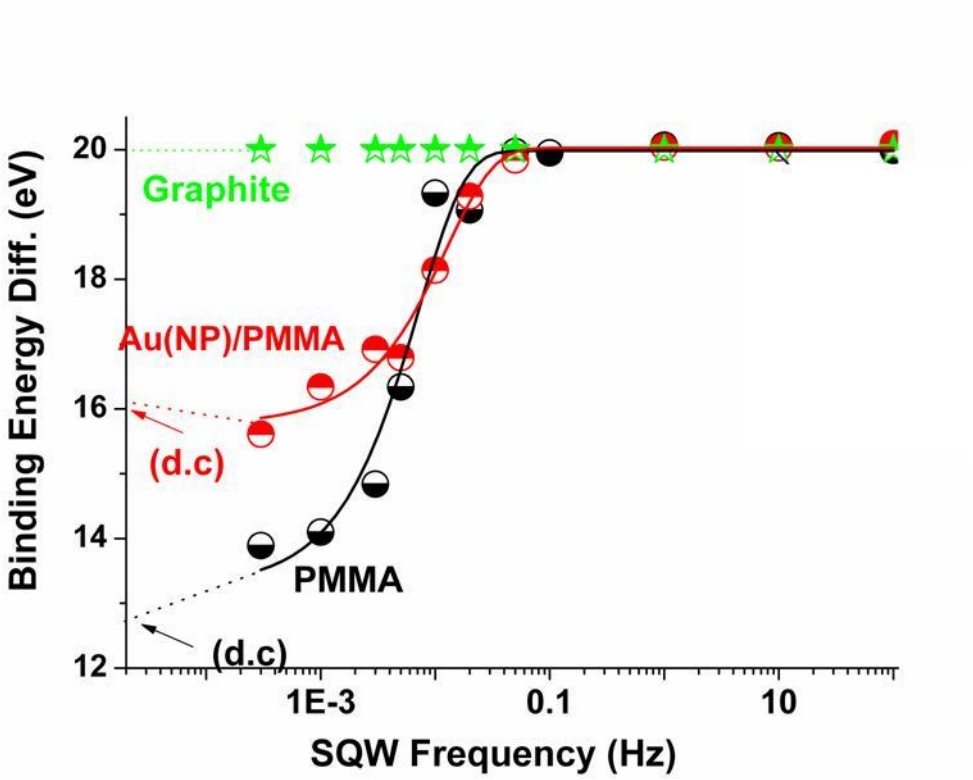

Figure 3.24 Measurement of dielectric behaviour of Graphite, PMMA and Au NP/PMMA films with SQW voltages at different frequencies.[§§§]

Table 3.1 Resistance and capacitance values calculated for Au NP/PMMA and PMMA films with SQW measurements

	R	***C***
PMMA	2.25 Mohm	6 μF
Au NP/PMMA	0.9 Mohm	20 μF

Another interesting feature observed at SQW measurements is the off-set in the line positions of charging samples at high frequencies. Figure 3.25 shows such a measurement performed on PMMA and Au NP/PMMA films and compared to conducting graphite spectrum. Off-set in line positions at non-conducting samples is observed because of IR-drop

[§§§] Reprinted from Applied Surface Science, Vol. 256, Yilmaz E., Suzer S., "Au nanoparticles in PMMA matrix: In situ synthesis and the effect of Au nanoparticles on PMMA conductivity", 6630-6633, Copyright (2010), with permission from Elsevier.

in such samples. As can be seen from the figure off-set at C lines of Au NP/PMMA sample is 0.3 eV whereas the off-set at PMMA sample is 1.3 eV, which is consistent with the proposed effect of gold nanoparticles on PMMA resistance at previously mentioned measurements. This is another result showing the decrease in resistance of PMMA films with the addition of gold nanoparticles.

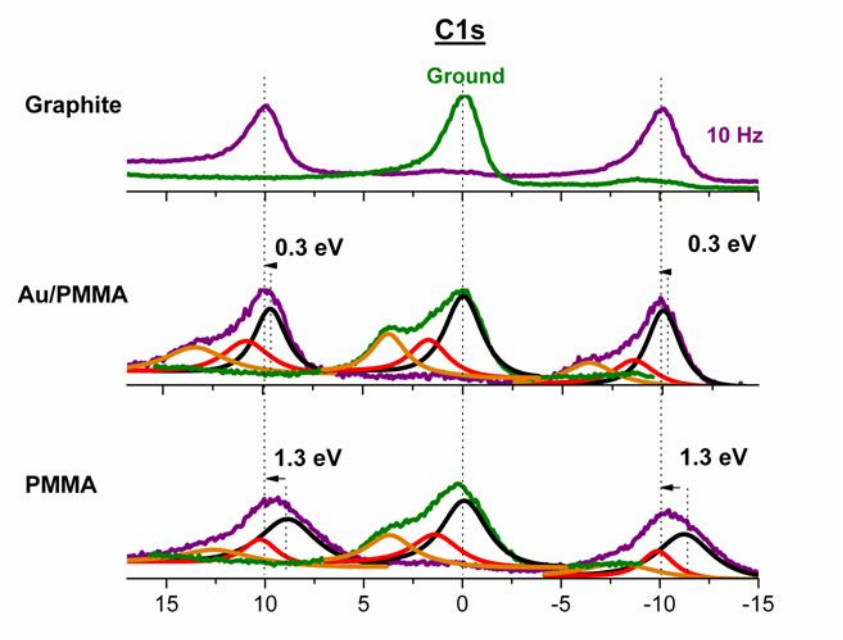

Figure 3.25 Off-set shift observed in the C lines of PMMA with and without gold nanoparticles compared to line positions of Graphite as a reference[****]

Another method that can harvest more information from the sample while applying SQW potentials is taking snapshot spectra from the sample in short time intervals to see the overall response of the sample to the changing potentials. Using this method one can see the behavior of the sample as we apply a potential and understand its charging properties better rather than just looking before and after states of the sample. Figure 3.26 shows snapshot spectra of PMMA/Au NP and only PMMA films. In this case 0.01 Hz +/-10 V SQW was applied to the sample and the effect of flood gun on the sample as it charges was observed.

[****] Reprinted from Applied Surface Science, Vol. 256, Yilmaz E., Suzer S., "Au nanoparticles in PMMA matrix: In situ synthesis and the effect of Au nanoparticles on PMMA conductivity", 6630-6633, Copyright (2010), with permission from Elsevier.

When -10 V is applied to the sample the O 1s peak first shifts to a lower binding energy but as time passes it starts to charge quickly and eventually the peak shifts all the way near +10 V peak position. But when we look at where the peak stops we can easily notice that for PMMA only film the peak shifts further away than the PMMA/Au NP film. This result presents a step-by-step visualization of the effect of Au NPs on the charging of the PMMA films also this method gives us a dynamic tool to observe how the charging event processes in time.

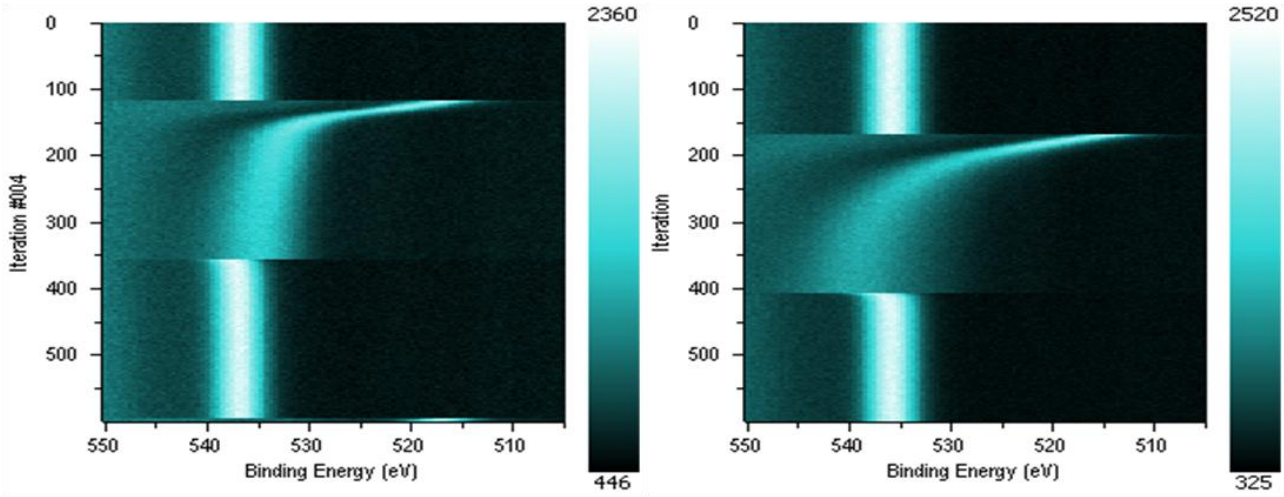

Figure 3.26 Snapshot spectra of PMMA/Au NPs film (left) and PMMA film (right) taken as a function of 0.01 Hz +/-10 V SQW voltage and the effect of flood gun.

I-V measurements for Au NP/PMMA films were also performed with a Keithley 2400 current/voltage sourcemeter. The film was deposited on gold electrodes on a non-conducting surface. The results shown at Figure 3.27 indicate there is no detectable conductivity for PMMA films containing Au^{3+} ions and Au NPs. The measurement medium was isolated from surroundings with a noise free box and several measurements were performed to prove consistency but the fluctuations in current were still available after many trials. This can be the result of poor electrical contact between electrode and the film. As mentioned before the measured current is very low in this type of materials and special techniques are needed to have reliable results. Even this finding also shows that the measurements performed with XPS is a lot more reliable and easier than the IV measurements, in which one has to work very hard to make good contacts with the sample especially if it's a polymer film that contact problem is a primary obstacle.

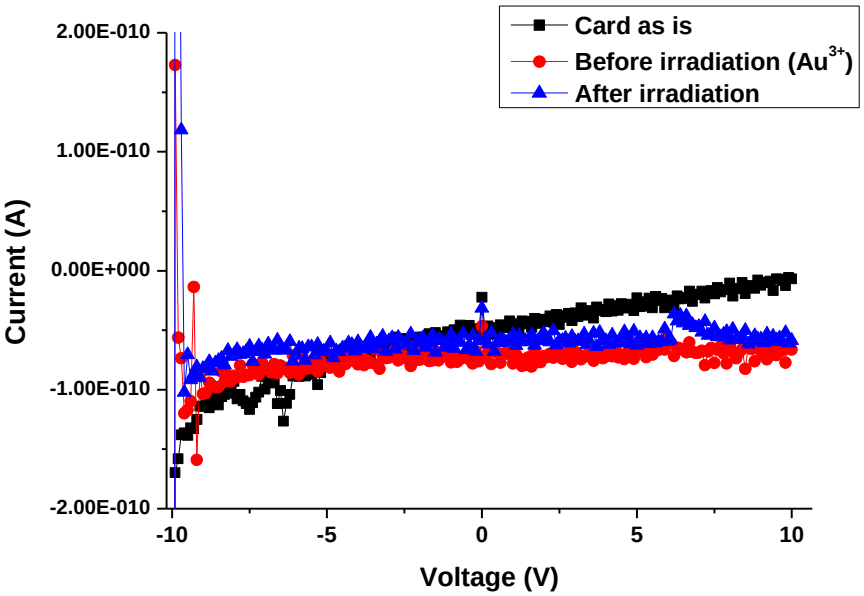

Figure 3.27 IV measurement performed on PMMA film containing Au3+ ions and Au nanoparticles

With charge resolved XPS technique successful measurements of resistance and capacitance of PMMA films with and without gold nanoparticles were achieved. This technique is advantageous over conventional resistance and capacitance measurement techniques for polymers, since large resistance values can be measured using charge resolved XPS without needing to have good contacts to the polymer surface. It was discovered that gold nanoparticles decrease the resistance and increase the capacitance of PMMA films.

3.4 Extra electrons on the PMMA Surface: Pendant Groups are Affected More than Skeleton Carbons

Electrification or electret formation is well-known to men for more than 2500 years. An "electret" is defined as a material that develops a permanent electrostatic potential due to extra charges, or has a permanent dipole moment. Electrons are spatially localized within atoms and molecules occupying atomic and molecular orbitals, and when larger particles or assemblies are considered interatomic and intermolecular delocalization of electrons becomes important, and dictate the electrical properties of metals and to some extent of semiconductors. However, for semiconductors additional electronic states due to doping or defects, imperfections at their surfaces and/or grain boundaries, as well within the lattice, commonly described as traps, impurity states, etc., contribute significantly to their electrical properties. For insulating materials like polymers (PMMA, PTFE, PVDF), salts, metal oxides, nitrides, and sulphides, etc., which are described as having larger band-gap values, where electrons are localized, leading to extremely low conductivities. In these materials, other electronic states, like interface and impurity states, defect sites, etc. completely dominate their electrical properties. In addition, electrical properties of these materials are strongly influenced by external stresses, like exposure to light, energetic particles, mechanical distortions, milling, etc., which are attributed to insertion of localized electrons and/or ions at interfaces, grain boundaries, cracks, or in bulk sites like cavities, which even lead to certain chemical oxidation-reduction reactions. [75] Among these, contact electrification has recently been in focus, due to the recent studies, proposing two different mechanisms as its cause, being electron transfer as opposed to ions or materials transfer with sound experimental findings on both side. [69-73]

One can probe the charges on an insulator surface in different ways. Wiles et al. proposes the use of an electrometer which measures the charge accumulated on a ferromagnetic sphere as it rolls over the polymer surface surrounded by a Faraday cage. [94] While Liu et al. shows the presence of cryptoelectrons as they conduct redox reactions on the surface of contact electrified polymers. [75] We are now proposing a different novel technique for analyzing this problem by using charge resolved XPS technique. As mentioned earlier, the charging on the surface can be controlled with the applied external bias, thus the response of the polymer surface to the induced charges and the accommodation of these charges can be

monitored using this technique. The understanding of how the charges are accommodated on the polymer surface can further our understanding of the electron storage capacity of the polymer surfaces at the molecular level, which might support the idea of electrons being the major source of the contact electrification.

In the experiments performed with PMMA films to understand the effects of gold nanoparticles on the polymer's electrical properties, a particular result was interesting. When the PMMA films were subjected to +/-10V external bias during the measurement, there was an observable broadening of the peaks. (Figure 3.23) Specifically, it was observed that the extent of the broadening was larger in +10 V than -10V external bias. This broadening of the peaks wasn't a result of structural damage on the polymer, since when the sample was grounded again and another spectrum was recorded the peaks returned back to their narrow profiles. Without causing a structural change on the polymer the induced charges on the surface were then creating reversible charging states according to our observation. We should note that, by applying +10 V external bias the surface became enriched with electrons and by applying -10 V external bias the surface was devoid of them. Any state created under these conditions directly relates to the trapping of charges on the polymer surface, which is a very important and vibrant research field because of its implications on the electrification of insulating materials.

For this study PMMA films were deliberately charged in XPS using flood gun as the external electron source and the applied external bias as an attractive/repulsive force for the electrons. Both DC and square wave potentials were applied to the substrates for static and dynamic measurements. During static measurements XPS spectra were collected in ground, -0.25 V and +0.25 V conditions as in shown in Figure 3.28. Interestingly a charging difference of 0.09 eV was clearly observed between C1s and O1s peaks when all the spectra were corrected taking C1s peak of PMMA backbone carbons at 285.0 eV as the reference for the neutral state. This difference in binding energy between C atoms and O atoms shows that, C atoms and O atoms response to accumulated charges differently when -0.25 V bias is applied. This is important for the fact that it experimentally shows the different affinity of C and O atoms towards the accommodated charges on the polymer surface. Another noteworthy point to mention is that difference of 0.09 eV observed in this case is a result of 0.25 V applied bias difference, which is very small but can cause a measurable change in the binding energies of C and O atoms and at larger biases the peaks become much broader.

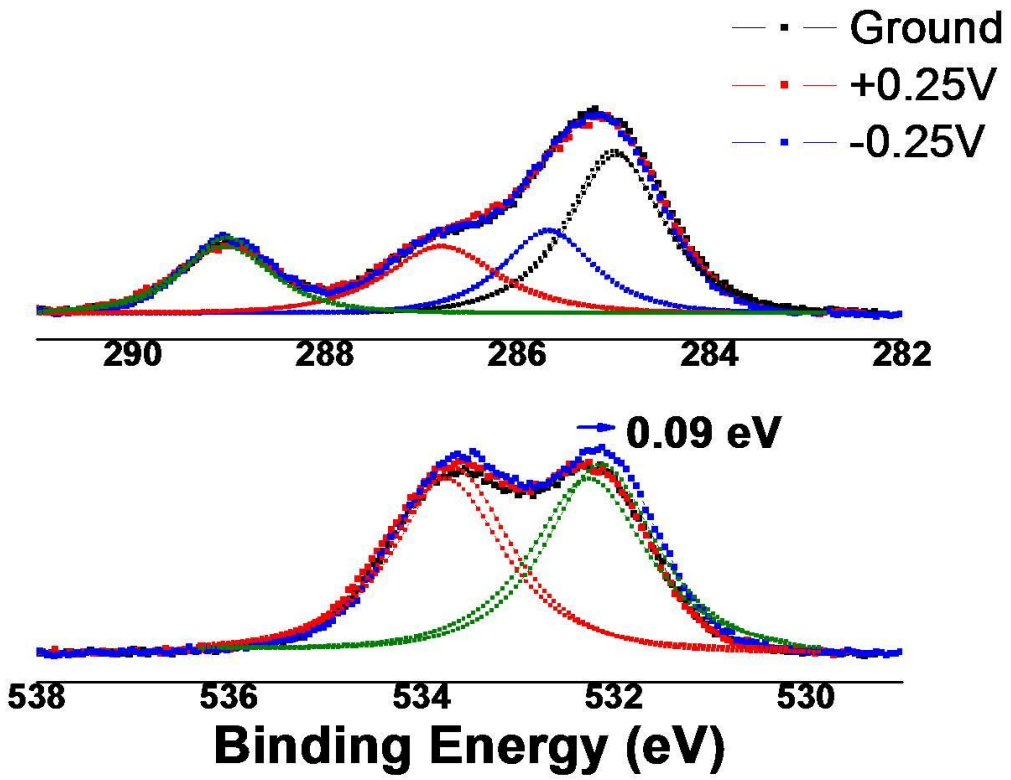

Figure 3.28 XPS spectra of carbon and oxygen 1s peaks of PMMA at Ground, -0.25 V and +0.25 V.

Another method to study charging is the dynamic measurement as mentioned earlier. In this case the movement of C and O peaks of a PMMA film in response to the +/-5 V applied SQW potential at 0.02 Hz is captured with snapshot measurements. Then the peaks are fitted for each spectrum for a better, quantified understanding of the movement as given in Figure 3.29**,** in these graphs reference values (given in Table 3.2) for the binding energies of C and O atoms are subtracted from the calculated values to see the binding energy difference due to charging more clearly. In the fitted graphs the charging difference between carbonyl group carbon and backbone carbon (Figure 3.29(a)) and also the methoxy group carbon and backbone carbon (Figure 3.29(b)) is seen clearly, while between the two oxygen atoms of carbonyl and methoxy group there is less difference. (Figure 3.29(c)) This is another evidence for the different affinities of different chemical groups in PMMA to the charges residing on the polymer surface. Also subtracting the binding energies of C1s backbone peaks from O1s peaks of carbonyl and methoxy groups results in the difference given in Figure 3.29(d). Although there is a large scatter in this measurement one can immediately notice two different

levels of binding energy difference for +5 V and -5V external biases. This result is in agreement with the result in Figure 3.28 showing the difference between carbon and oxygen atoms binding energies under charging conditions.

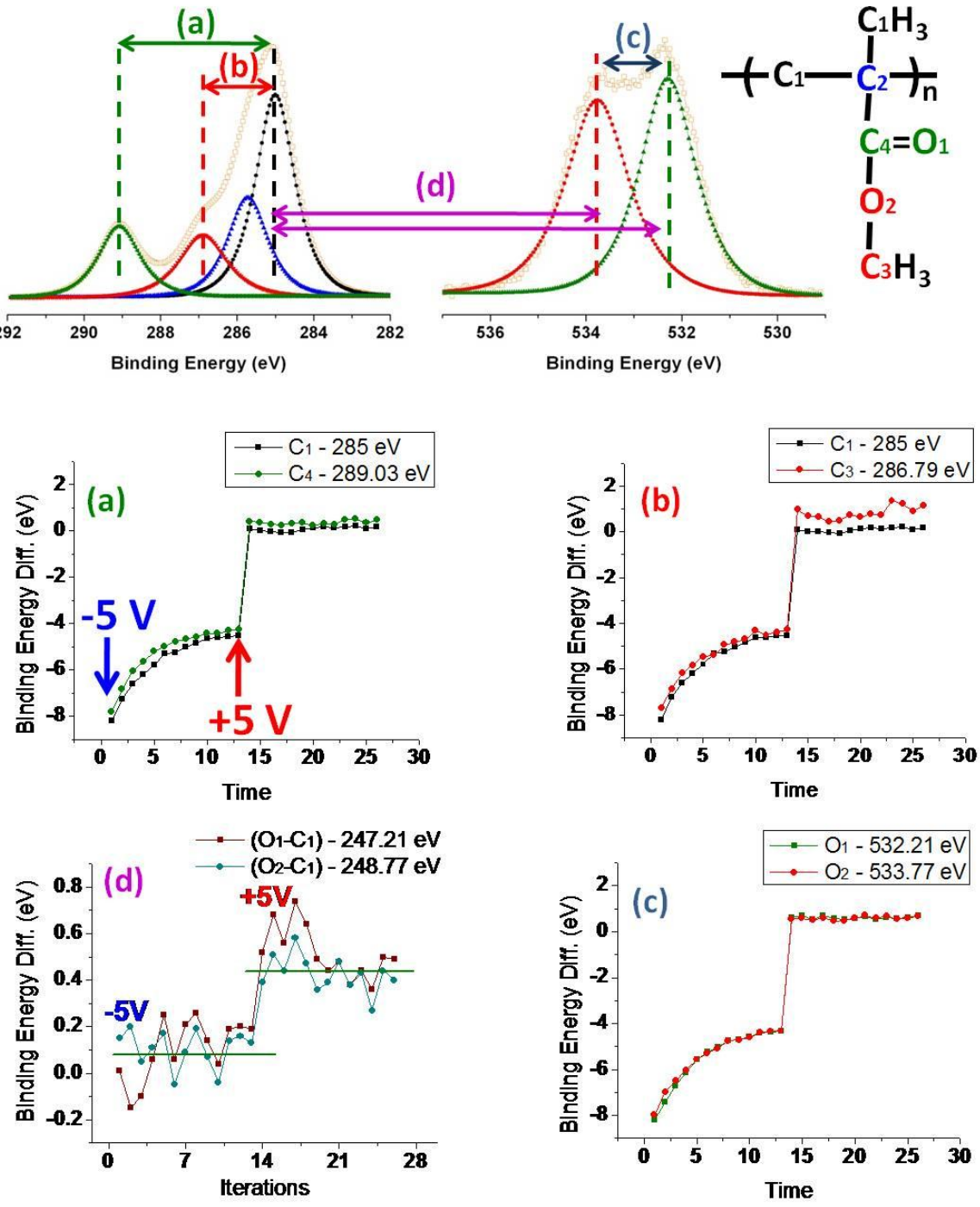

Figure 3.29 Fitted peak positions for dynamic measurement of -/+5 V at 0.002 Hz. (a) Comparison of binding energy change of carbonyl carbon and backbone carbon. (b) Comparison of binding energy change of methoxy carbon and backbone carbon. (c) Comparison of binding

Table 3.2 Reference binding energies of C1s and O1s peaks for PMMA and the binding energy differences between the reference O1s and C1s values.

C1s	*O1s*	*Binding Energy Differences (for Figure 3.29)*
C1: 285.00 eV	O1: 532.21 eV	O1-C1= 247.21 eV
C2: 285.72 eV	O2: 533.77 eV	O2-C1= 248.77 eV
C3: 286.79 eV		
C4: 289.03 eV		

Accompanying the binding energy shifts of C and O peaks of PMMA, there is also broadening of the peaks observed during our measurements. Judging from this broadening of the peaks and the binding energy shifts differing for different groups a visualization of charge distribution on the surface during a measurement can be expressed schematically as shown in Figure 3.30. As seen from the figure we think that charges are not uniformly distributed on the surface but there may be some charge accumulating spots surrounded by the highly electronegative groups like carbonyl and methoxy groups, leaning towards the trapped charges. This speculation is supported by the observation of shifting differences between the backbone and the pendant electronegative groups as well as the charging difference between carbon atoms and oxygen atoms of those electronegative groups under the same conditions as described earlier. A similar observation was also made recently by Baytekin et al. using Kelvin probe AFM to scan the surface of a contact electrified polymer. [95] They observed charge mosaics on the surface rather than uniformly distributed charging. The broadening of the peaks with applied external bias and the difference in charging of different groups may be a result of this non-uniform distribution.

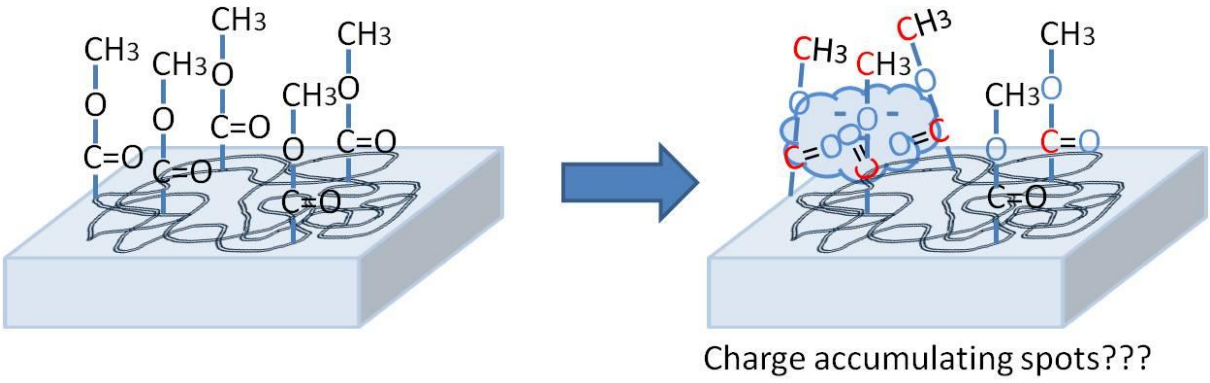

Figure 3.30 Scheme representing the non-uniform distribution of charges on the PMMA surface.

During measurements for the charge resolved XPS the surface is either loaded with electrons to make the surface negatively charged or electrons are repelled from the surface leaving the holes created by the photoelectric effect unneutralized to make the surface positively charged. Following how these cases affect the binding energies of different groups of the polymer, give us some insight to how the positive or negative charges reside on the surface when the charging event occurs. Another issue that can be addressed during such studies is the investigation of native charges on the polymer surface. According to the well known triboelectric series, some polymers are considered negatively charged and some polymers are considered positively charged. The detection of these native charges on the polymers can give important leads to the identity of charge carriers during contact or other electrification processes.

The fitted results of two different dynamic XPS measurements performed on PMMA with and without flood gun emission are given in Figure 3.31. As seen from the figure between +5 V and -5V measurements the binding energy difference is nearly 10 eV for flood gun off case, but at the very beginning of this measurement the presence of an excess negative charge can be observed. Moreover this excess negative charge can only be observed at the beginning of the measurement and cannot be seen in the following cycles. This observation is a solid proof for the presence of some negative charge on the PMMA surface prior to any

intervention.[††††] The issue of native negative charge of a polymer was also discussed before by Kornfeld in 1976 and he stated that polymers are not electrically neutral, structural defects and local charges are compensated by ions adsorbed from air. [71] There is no evidence if the polymer surface has adsorbed ions from the air in our case but the presence of negative charges on the surface can be observed clearly.

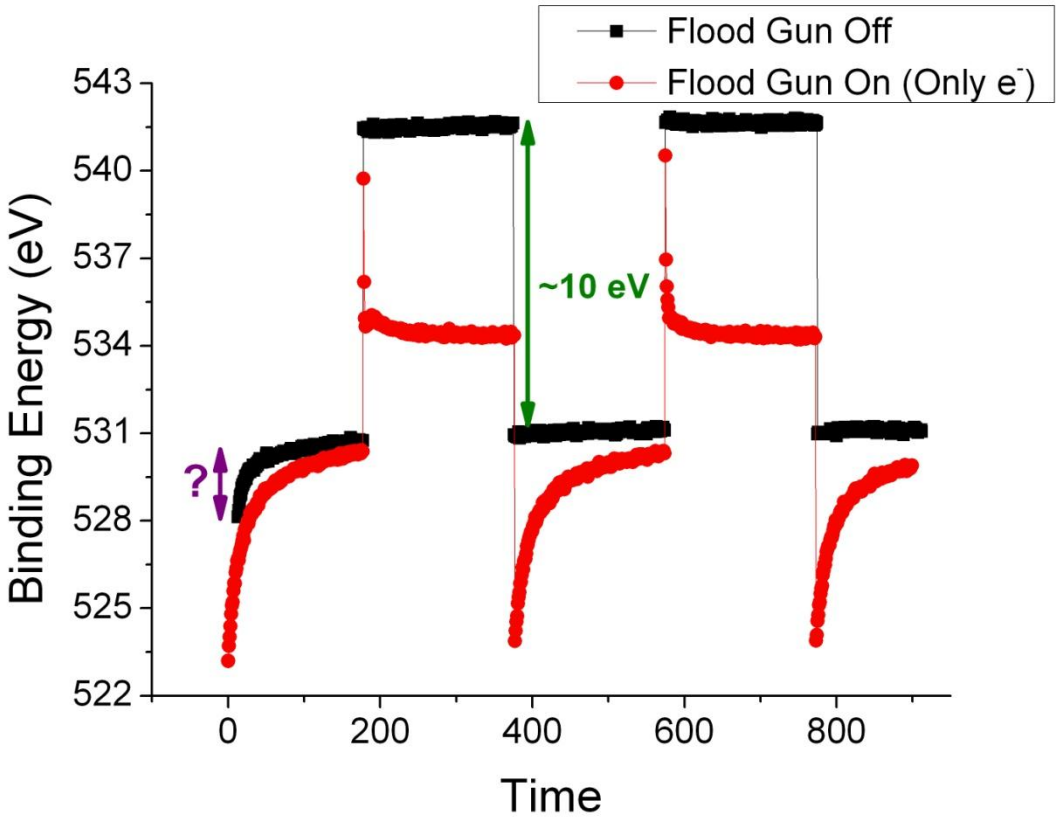

Figure 3.31 Fitted dynamic XPS measurements performed on a PMMA film with and without flood gun.

When the flood gun is turned on to emit only electrons during the measurement (Figure 3.31), the excess negative charging on the film can be seen even more pronounced. But in this case charging can be seen in all cycles during the experiment since the flood gun is

[††††] This measurement was performed on a virgin spot of the polymer. Prior to this measurement no other measurement was performed on the entire film. So neither x-ray and nor electron from the flood gun has contacted the film that can cause such a negative charging on the surface. For that reason the observed effect is believed to be purely native to the polymer.

continuously supplying electrons. In the measurement with flood gun, two charging processes can be observed. When the external bias is at -5 V, the surface releases the stored negative charge slowly until the bias is shifted to +5 V. When the external bias is shifted to +5 V, the polymer surface accumulates negative charge on the surface immediately and stays negatively charged until the next cycle. This behavior of the polymer towards the fast accumulation of electrons is another evidence of the high efficiency of PMMA surface towards the storage of electrons.

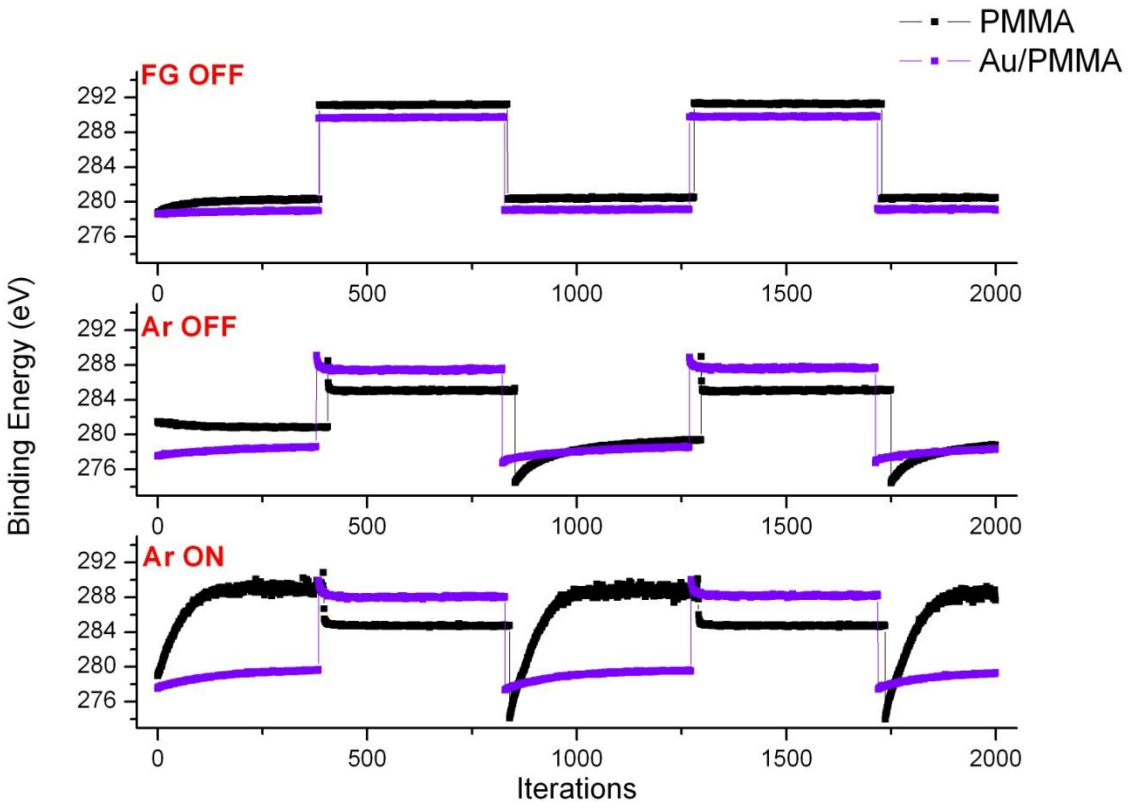

Figure 3.32 Fitted dynamic XPS measurements performed on PMMA and Au/PMMA films without flood gun, with flood gun without Ar and with flood gun with Ar.

In a parallel study, the effects of gold nanoparticles on the charge accumulation on PMMA surfaces were also investigated, For this PMMA films containing gold nanoparticles were prepared on Si substrates and the charging of these films were monitored without flood gun, with flood gun without Ar and with both flood gun and Ar. The fitted data on the resulting spectra is shown in Figure 3.32. As can be seen from the figure, when flood gun is off, gold nanoparticles addition seems to annihilate the negative charges observed at the

beginning of the measurement. For flood gun on cases with and without Ar, the decreased charge accumulation can be observed for the Au/PMMA film for both of the cases. These results support our observations on the increasing of conductivity of PMMA films with gold nanoparticle addition in our previously discussed studies.

The experiments performed with PMMA via charge resolved XPS technique, showed the affinity of PMMA surface for the storage of electrons on the surface and it was also observed that pendant groups and the backbone carbons response differently under charging conditions, due to accumulation of charges. This difference in response is thought to be due to the non-uniform distribution of charges on the polymer surface and relatively free movement of the pendant groups. According to our hypothesis, the pendant groups can surround and form charge accumulation spots and trap the surface charges in those spots. These observations are important insights for furthering of our understanding of the mechanism of electrification process on insulator materials like polymers and the effects of charge accumulation at the molecular level. Additionally, in studies performed on PMMA films containing gold nanoparticles, it was observed that gold nanoparticles decrease the charge accumulation on the PMMA films.

4 Conclusions

In our studies, we have synthesized gold nanoparticles within polymer matrices using photo irradiation. With this technique we obtain nanoparticle-polymer composites in one-step without any further procedure. The reduction of Au^{3+} ions and formation of Au nanoparticles are much slower in polymer matrix than in solution. So we can follow these two processes separately using UV-Vis spectrometer and different factors affecting these processes may be investigated. We probed the effects of heating, addition of another metal ion and phototosensitizers on reduction and nucleation and growth, and we assessed the effects of the given conditions on the reduction and nucleation and growth rates. Important information was gained with these studies about the reduction mechanism of gold ions and the role of polymer during reduction and nucleation and growth processes.

Photo-patterning is an important application of this synthesis method. Films of different thicknesses with different feature sizes can be produced with light-impermeable photomasks with this method. In our studies we discovered the presence of ion depleted regions, which contain no gold ions or nanoparticles and are formed by migration of gold ions at and near the border of the mask to the irradiated regions. Those regions can be observed as dark border regions at SEM and additional verification on the content of the ion depleted regions was also performed using fluorescence studies with Rhodamine 6G (R6G) molecules. Fluorescence studies conducted with the addition of R6G molecules to the patterned films concluded that, the ion depleted regions are indeed formed with the diffusion of gold ions at the border of the masked regions through the irradiated regions.

For characterization of the films we also perform charging studies with XPS using DC and SQW pulses. Thin films of PMMA with and without gold nanoparticles were probed with applied DC potentials and it was observed that gold nanoparticles decrease the resistance of PMMA films as shown by the previous studies in the literature. SQW potentials were also used for getting additional information about the electric properties of such films. The SQW potential measurements give us information about the capacitance properties of non-conducting samples and in our experiments we saw the effect of gold nanoparticles on the capacitance of the PMMA films with this method. Gold nanoparticles increased the capacitance of PMMA films and decreased the resistance of the PMMA films as the summary of our studies. These results were not new, but the point we want to emphasize is that these measurements are very hard to do using normal electrical IV measurement since making good

electrical contacts to polymer films is difficult and also the measured current values are very low. But in this study we reliably have shown that such measurements can be made by XPS non-contact, more easily and accurately.

Another important process we investigated using charge resolved XPS technique is the charge accumulation on the polymer surfaces and the effect of gold nanoparticles on this process. Probing the charge accumulation on polymer surfaces may give us information on the identity of charge carrying groups during contact and other forms of electrification of electrets. The studies conducted to understand the charge accumulation on the PMMA surface showed that, PMMA surface is very susceptible to accumulate negative charges on its surface and there are even native negative charges on the surface prior to any treatment. This observation partly supports the other studies claiming that the electrons are the charge carriers during the contact electrification of insulators. Another observation done during these experiments was that, the carbon and oxygen atoms of the pendant groups were reacting differently than the carbon atoms of the polymer backbone when the surface was charged. Presence of charge accumulation spots, surrounded by highly electronegative groups leaning towards those charges, may be leading to this observation. Additionally the effect of gold nanoparticles, on this charge accumulation process was also monitored during these studies. And the decreasing charge accumulation with the addition of gold nanoparticles was observed, supporting our previous observations on the effect of gold nanoparticle on the conductivity of the PMMA films.

5 List of Abbreviations

DC	Direct current
FG	Flood gun
FT-IR	Fourier Transform Infrared
NP	Nanoparticle
PDMS	Poly(dimethyl siloxane)
PMMA	Poly(methyl methacrylate)
PS	Poly(styrene)
PVA	Poly(vinyl alcohol)
R6G	Rhodamine 6G
SEM	Scanning electron microscope
SERS	Surface enhanced Raman spectroscopy
SPR	Surface plasmon resonance
SQW	Square wave
UV	Ultraviolet
UV-Vis	Ultraviolet-Visible
XPS	X-ray photoelectron spectroscopy

6 References

1. M. C. Daniel and D. Astruc, Chemical Reviews **104** (1), 293-346 (2004).
2. K. Watanabe, D. Menzel, N. Nilius and H. J. Freund, Chemical Reviews **106** (10), 4301-4320 (2006).
3. A. N. Shipway, E. Katz and I. Willner, Chemphyschem **1** (1), 18-52 (2000).
4. R. Hoffmann, Angewandte Chemie-International Edition in English **26** (9), 846-878 (1987).
5. G. Schmid, Chem. Rev. **92** (8), 1709-1727 (1992).
6. M. Brust, D. Bethell, C. J. Kiely and D. J. Schiffrin, Langmuir **14** (19), 5425-5429 (1998).
7. T. Goodson, O. Varnavski and Y. Wang, International Reviews in Physical Chemistry **23** (1), 109-150 (2004).
8. X. Li, J. W. M. Chon and M. Gu, Australian Journal of Chemistry **61** (5), 317-323 (2008).
9. A. T. Bell, Science **299** (5613), 1688-1691 (2003).
10. M. S. Chen and D. W. Goodman, Science **306** (5694), 252-255 (2004).
11. L. He, M. D. Musick, S. R. Nicewarner, F. G. Salinas, S. J. Benkovic, M. J. Natan and C. D. Keating, Journal of the American Chemical Society **122** (38), 9071-9077 (2000).
12. R. P. Bagwe, X. J. Zhao and W. H. Tan, Journal of Dispersion Science and Technology **24** (3-4), 453-464 (2003).
13. M. Haruta, T. Kobayashi, H. Sano and N. Yamada, Chem. Lett. (2), 405-408 (1987).
14. M. Haruta, N. Yamada, T. Kobayashi and S. Iijima, J. Catal. **115** (2), 301-309 (1989).
15. H. Sakurai and M. Haruta, Catalysis Today **29** (1-4), 361-365 (1996).
16. A. Ueda, T. Oshima and M. Haruta, Applied Catalysis B-Environmental **12** (2-3), 81-93 (1997).
17. T. Sato, H. Ahmed, D. Brown and B. F. G. Johnson, J. Appl. Phys. **82** (2), 696-701 (1997).

18. L. E. Brus, M. Bawendi, W. L. Wilson, L. Rothberg, P. J. Carroll, T. M. Jedju and M. L. Steigerwald, Abstracts of Papers of the American Chemical Society **201**, 409-INOR (1991).

19. L. F. Chi, M. Hartig, T. Drechsler, T. Schwaack, C. Seidel, H. Fuchs and G. Schmid, Applied Physics a-Materials Science & Processing **66**, S187-S190 (1998).

20. M. Valden, X. Lai and D. W. Goodman, Science **281** (5383), 1647-1650 (1998).

21. A. P. Alivisatos, K. P. Johnsson, X. G. Peng, T. E. Wilson, C. J. Loweth, M. P. Bruchez and P. G. Schultz, Nature **382** (6592), 609-611 (1996).

22. G. P. Mitchell, C. A. Mirkin and R. L. Letsinger, Journal of the American Chemical Society **121** (35), 8122-8123 (1999).

23. T. A. Taton, R. C. Mucic, C. A. Mirkin and R. L. Letsinger, Journal of the American Chemical Society **122** (26), 6305-6306 (2000).

24. Y. W. C. Cao, R. C. Jin and C. A. Mirkin, Science **297** (5586), 1536-1540 (2002).

25. A. Campion and P. Kambhampati, Chem. Soc. Rev. **27** (4), 241-250 (1998).

26. Y. J. Kim, R. C. Johnson and J. T. Hupp, Nano Letters **1** (4), 165-167 (2001).

27. C. Guan, C. L. Lu, Y. R. Cheng, S. Y. Song and B. Yang, J. Mater. Chem. **19** (5), 617-621 (2009).

28. C. L. Lu, C. Guan, Y. F. Liu, Y. R. Cheng and B. Yang, Chemistry of Materials **17** (9), 2448-2454 (2005).

29. Y. Imai, A. Terahara, Y. Hakuta, K. Matsui, H. Hayashi and N. Ueno, Polymer Journal **42** (2), 179-184 (2010).

30. J. L. H. Chau, C. T. Tung, Y. M. Lin and A. K. Li, Mater. Lett. **62** (19), 3416-3418 (2008).

31. Y. F. Liu, C. L. Lu, M. J. Li, L. Zhang and B. Yang, Colloids and Surfaces a-Physicochemical and Engineering Aspects **328** (1-3), 67-72 (2008).

32. T. Hanemann, J. Hausselt and E. Ritzhaupt-Kleissl, Microsystem Technologies-Micro-and Nanosystems-Information Storage and Processing Systems **15** (3), 421-427 (2009).

33. Y. Q. Li, Y. Yang, S. Y. Fu, X. Y. Yi, L. C. Wang and H. D. Chen, Journal of Physical Chemistry C **112** (47), 18616-18622 (2008).

34. H. M. Xiong, Y. Xu, O. G. Ren and Y. Y. Xia, Journal of the American Chemical Society **130** (24), 7522-+ (2008).

35. R. F. Ziolo, E. P. Giannelis and R. D. Shull, Nanostructured Materials **3** (1-6), 85-92 (1993).

36. R. F. Ziolo, E. P. Giannelis, B. A. Weinstein, M. P. Ohoro, B. N. Ganguly, V. Mehrotra, M. W. Russell and D. R. Huffman, Science **257** (5067), 219-223 (1992).

37. C. M. Yang, H. Y. Li, D. B. Xiong and Z. Y. Cao, Reactive & Functional Polymers **69** (2), 137-144 (2009).

38. A. Masotti, A. Pitta, G. Ortaggi, M. Corti, C. Innocenti, A. Lascialfari, M. Marinone, P. Marzola, A. Daducci, A. Sbarbati, E. Micotti, F. Orsini, G. Poletti and C. Sangregorio, Magnetic Resonance Materials in Physics Biology and Medicine **22** (2), 77-87 (2009).

39. Z. Y. Wang, G. Liu, J. Sun, B. Y. Wu, Q. Y. Gong, B. Song, H. Ai and Z. W. Gu, Journal of Nanoscience and Nanotechnology **9** (1), 378-385 (2009).

40. S. A. Meenach, A. A. Anderson, M. Suthar, K. W. Anderson and J. Z. Hilt, Journal of Biomedical Materials Research Part A **91A** (3), 903-909 (2009).

41. B. Thiesen and A. Jordan, International Journal of Hyperthermia **24** (6), 467-474 (2008).

42. J. L. Arias, M. Lopez-Viota, J. Lopez-Viota and A. V. Delgado, Int. J. Pharm. **382** (1-2), 270-276 (2009).

43. Y. F. Zhu, S. Kaskel, T. Ikoma and N. Hanagata, Microporous and Mesoporous Materials **123** (1-3), 107-112 (2009).

44. C. Albornoz and S. E. Jacobo, J. Magn. Magn. Mater. **305** (1), 12-15 (2006).

45. A. M. Schmidt, Macromolecular Rapid Communications **26** (2), 93-97 (2005).

46. P. Murugaraj, D. Mainwaring and N. Mora-Huertas, *Dielectric enhancement in polymer-nanoparticle composites through interphase polarizability*. (AIP, 2005).

47. S. K. Bhattacharya and R. R. Tummala, Journal of Materials Science-Materials in Electronics **11** (3), 253-268 (2000).

48. S. K. Bhattacharya and R. R. Tummala, Microelectronics Journal **32** (1), 11-19 (2001).

49. J. W. Paquette, K. J. Kim, J.-D. Nam and Y. S. Tak, Journal of Intelligent Material Systems and Structures **14** (10), 633-642 (2003).

50. P. G. Bruce, B. Scrosati and J. M. Tarascon, Angewandte Chemie-International Edition **47** (16), 2930-2946 (2008).

51. W. M. Zhang, J. S. Hu, Y. G. Guo, S. F. Zheng, L. S. Zhong, W. G. Song and L. J. Wan, Advanced Materials **20** (6), 1160-+ (2008).

52. M. S. Park, Y. M. Kang, J. H. Kim, G. X. Wang, S. X. Dou and H. K. Liu, Carbon **46** (1), 35-40 (2008).

53. S. Panigrahi, S. Kundu, S. K. Ghosh, S. Nath and T. Pal, Journal of Nanoparticle Research **6** (4), 411-414 (2004).

54. J. Turkevitch, P. C. Stevenson and J. Hillier, Discussions of the Faraday Society **11**, 55-75 (1951).

55. G. Frens, Nature Phys. Sci. **241**, 20-22 (1973).

56. M. Brust, J. Fink, D. Bethell, D. J. Schiffrin and C. Kiely, Journal of the Chemical Society-Chemical Communications (16), 1655-1656 (1995).

57. M. Brust, M. Walker, D. Bethell, D. J. Schiffrin and R. Whyman, Journal of the Chemical Society-Chemical Communications (7), 801-802 (1994).

58. F. Vitale, L. Mirenghi, E. Piscopiello, G. Pellegrini, E. Trave, G. Mattei, I. Fratoddi, M. V. Russo, L. Tapfer and P. Mazzoldi, Materials Science & Engineering C-Biomimetic and Supramolecular Systems **27** (5-8), 1300-1304 (2007).

59. S. Horiuchi, M. I. Sarwar and Y. Nakao, Advanced Materials **12** (20), 1507-1511 (2000).

60. E. Gachard, H. Remita, J. Khatouri, B. Keita, L. Nadjo and J. Belloni, New J. Chem. **22** (11), 1257-1265 (1998).

61. F. Karadas, G. Ertas, E. Ozkaraoglu and S. Suzer, Langmuir **21** (1), 437-442 (2005).

62. A. S. Korchev, T. Konovalova, V. Cammarata, L. Kispert, L. Slaten and G. Mills, Langmuir **22** (1), 375-384 (2006).

63. A. Alexandrov, L. Smirnova, N. Yakimovich, N. Sapogova, L. Soustov, A. Kirsanov and N. Bityurin, Appl. Surf. Sci. **248** (1-4), 181-184 (2005).

64. M. Sakamoto, T. Tachikawa, M. Fujitsuka and T. Majima, Advanced Functional Materials **17** (6), 857-862 (2007).

65. S. Horiuchi, T. Fujita, T. Hayakawa and Y. Nakao, Advanced Materials **15** (17), 1449-1452 (2003).

66. E. Yilmaz, G. Ertas, E. Bengu and S. Suzer, Journal of Physical Chemistry C **114** (43), 18401-18406 (2010).

67. B. Ulgut and S. Suzer, The Journal of Physical Chemistry B **107** (13), 2939-2943 (2003).

68. S. Suzer, A. Dana and G. Ertas, Anal. Chem. **79** (1), 183-186 (2006).

69. J. J. Cole, C. R. Barry, R. J. Knuesel, X. Y. Wang and H. O. Jacobs, Langmuir **27** (11), 7321-7329 (2011).

70. A. F. Diaz and D. Fenzelalexander, Langmuir **9** (4), 1009-1015 (1993).

71. M. I. Kornfeld, J. Phys. D: Appl. Phys. **9**, 10 (1976).

72. C. Y. Liu and A. J. Bard, Chem. Phys. Lett. **480** (4-6), 145-156 (2009).

73. L. S. McCarty and G. M. Whitesides, Angewandte Chemie-International Edition **47** (12), 2188-2207 (2008).

74. C. Y. Liu and A. J. Bard, Nature Materials **7** (6), 505-509 (2008).

75. C. Y. Liu and A. J. Bard, Journal of the American Chemical Society **131** (18), 6397-6401 (2009).

76. J. J. Cole, C. R. Barry, X. Y. Wang and H. O. Jacobs, Acs Nano **4** (12), 7492-7498 (2010).

77. L. S. McCarty, A. Winkleman and G. M. Whitesides, Journal of the American Chemical Society **129** (13), 4075-4088 (2007).

78. A. Diaz, D. Fenzelalexander, D. Wollmann and J. A. Barker, Langmuir **8** (11), 2698-2706 (1992).

79. A. F. Diaz, D. Wollmann and D. Dreblow, Chemistry of Materials **3** (6), 997-999 (1991).

80. F. Carpi, S. Bauer and D. De Rossi, Science **330** (6012), 1759-1761 (2010).

81. P. Brochu and Q. B. Pei, Macromolecular Rapid Communications **31** (1), 10-36 (2010).

82. S. Balci, O. Birer and S. Suzer, Polymer **45** (21), 7123-7128 (2004).

83. A. S. Korchev, T. S. Shulyak, B. L. Slaten, W. F. Gale and G. Mills, Journal of Physical Chemistry B **109** (16), 7733-7745 (2005).

84. A. Kudelski and B. Pettinger, Chem. Phys. Lett. **321** (5-6), 356-362 (2000).

85. P. Xu and H. Yanagi, Chemistry of Materials **11** (10), 2626-2628 (1999).

86. T. Tanaka, K. Yamaguchi and S. Yamamoto, Opt. Commun. **212** (1-3), 45-50 (2002).

87. T. Sen and A. Patra, Journal of Physical Chemistry C **112** (9), 3216-3222 (2008).

88. F. Faupel, R. Willecke and A. Thran, Materials Science & Engineering R-Reports **22** (1), 1-55 (1998).

89. W. H. Teh, C. T. Liang, M. Graham and C. G. Smith, Journal of Microelectromechanical Systems **12** (5), 641-648 (2003).

90. V. Raja, A. K. Sharma and V. Rao, Mater. Lett. **58** (26), 3242-3247 (2004).

91. W. Zheng and S. C. Wong, Composites Science and Technology **63** (2), 225-235 (2003).

92. M. K. Abyaneh, R. Pasricha, S. W. Gosavi and S. K. Kulkarni, Nanotechnology **17** (16), 4129-4134 (2006).

93. M. C. Salvadori, M. Cattani, F. S. Teixeira and I. G. Brown, Appl. Phys. Lett. **93** (7) (2008).

94. J. A. Wiles, B. A. Grzybowski, A. Winkleman and G. M. Whitesides, Anal. Chem. **75** (18), 4859-4867 (2003).

95. H. T. Baytekin, A. Z. Patashinski, M. Branicki, B. Baytekin, S. Soh and B. A. Grzybowski, Science **333** (6040), 308-312 (2011).

7 Appendix

7.1 Publications

- Yilmaz E, Ertas G, Bengu E, Suzer S, The Journal of Physical Chemistry C, Vol.114(43), Pages: 18401-18406, 2010
- Yilmaz E, Suzer S, Applied Surface Science, Vol.256, Issue: 22, Pages: 6630- 6633, 2010
- Ozkaraoglu E, Tunc K, Suzer S, Polymer, Volume: 50, Issue: 2, Pages: 462-466, 2009
- Ozkaraoglu E, Tunc I, Suzer S, Surface & Coatings Technology, Volume: 201, Issue: 19-20, Pages: 8202-8204, AUG 5 2007
- Karadas F, Ertas G, Ozkaraoglu E, Suzer S, Langmuir, Volume: 21, Issue: 1, Pages: 437-442, JAN 4 2005

7.2 Conference Presentations

- Yilmaz E, Suzer S, "UV Induced Synthesis and XPS Characterization of Gold Nanoparticle-PMMA Composites", Poster Presentation, AVS 57th International Symposium & Exhibition, October 17-22 2010, Albuquerque, New Mexico, USA
- Yilmaz E, Suzer S, "Photo-patterning of PMMA Films with Gold Nanoparticles", Oral Presentation, 6th Nanoscience and Nanotechnology Conference, June 15-18 2010, Izmir, TURKEY
- Ozkaraoglu E, Suzer S, "Gold Nanoparticles in PMMA Matrix: in-situ Synthesis and Gold Nanoparticle-PMMA interactions", Oral Presentation, 13th European Conference on Applications of Surface and Interface Analysis, October 18-23 2009, Antalya, TURKEY
- Ozkaraoglu E, Suzer S, "Gold Nanoparticles in PMMA Matrix: in-situ Synthesis and Gold Nanoparticle-PMMA interactions", Oral Presentation, 8th International Conference on Advanced Polymers via Macromolecular Engineering, October 4-7 2009, Dresden, GERMANY

- Ozkaraoglu E, Suzer S, “Gold Nanoparticles in PMMA Matrix: in-situ Synthesis and Gold Nanoparticle-PMMA interactions”, Oral Presentation, 26th European Conference on Surface Science, August 30 - September 4 2009, Parma, ITALY
- Ozkaraoglu E, Suzer S, “UV Induced in-situ Synthesis of Gold Nanoparticles within PMMA Films”, Oral Presentation, 5th Nanoscience and Nanotechnology Conference, June 9-11 2009, Eskisehir, TURKEY
- Ozkaraoglu E, Tunc I, Suzer S, “UV and X-Ray Induced Production of Au and Pt Mono/Bimetallic Nanoparticles within Polymer Films”, Poster Presentation, 12th European Conference on Applications of Surface and Interface Analysis, September 9-14 2007, Brussels, BELGIUM
- Ozkaraoglu E, Tunc I, Suzer S, “Synthesis and Characterization of Gold Nanoparticles with UV radiation and/or X-rays within Polymer Films”, Oral Presentation, 10th National Spectroscopy Conference, July 4-7 2007, Izmir, TURKEY